Variability of precipitation in complex terrain and the investigation of representativeness of a single point measurement for the Matre Hydro System, Western Norway.

Master thesis in Meteorology

Mette Sundvor Skjerdal

June 2009

UNIVERSITY OF BERGEN
GEOPHYSICAL INSTITUTE

The work of this thesis has been performed as a cooperation between Geophysical Institute, University of Bergen and the Norwegian power company BKK (Bergenshalvøens Kommunale Kraftselskap).

University of Bergen
Geophysical Institute

Bergenshalvøens Kommunale
Kraftselskap

Acknowledgements

The process of having a practial thesis in Meteorology have been both informative and challenging, and I am thankful to have had the opportunity to explore geophysics in this way. First of all I would like to thank all people participating in the field part of this thesis: Tor de Lange, Joachim Reuder, Fredrik Villanger, Sven-Ole Berland and Bård Monsen. A special thanks to Tor de Lange for performing the practical part of the calibrations.

In the work of this thesis, I would especially thank my supervisors Joachim Reuder and Fredrik Villanger for skillful guidance, constructive feedback and help through the whole process making this thesis.

Thanks to Gard Hauge at Storm Weather Center for providing data from the MM5 model, and to Øyvind Breivik at the Norwegian Meteorological Institute for providing data from the HIRLAM4 model. Thanks to Marius Jonassen for great software support and to Berit Hagen for making analysis maps available. Thanks to Leiv O. Oppedal for allowing me to place a rain gauge in his garden for several months. Also thanks to the reviewers, Silje Nordtveit, Stephanie Mayer and Marius Jonassen, for their suggestions.

A special thanks to all friends and students at the Geophysical Institute for making this time great and unforgettable! Finally, thanks to friends, family, and my fantastic boyfriend Sven-Ole for having supported and encouraged me through the whole thesis.

Abstract

Orography is strongly affecting precipitation. Especially over complex terrain, the precipitation fields can show high spatial variability even over very small scales. In cooperation between the power company BKK (Bergenshalvøens Kommunale Kraftselskap) and the Geophysical Institute, University of Bergen, 20 rain gauges and two weather stations have been deployed between 22 and 898 meters above sea level in the catchment area of the Matre Hydro System in Western Norway in the period April - October 2008. The derived high resolution data set in space and time was used to investigate the horizontal variability and the altitude dependence of precipitation in complex terrain under different synoptic conditions in this catchment area. An average vertical increase of precipitation amount with altitude of 5.2 % / 100 m was found. The precipitation amounts normalized to the altitude of the reference Station at Stordal allow for the investigation of the horizontal precipitation gradient in the area. This gradient is found to be southwest-northeast oriented, with approximately 115 % of the overall reference amount in the southwest and 85 % in the northeast. By this the representativeness of BKKs single point measurement at Stordal on the total precipitation amount of the whole catchment area has been addressed.

Another purpose of the project was also to study the representativeness of a used single point ECMWF forecast for the reference station at Stordal. During the measurement period the model forecasted in total only about 5 % less then the observed amount, however it showed a smoothing tendency compared to the observations. The potential for improvement of precipitation prediction by use of operational model runs with higher horizontal resolution has also been addressed. Both tested model configurations MM5, with a horizontal resolution of 12 km, and HIRLAM4, with a horizontal resolution of 4 km, were not able to improve the point forecast quality for Stordal.

An important part of the thesis was dedicated to a thorough characterization of the used HOBO rain gauges by laboratory tests and field comparisons. This included laboratory calibration, laboratory investigation of the effects of non-level mounting on sampling efficiency and a field comparison with official measurements that showed an accordance of better than 1 % for total precipitation amounts.

Contents

1 Introduction

The western part of Norway is the area which experiences the highest amounts of precipitation in Norway. The position in the westerlies, where relatively mild and humid air gets directed toward the shore and land, is contributing to the high precipitation amounts. Orography is strongly affecting precipitation, and the topography and high mountains in Western Norway give very favorable conditions for orographic enhanced precipitation (e.g. Spinnangr (1943a), Spinnangr (1943b), Smith (1979)). Over complex terrain, precipitation fields can show high spatial variability even over very small scales. High annual precipitation amounts combined with large and low populated mountain areas for water collection and storage make Western Norway a favorable region for hydroelectric power production.

The producers of hydroelectric power continuously want the water resources to be utilized in the best suited way. This requires a continuous control and supervision of the water resources. Therefore, accurate precipitation observations and reliable precipitation forecasts for the next days are of uttermost economic importance for the power companies. The catchment areas in Norway are often large and contain large topographical variations from sea level up to more than 1000 m within short horizontal distances, which causes high variability in the distribution of precipitation. Nevertheless the power companies typically operate with one or only very few measurement sites even in those complex areas. In case of the Matre Hydro System (MHS), which is situated in a large mountain region at the border between the counties of Hordaland and Sogn og Fjordane (Figure 1), the Norwegian power company BKK (Bergenshalvøens Kommunale Kraftselskap), uses one single rain gauge at Stordal to describe the actual and past precipitation situation in the whole catchment area of around 200 km^2.

The main motivation of this work was to investigate the representativeness of such single point measurement for a larger area of complex terrain, which requires a detailed picture of the horizontal variability and the altitude dependency of precipitation in the area. This demands high resolution measurements in space and time. Such measurements are sparse and corresponding data are not available on an operational basis. Therefore a measurement campaign has been performed in the MHS in cooperation between BKK and the Geophysical Institute, University of Bergen. During the period April - October 2008, 20 rain gauges and two automatic weather stations have been deployed at altitudes between 22 and 898 m above sea level in the catchment area of the MHS. All instruments have been deployed in the area limited by the red frame in Figure 1. This setup allows the observation of the spatial distribution of precipitation over several months under different synoptic situations and wind directions. In particular knowledge will be gained on the relationship of precipitation amounts between the BKK reference station Stordal and the different rain gauge stations specifically installed during the campaign.

To estimate the precipitation expected during the next days, BKK uses a single point

forecast from the ECMWF model with a resolution of 25 km for the location of Stordal. Another purpose of this work was the validation of the ECMWF single point forecast against rain gauge measurements for the reference station. One of the main problems of precipitation modelling for complex terrain is the insufficient resolution of the topography for rather coarse resolutions of e.g. 25 km. Therefore the potential for improvement of precipitation prediction by use of operational model runs with higher horizontal resolution has also been addressed. For this purpose, the models MM5, with a horizontal resolution of 12 km, and HIRLAM4, with a horizontal resolution of 4 km, are used.

For the precipitation measurements HOBO RG2-M rain gauges have been utilized. Rain gauge measurements are subject to specific sources of errors, e.g. undercatch due to wind, evaporation and splash-out (e.g Førland et al. (1996), Yang et al. (1998)). Nevertheless those instruments provide the only reasonable instrumentation for the measurement in mountainous areas. Precipitation radar is not suitable for the purpose due to substantial limitations in complex terrain (Dinku et al. (2002)). Consequently another important part of this thesis is a thorough laboratory and field characterization of the HOBO instruments to minimize the related uncertainties. The focus in this context was set to the laboratory calibration of the instruments and a validation against official measurements.

Of course improvement in knowledge of the precipitation distribution in complex terrain is not only economically relevant with respect to power production. High precipitation events regularly cause flooding and landslides in Western Norway (e.g. Karlsen (2007)). This implies an undesirable risk for the community. A better understanding of the spatial distribution will increase flood forecast capabilities and therefore reduce the risk of related natural hazards.

The thesis is organized as follows; chapter two presents some general theory concerning different orographic precipitation mechanisms. The theory chapter ends with an overview of some of the previous studies on precipitation in Western Norway. The third chapter describes the instruments used in this thesis. Field and laboratory tests of the HOBO rain gauges are presented in chapter four. The fifth chapter presents the instrumental setup in the Matre-campaign. A description of error sources regarding precipitation measurements and a short description of the MHS is also included in this chapter. Chapter six presents the overall meteorological conditions during the campaign. This chapter also includes a comparison between the observed and forecasted wind conditions. In chapter seven the precipitation distribution at the reference location is described. A comparison of the reference station and the single point forecast from the ECMWF model is also addressed in this chapter. Chapter eight presents the precipitation distribution in the MHS. This chapter also includes a comparison of the observed precipitation in the campaign and the run-off in a normal period. In chapter nine, attention is given to case studies. In chapter ten, a model comparison is performed. The measurement period is compared to a normal period in chapter eleven. A summary and conclusion will be presented in chapter twelve.

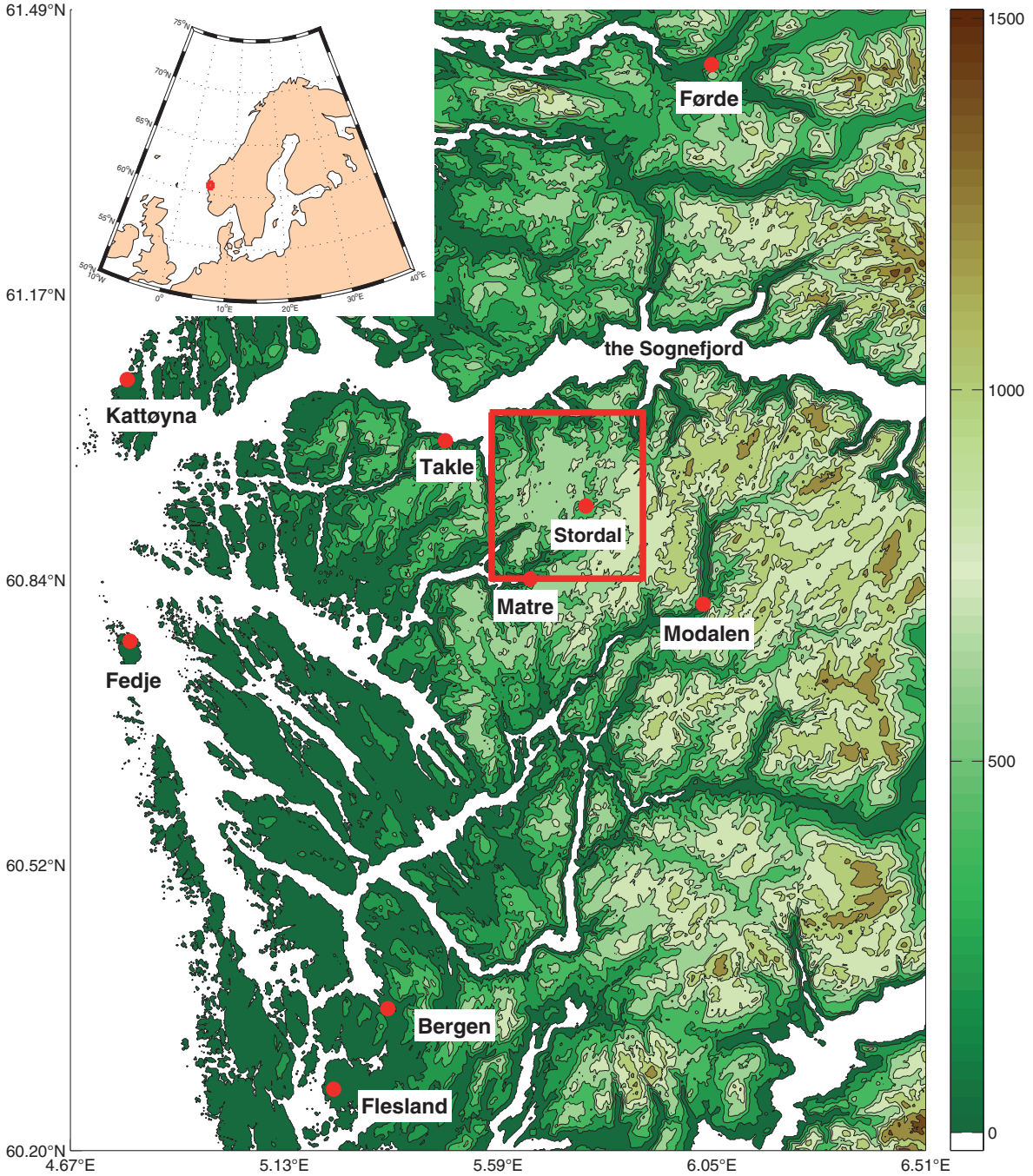

Figure 1: *The measurement area is located inside the red frame, and Matre denotes the southernmost station in the Matre-campaign. Meteorological stations maintained by the Norwegian Meteorological Institute are situated at Bergen, Flesland, Fedje, Takle, Modalen and Førde. The colorbar denotes the elevation above sea level [m].*

2 Theory

2.1 Cloud and hydrometeor formation

Clouds form when the moisture in the air exceeds its ability to carry water as vapor, accordingly when the air parcel reaches saturation. The relative humidity, expressed in percent, is the ratio of the amount of water vapor in dry air (actual mixing ratio, w) to the amount of water vapor the air can hold (saturation mixing ratio, w_s). Relative humidity can thus be expressed as

$$RH = 100\frac{w}{w_s} \cong 100\frac{e}{e_s}, \tag{1}$$

where e is the partial pressure of water vapor in the parcel and e_s is the saturation vapor pressure. When the relative humidity is 100 %, an air parcel is referred to as saturated. In this state, the rate of condensation is equal to the rate of evaporation. As described by the Clausius-Clapeyron relationship, the saturation vapor pressure, e_s, is a function of temperature. With a high accuracy, e_s may be written as

$$e_s(T) = 6.112exp\left(\frac{aT}{b+T}\right), \tag{2}$$

where e_s is in hPa, T is in degree Celsius, a = 17.67 and b = 243.5 °C (e.g. Rogers (1989)). The expression is, according to Bolton (1980), accurate to within 0.3 % for temperatures between -35 °C and +35 °C. As seen in Figure 2, saturation vapor pressure changes exponentially with temperature.

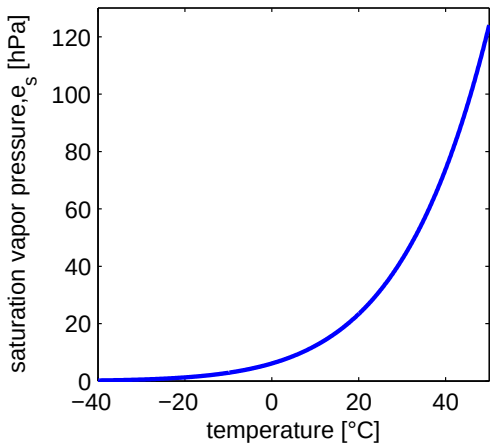

Figure 2: *Relationship between temperature and saturation water vapor pressure, e_s.*

When the air contains more water vapor than needed to produce saturation, it becomes supersaturated. Homogeneous nucleation, the formation of droplets from vapor in pure environment, requires supersaturation levels of several hundred percents. Supersaturation of only a few percent is observed in the atmosphere. This indicates that droplets in the atmosphere form through heterogeneous nucleation, where all condensation occurs on wettable aerosol particles, so-called cloud condensation nucleii (CCN).

Droplet growth is controlled by the ambient conditions inside a cloud, and the process is divided into warm and cold droplet growth. In warm clouds, that is clouds where the temperature in the cloud is above 0 °C, the cloud droplets at first grow by condensation on a CCN. The rate of increase in the radius of a droplet growing with condensation decreases with time because growing droplets consume water vapor faster than it is made available, and therefore the droplets rarely grow large enough to become a rain drop by condensation only. Further growth from the relatively small size achieved by condensation to the size of raindrops occurs by collision and coalescence due to the different vertical velocity of droplets of different size. The cloud droplet leaves the cloud as a raindrop when it becomes too heavy and the upcraft too weak.

In cold clouds with temperatures below 0 °C, water droplets can coexist with ice particles down to about -40 °C, and are referred to as supercooled droplets. If a cloud contains both ice particles and supercooled droplets, it is said to be a mixed cloud. The saturation vapor pressure over ice is less than that over liquid water at the same temperature, therefore the ice particles in a mixed cloud will grow by water vapor diffusion at the expense of the droplets. This causes a rather fast initial growth of ice crystals, which start to fall. In mixed clouds, ice particles will increase further in mass by riming, which means that ice particles are colliding with supercooled droplets that freeze onto them. In addition, in glaciated clouds, clouds which consist only of ice particles, ice particles can grow by colliding and aggregating with one another. The ice particles collide with each other if their terminal fall speeds are different. The probability of two colliding crystals aggregating increases with increasing temperature, and is likely above -5 °C due to more "sticky" ice surface (e.g. Wallace and Hobbs (2006)).

2.2 Orographic precipitation mechanisms

Orographic precipitation is precipitation induced or enhanced by the ascent of moist air over an elevated barrier such as a mountain range. Important factors for orographic precipitation are wind speed and direction, humidity, sloping of the terrain and the vertical profile of temperature (e.g. Smith (1979)). The vertical velocity, caused by forced elevation, has a particular high importance for the precipitation amount and distribution. The forced vertical velocity w is determined by the sloping of the terrain $\nabla_h \mathrm{H}$ (where H is the height of the terrain and $\nabla_h \mathrm{H} = \frac{dH}{dx} + \frac{dH}{dy}$ and the horizontal

wind $\vec{U}$ in the lower stratum of the air:

$$w = \vec{U} \bullet \nabla_h H \tag{3}$$

Orographic enhanced precipitation occurs in several ways and under different weather conditions. Smith (1989) operates with four basic mechanisms for production of orographic rainfall: The smooth forced ascent, the "seeder-feeder"-mechanism, triggered convection by forced ascent or blocking and diurnally forced convection.
The smooth forced ascent, which is the classic view of orographic precipitation, is described by a moist airflow ascending on the windward side of the mountain (Figure 3(a)). The airflow cools adiabatically, resulting in condensation and precipitation. On the leeside of the mountain range, rainfall is usually lower due to descending and additional evaporation of cloud and rain droplets in the prevailing airflow. The leeside of an orographic barrier is often denoted as rain shadow. According to Smith (1979) and Smith and Barstad (2004), this mechanism is a good description of the precipitation distribution for wide mountain ranges (about 100 km).
A parameter used to characterize the flow over mountains is the dimensionless mountain height $\hat{h}$ = hN/U, where U is the wind speed component normal to the mountain, N the Brunt-Väisälä frequency (stability parameter) and h is the mountain height. If the dimensionless mountain height is below $\hat{h}_{crit} = 1.6 \pm 0.1$ (Smith and Grønås (1993)), it is assumed that the particles have sufficient energy to flow over the mountain. For standard stability, N=0.01 s^{-1} and mountain height h$\sim$1000 m (approximately the most elevated point in the measurement area), U needs to be larger than 6-7 m/s to avoid blocking. For Southern Norway overall, the mountain height is approximately 1500 m, and the corresponding numbers are 9-10 m/s. Airflows which hit the coast of Norway during a low pressure system will typically have wind speeds above the mentioned values, and therefore the airflow is assumed to be blocked to a small extent. The measurement area is therefore to a large extent believed to experience smooth forced ascent during frontal passages. For more narrow mountains, the classic view of the concept of forced ascent may differ. Smith (1979) pointed out that the time between ascent on the windward side and descent on the leeside may be shorter than hydrometeor formation. The linear model of orographic precipitation of Smith and Barstad (2004), which included key parameters of orographic precipitation as airflow dynamics, cloud time scales and advection, and downslope evaporation, indicated that as the mountain width decreases, the location of the maximum precipitation shifts from the windward slope to the hilltop.

An enhancement mechanism of orographic precipitation is the "seeder-feeder" mechanism (e.g Bergeron (1965)), which is visualized in Figure 3(b). The mechanism was proposed to explain the enhancement of precipitation over low-level orography that was too small to generate precipitation themselves because air passes too quickly for hydrometeor formation. A large-scale precipitation cloud at upper levels, the "seeder", is assumed to be precipitating with no influence from the orography below. The "feeder"-

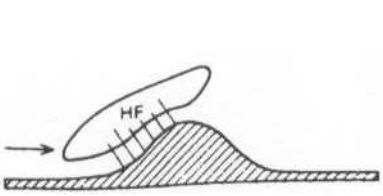

(a) Smooth forced ascent.

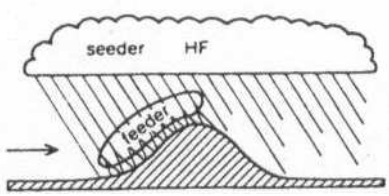

(b) Seeder feeder mechanism.

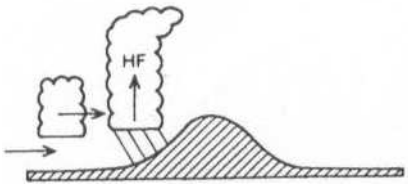

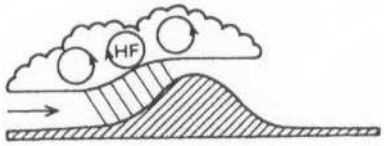

(c) Triggering penetrative or shallow convection.

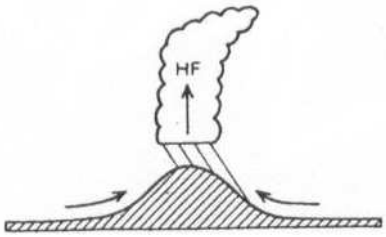

(d) Diurnal convection.

Figure 3: *Four idealized mechanisms for orographic precipitation. HF = hydrometeor formation. Illustrations from Smith (1989).*

cloud is assumed to be caused by low level ascent over the hill. The falling hydrometeors from the seeder cloud collect cloud droplets and additional moisture when falling through the feeder cloud, by coalescence and riming, and enhanced precipitation over the hill is achieved. In practice, the seeder, which might be influenced by the terrain and feeder cloud, may be combined to one cloud, and the pure seeder-feeder mechanism is therefore an idealization.

Another mechanism of the atmospheric response to orography is that forced lifting can trigger instability (Figure 3(c)). The existence of convection adds additional complexity to orographic precipitation. If an air parcel is instable due to vertical disturbances, forced lifting may trigger convection and thus condensation and hydrometeor formation. Smith (1982) introduced a theory concerning blocking and differential advection causing fronts to overturn, triggering conditional instability in stratiform layers.

The fourth mechanism described by Smith (1989) is diurnally forced convection, which is a regular and predictable type of orographic precipitation that occurs in warm seasons over mountainous regions. The daily heating of the sun-facing slopes generates warm upslope winds, which can trigger deep convection (Figure 3(d)). Precipitation in the

afternoon, often afternoon thunderstorm in the summer, is produced over the peaks or downwind if there is a cloud drift. Convective induced precipitation events have been observed in the Matre-campaign, and a convective situation is discussed in section 9.2.

In addition to these four basic mechanisms, Mass (1981) pointed out that an atmospheric flow which has split around a mountain may experience a convergence zone in the lee of the range, where ascents and often precipitation occurs. Yet another mechanism is costal convergence, which is caused by the difference in friction between land and ocean. This may result in ascending motion and precipitation, and needs to be taken into consideration as a possible precipitation mechanism for the Matre area.
Spillover denotes the amount of orographic precipitation that reaches the lee slope of a mountain range. In a study of Sinclair et al. (1997) concerning the distribution of precipitation in the Southern Alps of New Zealand, the spillover was found to increase with wind speed and decrease with increasing static stability. From a spillover factor, a measure of leeside precipitation to the total precipitation, utilized by Jiang and Smith (2003), it followed that spillover was dependent on advection-, fallout- and sublimation time. From the factor, spillover was found increasing with fallout time and decreasing with advection time, and the spillover was small for a wide mountain and larger for a narrow mountain. Local spillover effects might be present in the Matre-area.

2.3 Previous studies on precipitation in Western Norway

Several studies concerning precipitation in Western Norway have been performed. An overview of some of them, concerning the area of interest, is given in the following. Several studies on precipitation in Southern Norway for different synoptically situations, are described in Spinnangr (1943a), Spinnangr (1943b), Spinnangr and Johansen (1954) and Spinnangr and Johansen (1955). A maximum zone of precipitation about 30-50 km inland of the western coast of Southern Norway was found in the investigation of air currents passing from a westerly (SW,W,NW) direction (the westernmost part of the measurement area in the Matre campaign is located about 40 km from the coast). The orography in Southern Norway was shown to have a distinct influence on the distribution of precipitation, and a southwesterly wind direction gave an especially large precipitation amount in Western Norway. The maximum zone was found to have the smallest distance to the coast where the coast mountains were highest, and eastward of this maximum zone the precipitation decreased inward and upward to the head watershed between Western and Eastern Norway. In Spinnangr and Johansen (1955), the decrease of precipitation amount from the maximum zone to the head watershed is believed to be caused by the showers having emptied their content of water when passing the middle districts. The formation of new showers will be hampered because the supply of moisture from below is cut off over land as compared with the sea surface.

According to Andersen (1973), H. Johansen introduced a synoptic weather type classification particularly for West-Norwegian conditions. The classification is based upon the 24-hourly 1000 hPa gradient wind field over Western Norway, and the weather

types are defined by the eight main wind directions plus a class of variable direction. The wind fields are divided into 'cyclonic' and 'anticyclonic'. Andersen (1973) studied monthly precipitation distribution for Southern Norway with the aid of the H. Johansen weather types. In a cyclonic S weather type, great amounts of precipitation were observed from Rogaland to Vestfold, and from Rogaland to around Sogn og Fjordane, with decreasing amount further north. As expected, large amount of precipitation is measured in Western Norway in a cyclonic weather type with SW or SSW wind. A westerly wind direction and cyclonic weather type gave the greatest amount of precipitation south of Stad. The results in Nordø and Hjortnæs (1966) showed a close relationship between the geostophic wind perpendicular to large-scale mountain ranges and precipitation on local, national and continental scales. Especially good was the correlation of westerly wind and precipitation in Norway. In Skaar (1976) an investigation concerning the climate condition and precipitation distribution of the Sognefjord region was made. 11 meteorological stations and 26 precipitation stations operated by The Norwegian Meteorological Institute were situated in the region. In addition, in the period from 1963-1966, about 100 temporary climatic stations were mounted. It is however important to indicate that no precipitation measurements were done inside the area studied in this master thesis. The nearest measurements were made somewhat south of Matre and north of the easternmost rain gauge in the Matre-campaign. In the years 1964-1966, a great year-to-year variation in amounts were found by Skaar (1976), but the distributions show relatively small variations in their configurations. Common for the years 1964-66 are the maximum zones situated about 20-30 km inland from the coast, one on each side of the Sognefjord. South of the fjord the amounts were found to decrease gradually from the western maximum, and 70-80 km from the coast, the amounts were reduced to about 1/3. On the northern side, the maximum zone had a greater west to east extension. The distribution of mean precipitation amounts in the period April - October 1964-66 is given in Figure 4. The red dots give the southern, northern, western and easternmost HOBO rain gauge location in the Matre-campaign. According to Skaar (1976), the distribution in Figure 4 has in broad outlines much in common with the traditional distribution of annual precipitation amounts. The driest areas were found in the lower parts of the valleys and in the eastern districts of the Sognefjord. However, the local distribution differs much from one valley to another. This variation was explained, not only from local topography and the geostrophic wind field, but also from a local wind field. Pursuant to Skaar (1976), fronts passing from a south-western direction, accordingly southern and south-western weather types, give the main part of the precipitation in this region. However, in late spring and summer, elements of north-western weather types were often present, and unstable air masses could give a greater contribution of convective precipitation. The distribution of convective precipitation was often separated in different local maxima and minima, moreover, the eastern districts got relatively greater precipitation totals. For Western Norway, Førland (1979) showed that normal annual precipitation (for the period 1931-1960) increases with about 50 mm/km from the coast to about 45 km from the coast, and from 45 km to 70 km from the coast the precipitation decreased with 30 mm/km.

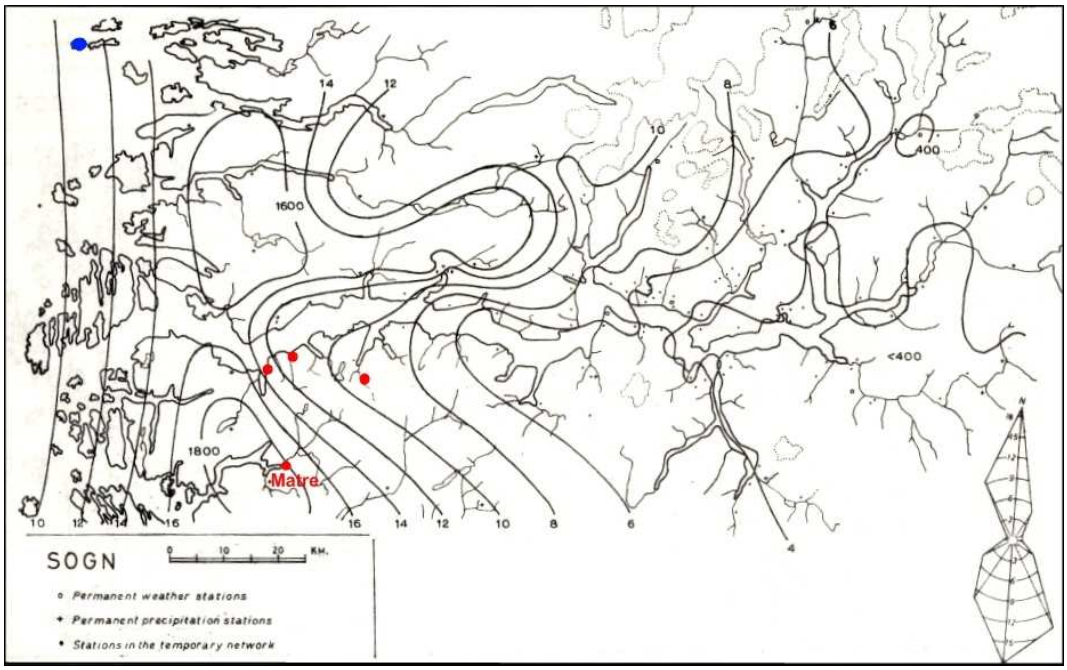

Figure 4: *Distribution of mean precipitation amounts for April-October, 1964-66. Inserted distribution of corresponding wind frequencies, in percent, at Kinn (blue dot). Red dots give the outermost HOBO rain gauge locations in N,S,W and E directions. Figure from Skaar (1976).*

For Norway, various investigations of the precipitation gradient with height have been performed. For the Fillefjell-area, Sælthun (1972) found the increase in precipitation amount about 1000 meter above see level to be approximately 5.0 % / 100 m. For measurements done at three locations at Hardangervidda, Skartveit (1976) found from July to September 1969-1972 that the average seasonal precipitation increased with approximately 8.0 % / 100 m. Førland (1979) studied the precipitation height dependence several places, among them, Vestlandet. A positive vertical gradient below 150-300 m a.s.l is found, while for higher altitudes the trend is more or less contrary, the precipitation amounts decrease with increasing altitude. Førland did not conclude that precipitation amounts do not increase with increasing altitude above 300 meters, and emphasized that potential precipitation amounts are decreasing while the air masses are transported from the coast and inwards, and that this must be taken into consideration. Another suggested and possible reason is the negative wind influence on gauge catch high above sea level. This is also present in Førland (1984), where the highest mounted station experienced smaller amounts of precipitation than the close by mounted stations at a lower altitude, which is believed to be due to stronger wind at the stations highest above sea level.

3 Instrumentation

This chapter gives an overview of the instruments used in this master project. A description of the calibration of HOBO rain gauges is also addressed in this chapter.

3.1 HOBO RG2-M rain gauge

3.1.1 Specifications of the HOBO rain gauge

HOBO RG2-M data logging rain gauges have been used during the measurement periods to measure the precipitation in both the Matre area and in projects at the Geophysical Institute. The data logging rain gauge is a self-contained, battery-operated rainfall data collection and recording system (Figure 7). The rain gauge uses the tipping-bucket principle which consists of two connected buckets. When a bucket is full of water, the weight of the water makes it tip, causing the former to be emptied and putting the latter in collecting position. One tip of the bucket occurs for each 0.2 mm of rainfall. The corresponding time for each tip is recorded by the HOBO Event data logger, which is integrated within each rain gauge. The accuracy of precipitation amount measurement is given as ± 2.0 % by the manufacturer (Onset (2001)). To avoid debris getting into the funnel and clog the orifice, a protective grid is mounted rigidly at the top of the rain gauge. The HOBO rain gauges are not equipped with any kind of heating or antifreeze solution, and do not possess any windshield.

3.1.2 Description of the calibration of the HOBO rain gauges

Calibration of the HOBO rain gauges is performed using the method described in the manual (Onset (2001)), and summarized in short here. For calibration, the rain gauges were mounted in a level position. A water container with a very small hole in the bottom is placed in the top funnel of the rain gauge with the hole not over the orifice. The water container is filled with exactly 373 ml of water that should drop into the gauge in not less than one hour. It is important that the rain gauges are calibrated with a controlled rate of flow of water through the tipping-bucket mechanism, and it should take at least 36 seconds to fill one side of the tipping bucket. This represents a maximum precipitation intensity of 20 mm/hour. Decreasing the rate of flow will not affect the calibration. If the flow rate in the calibration is increased, a properly calibrated instrument will read too low values. The reason for this is that some time is required for the bucket filled with water to tip. During the first 50 % of the tipping time, water continues to flow into the filled bucket. For the remaining last 50 % of the tipping time, the water flows into the empty bucket. The amount of water flowing during the first 50 % of the tipping time represents an error, the faster the flow, the greater the error. When the flow rate is 20 mm/hr or less, the water drips into the bucket instead of flowing. Under this condition no water is added to the already full moving bucket.

A calibration performed as described should result in 100±2 tips. If the number of tips is outside this interval, the screws located on the bottom outside the rain gauge housing should be adjusted to increase or decrease the number of tips. There are two screws which should be adjusted equally. Turning the screws clockwise (counterclockwise) increases (decreases) the number of tips per measured amount of water. A 1/4 turn on both screws will increase or decrease the number of tips by approximately one tip.

3.2 Automatic weather station

Automatic weather stations from Aanderaa Data Instruments (AADI) have been used to measure meteorological parameters during the field campaigns. The stations are battery-powered and the data were stored on-site in a removable data storage unit. The stations were equipped with sensors for temperature, relative humidity, wind speed, wind gust and wind direction. The sampling interval during the campaigns has been set to 10 minutes. Figure 5 shows the automatic weather station at Blåfjell in the MHS.

3.3 SIAP rain gauge

The precipitation sensor SIAP UM7525R is maintained by BKK and situated at the power station area at Stordal. This rain gauge will be compared to the HOBO rain gauges at this location. The SIAP rain gauge, like the HOBO rain gauges, uses a tipping-bucket principle and enables a resolution of 0.2 mm. The accuracy given by the manufacturer is ±0.2 mm for rain rates < 5 mm/h, and ±2.0 % for rain rates > 5 mm/h (SIAP (2001)). In the SIAP rain gauge, a heater with a thermostat is integrated in the tipping buckets assembly, and the rain gauge is therefore able to monitor solid precipitation. The rain gauge is protected by a wind shield. Data from the SIAP rain gauge enable a resolution of 1 h. Figure 8 shows the SIAP rain gauge located at Stordal power station.

3.4 Manual precipitation measurements

The official precipitation registrations performed by the Norwegian Meteorological Institute (DNMI) at the station Bergen-Florida are measured manually. The precipitation is collected in a water collector and read off in a graduated glass. Precipitation as snow gets melted before registration. The collector is protected by a low funnel-shaped wind shield, and the mounting height of the manual water collector is approximately 180 cm. The measurements enable a resolution of 0.1 mm. Precipitation measured by DNMI at the station Bergen-Florida are compared with HOBO rain gauges in section 4.3. Figure 6 shows the manual rain gauge.

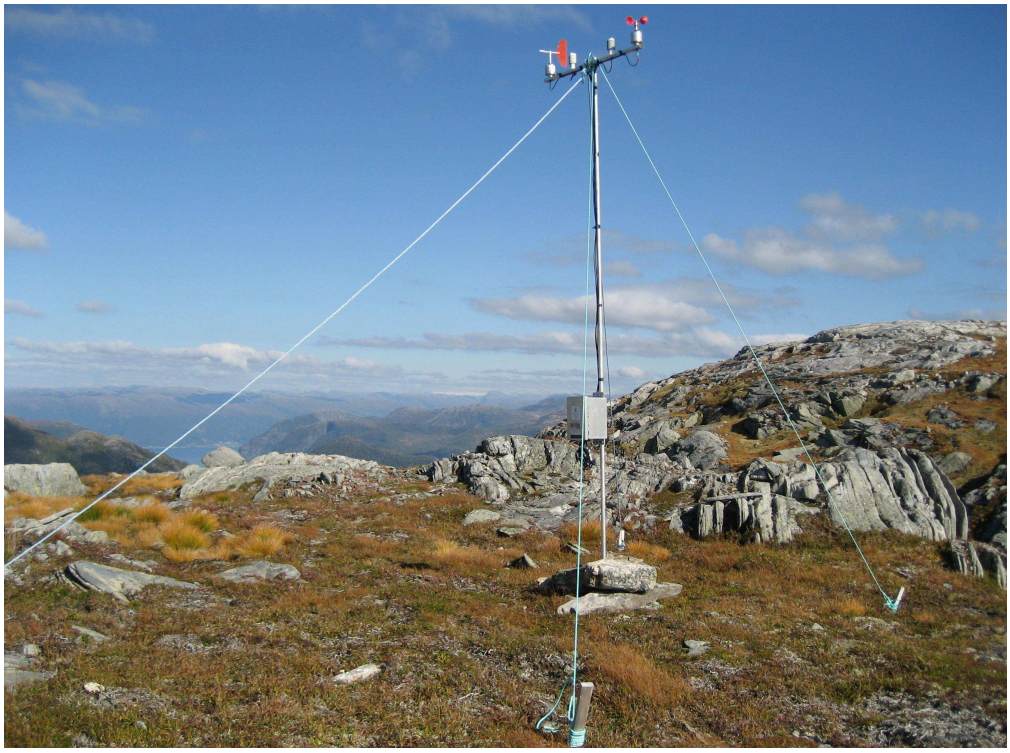

Figure 5: *Automatic weather station at Blåfjell. View towards northwest.*

Figure 6: *Manual rain gauge maintained by DNMI at Bergen-Florida.*

Figure 7: *HOBO RG2 data logging rain gauge.*

Figure 8: *SIAP rain gauge situated at the power station area at Stordal.*

4 Field and laboratory tests of the HOBO rain gauges

The data logging rain gauges HOBO RG2-M are widely used in scientific projects at the Geophysical Institute. It is therefore important to know the accuracy and variability of the rain gauges and how well the rain gauges coincide with the official precipitation measurement. These topics are discussed in section 4.2 and 4.3, respectively. Rain gauges used in field campaigns are usually unattended. Even under regular supervision and adjustment of the equipment, it may get out of the leveled position. Errors from this source have generally been assumed to be negligible, because levelness is often taken for granted. To investigate the potential effect of non-level mounting on the sampling efficiency of HOBO rain gauges, corresponding laboratory tests have been performed. Laboratory experiments concerning this subject are discussed in section 4.1.

4.1 Laboratory experiments with HOBO rain gauges out of level

4.1.1 Description

Two similar experiments were performed in May and July 2008. In the first experiment, two data logging HOBO rain gauges were used (serial numbers 20857 and 20806). In the second experiment, only one rain gauge was used (serial number 20859). The rain gauges were mounted on a board with an adjustable tilt angle, see Figure 9. A water container with an adjustable outlet was placed above each rain gauge. The water container was filled with 373 ml of water, which, according to Onset (2001), is the amount of water recommended for calibration of the HOBO rain gauges. The outlet in the water container was adjusted in accordance with the recommendation given by the supplier, as described in section 3.1.2.

The experiments were made for three different orientations of the tipping bucket with respect to the tilting angle of the board, see Figure 10. In the first experiment, four different tilting angles between 0.9° and 6.6° were utilized. In the second experiment, six different tilting angles between 0.5° and 5.5° were applied. The HOBO rain gauges were horizontally mounted (tilting device=0°) before and after the sequence of angles to compare the results. In addition rain gauge 20859 was, before the second experiment, tested ten times horizontally mounted to investigate the stability of the results.

4.1.2 Results

Rain gauge 20857 was calibrated and adjusted before this experiment. Rain gauge 20806 was tested and it showed a satisfactory value, and was therefore not adjusted. In spite of this, rain gauge 20806 showed a reduced number of tips in this experiment. Rain gauge 20859 was not calibrated, and also showed a reduced number of tips. However, this is not affecting this laboratory study because the result is based on the relative

Figure 9: *Laboratory setup for the test of non-level mounting on the sampling efficiency of HOBO rain gauges.*

	Serial number 20859
Angle [°]	# tips
0	96
0	96
0	96
0	90 [1]
0	95
0	94
0	94
0	93
0	93
0	94

Table 1: *Results from rain gauge 20859 horizontally mounted.*

deviation from the number of 0°-tips for each particular rain gauge.

Table 1 shows the result from the test with rain gauge 20859 when the variability was addressed. The mean value of the 0° tips is 94.6±1.7, or ± 1.8 %. To get a larger data

[1] In this episode the locking mechanism in the water container did not work properly, and the water ran out of the container in only 21 minutes. Because of this, the episode is left out of the calculations.

(a) Tipping bucket parallell to the board

(b) Tipping bucket perpendicular to the board

(c) Tipping bucket 45° to the board

Figure 10: *Orientations of the tipping bucket in the rain gauge with respect to the board.*

basis, the datas of the 0°-tips from experiment 2, presented in Table 2, are included in this calculation (also rain gauge 20859). According to the HOBO manual, the accuracy for the HOBO rain gauges is ±2 % (Onset (2001)), and our result is within this specification.

Table 2 shows the result from experiment 2 (experiment 1 is considered afterwards). As already stated, the mean value from the tips in Table 1 together with the 0° tips in experiment 2 is 94.6 ± 1.7. According to basic statistics, if the measured values are assumed normally distributed, there is a probability of 68.3 % that the measured values are less than one standard deviation away from the mean value. The probability is 95.4 % when considering two standard deviations. The value for 5.5° for the parallel case in experiment 2 is more than two standard deviations away from the mean value, and indicates therefore a weak tendency for the rain gauge to measure smaller amounts of water with increasing tilt angle. In the case where the tipping bucket is perpendicular to the board, a larger number of tips are seen for the highest tilt angles, with the largest value for 3.5°. In the other case where the tipping bucket is 45° to the board, there is no clear effect of non-level mounting on the sampling efficiency.

The results from experiment 1 are shown in Table 3. For rain gauge 20857 the mean value of the 0° tips for the parallel case is 97.2 ± 4.2. The corresponding mean value for rain gauge 20806 is 92.3 ± 2.4. The tendency seen for the perpendicular case in experiment 2 does not exist in experiment 1, and is therefore believed to occur by chance. Inaccurate amount of water in the water container in experiment 1 may also be an explanation. For both rain gauges 20857 and 20806, the number of tips decreases with increasing tilt angle for the parallel case. For rain gauge 20857 the number of tips when the tilt angle is 6.3° is more than two standard deviations away from the mean value. For rain gauge 20806 the corresponding number of tips is more than four standard deviations away from the mean value. In this experiment, only cases where the tipping bucket is parallel to the tilting device seem to be affected.

Angle[°]	*Ori.*	Serial number 20859 # tips	% of 0°-average
0		93	-
0.5		92	97.3%
1.5	a)	92	97.3%
2.5		91	96.2%
3.5		91	96.2%
4.5		91	96.2%
5.5		89	94.1%
0		92	-
0		94	-
0.5		94	99.4%
1.5	b)	97	102.5%
2.5		97	102.5%
3.5		101	106.8%
4.5		98	103.6%
5.5		98	103.6%
0		98	-
0		97	-
0.5		98	103.6%
1.5	c)	97	102.5%
2.5		95	100.4%
3.5		97	102.5%
4.5		94	99.4%
5.5		95	100.4%
0		94	-

Table 2: *Experiment 2. The orientation is indicated in column two, where a),b) and c) is analogous to Figure 10.*

The investigations in this section show a tendency of undersampling with increasing angle when the tipping bucket in the rain gauge is parallel to the board. According to Table 3, the maximum underestimation is around 10 % for a the tilt angle of 6.6°.

The ideal test conditions in a laboratory are difficult to achieve outdoors. The laboratory tests described in this section are therefore corresponding to calm condition in the field (vertical rainfall). The sampling efficiency of the rain gauge is also being influenced by the pickup area of the gauge. In calm conditions, this varies pursuant to the tilt angle, and increasing tilt angle results in decreasing pickup area. The pickup area in calm conditions is elliptical, and equal to $\pi r^2 \cos\alpha$, where r is the radius of the rain gauge for a tilt angle α (see Figure 11). This has not been taken into consideration in the laboratory test, where the water has been falling in a straight stream into the

Angle[°]	*Ori.*	Serial number 20857 # tips	% of 0°-average	Serial number 20806 # tips	% of 0°-average
0		103	-	96	-
0.9		102	104.9%	94	101.8%
1.4	a)	99	101.9%	91	99.6 %
3.3		96	97.7%	89	96.4 %
6.6		88	90.5%	81	87.8 %
0		99	-	94	-
0		100	-	92	-
0.9		97	99.8%	90	97.5%
1.4	b)	97	99.8%	90	97.5%
3.3		98	100.8%	88	95.3%
6.6		95	97.7%	90	97.5%
0		94	-	91	-
0		95	-	92	-
0.9		95	97.7%	90	97.5%
1.4	c)	96	98.8%	89	96.4%
3.3		97	99.8%	89	96.4%
6.6		94	96.7%	88	95.3%
0		92	-	89	-

Table 3: *Experiment 1. The orientation is indicated in column two, where a),b) and c) is analogous to Figure 10.*

(a) Rain gauge tilted an angle α.

(b) Tilted rain gauge seen from above with radius r.

Figure 11: *Tilted rain gauge with radius r and angle α.*

rain gauges. In the presence of wind during field deployment, the sampling efficiency is in addition affected by the wind direction and the orientation of the oblique rain gauge. If the rain gauge is tilted towards the main wind direction, the sampling efficiency will be higher compared to a tilt of the rain gauge to the opposite site. From calculations, Rinehart (1983) showed that instruments that are out of level by 2° in the presence of winds of 10 m/s can produce errors in the order of 9 %. To determine the possible extent of this source of error, Rinehart (1983) examined 19 gauges for levelness. The overall average tilt was 2.3°. A correction of out-of-level errors is a difficult task and the complete wind and precipitation data records would be necessary in each case. Efforts to eliminate out-of-levelness as a problem would be worthwhile. Other conditions influencing rain gauge measurements will be described in section 5.1.

4.2 Variability of the HOBO rain gauges

4.2.1 Description

To test the variability of the data logging rain gauges HOBO RG2-M, 12 instruments have been operated in parallel during a two month intercomparison campaign from January to March 2008. The rain gauges were placed outdoors at the Geophysical Institute, inside the measurement field of DNMI at the station Bergen-Florida. The setup of the rain gauges is shown in Figure 12(a) and 12(b). The HOBO rain gauges were located close to each other to obtain as similar conditions as possible. The height of the rain gauges was 180 cm above ground. Measurements of wind direction, wind speed and temperature were performed by an automatic weather station of Aanderaa Data Instruments situated next to the HOBO rain gauges. These data enable a 10 minutes resolution. Wind direction was measured 4.05 meters above ground level, wind speed was measured both 4.05 meters and 2.25 meters and temperature was measured 2.25 meters above ground level.

4.2.2 Results

One rain gauge (serial number 20840) had trouble with the data logging unit, and only one month of data became available from this rain gauge. This rain gauge is therefore omitted from the evaluation.

In this section, the total amount of registered precipitation is considered, regardless of type of precipitation. The total amount of precipitation during the comparison campaign for each rain gauge is shown in Figure 13. One rain gauge (serial number 20548) measured considerably smaller amounts compared to the other rain gauges. Due to this, data from this rain gauge have been removed from the calculations. Rain gauge 20547 showed unstable behavior during calibration after the measurement period, and has therefore also been removed from further evaluation. These rain gauges were neither used in the Matre-campaign. The mean value of the remaining nine rain gauges is 755.0 mm with a standard deviation of 23.8 mm. Therefore, the total precipitation amount

(a)

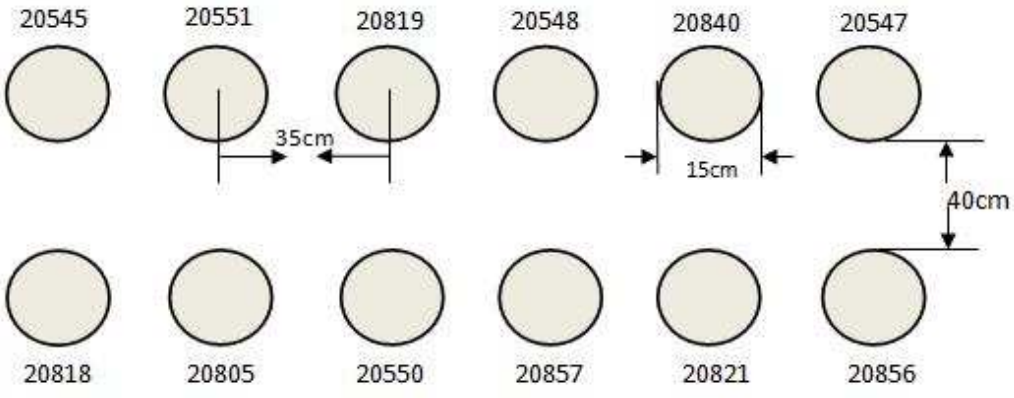

(b)

Figure 12: *Setup of the 12 HOBO rain gauges inside the metering panel of DNMI at the station Bergen-Florida.*

measured by these rain gauges coincides within ±3.2 %. Because of the somewhat large variability between the measured precipitation amounts, the rain gauges in the field have been checked for wind direction-dependence. The dominating wind direction during the measurement period was southerly and southeasterly, but also components of westerly wind were present. No clear pattern in precipitation amount with respect to the mounting position of the gauges was discovered.

The rain gauges used in this experiment have also been used in several other field campaigns. With the exception of the calibration performed by the manufacturer when the

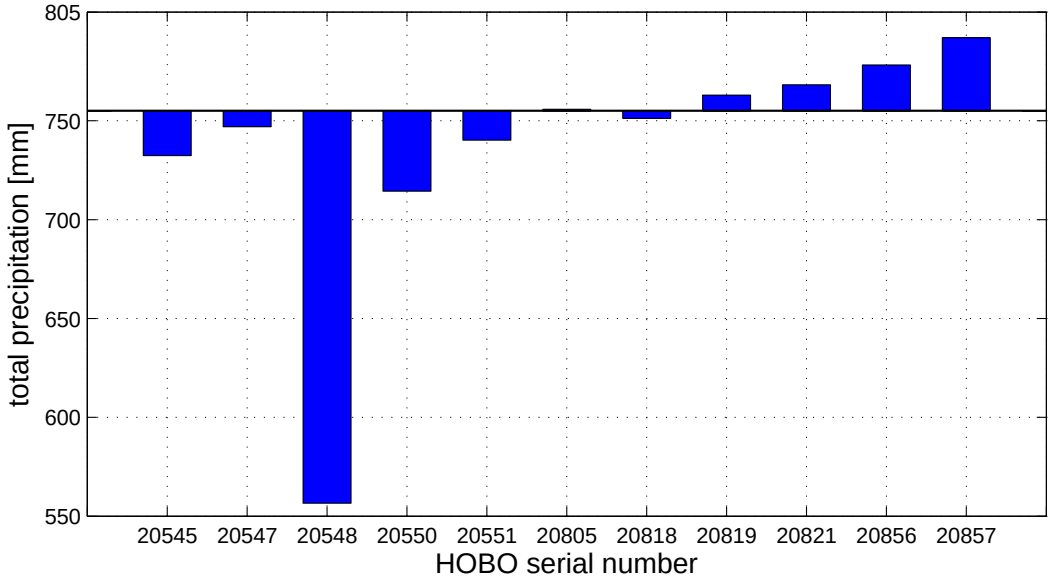

Figure 13: *Total precipitation amount during the field experiment. The precipitation amount for each rain gauge is plotted with starting point at the mean value for the rain gauges. Rain gauge 20547 and 20548 is not included in the calculation of the mean value.*

rain gauges were new, the rain gauges have not been calibrated. These rain gauges were, after the measurement period at the station Bergen-Florida, calibrated in a laboratory in accordance with the description given in section 3.1.2. The calibration was performed in April 2008. Table 4 gives an overview of the number of tips for each rain gauge achieved in this calibration. Each rain gauge was only tested once, and set to 'ok' if the number of tips were in the interval 98 to 102. If the number of tips was outside this interval, the screws located on the outside of the rain gauge housing were adjusted

HOBO serial number	# tips after lab.test	Correction factor
20545	92	1.087
20550	91	1.099
20551	96	1.042
20805	97	1.031
20818	97	1.031
20819	100	1.000
20821	99	1.010
20856	97	1.031
20857	99	1.010

Table 4: *Overview of the calibration performed in April 2008.*

until the number of tips was inside the desired interval. Since the rain gauges have been used several times before this field campaign, the calibration done by the manufacturer is no longer assumed to be valid. The correction factor for the presented intercomparison is calculated as 100 divided by the number of tips from the April 2008-calibration for each rain gauge. The original raindata from each gauge have in the following been multiplied by the corresponding correction factor in Table 4. Figure 14 shows both the corrected and uncorrected total amount of precipitation during the measurement campaign. The mean value of accumulated precipitation after correction is 783.0 mm with a standard deviation of 13.7 mm. The corrected total precipitation amount coincides within ±1.8 %.

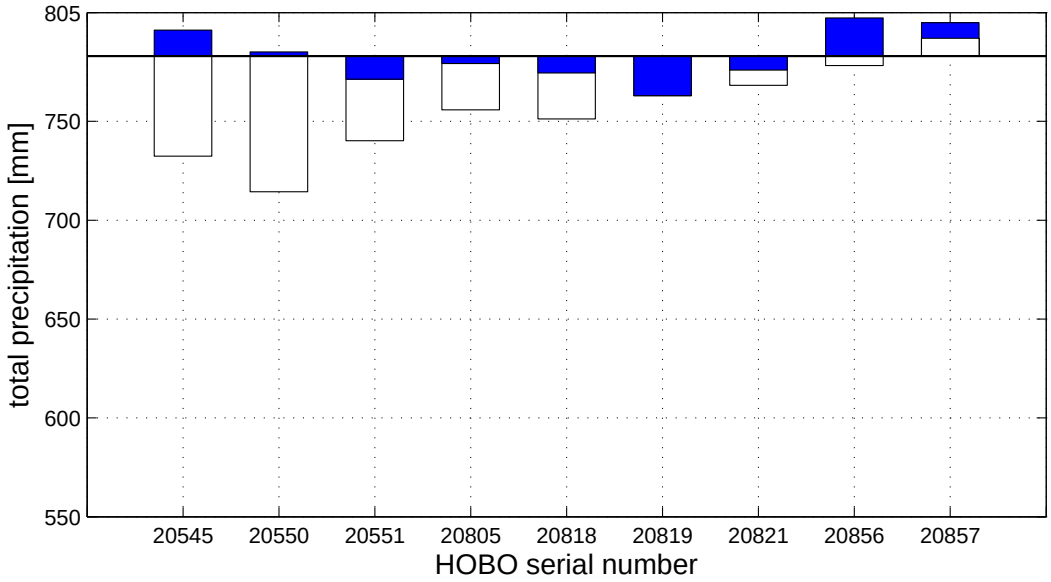

Figure 14: *The total precipitation amount for each rain gauge is plotted with a starting point at the mean value for the corrected rain gauges. The blue bars indicate the corrected values in accordance with the calibration performed in April 2008 just after the intercomparison. The white bars indicate the precipitation amounts before correction.*

4.3 Comparison: HOBO rain gauges and official precipitation registration

4.3.1 Description

The rain gauges discussed in the previous section have during the measurement period been operated a few meters away from the official precipitation registration performed by DNMI at the station Bergen-Florida. The calculations in this section are based on data from DNMI and the corrected data from the mentioned nine HOBO rain gauges from the previous section. For the purpose of comparison, the HOBO rain gauges were placed at the same height, 180 cm above ground level, as the measurements by DNMI. Temperature measurements are made close to the HOBO rain gauges by an air temperature sensor of Aanderaa Data Instruments. By daily precipitation sums of the HOBO rain gauges in this section, is meant the average over all nine HOBO rain gauges for the reference time interval 06 UTC - 06 UTC. 24 h precipitation sums assigned e.g. 14th of January have arrived between 06 UTC 13th of January to 06 UTC 14th of January.

4.3.2 Results

An overview of the measured precipitation and temperature during the measurement period is given in Figures 15(a) and 15(b). The official precipitation registrations for Bergen-Florida are included by way of the red crosses in Figure 15(a). As seen in the last-mentioned figures, there have been periods with both temperatures below 0 °C and precipitation at the same time. Figure 15(c) shows the ratio between the daily precipitation sums observed by DNMI and the HOBO rain gauges for precipitation values greater than 0.4 mm/24h. Compared to the measurements done by DNMI, the mean value of the accumulated precipitation for the HOBO rain gauges during the entire period is underestimated by 2.6 %. The corresponding number for the HOBO rain gauge which measured the maximum and minimum amount of precipitation is 0.2 % and 5.1 %, respectively. In similar comparisons reported by Reuder et al. (2007), two HOBO rain gauges were operating in parallel to the measurements of DNMI in May and June 2007. The rain gauges underestimate monthly integrated precipitation by 2 % (June) to 6 % (May). In this study the most probable cause for the underestimation of the HOBO rain gauges was the evaporation loss and splash out due to the protective grid of the rain gauges. However, as seen from the previous section, underestimation of the rain gauges due to absent calibration may also be of significance.

During the measurement period some of the precipitation was snow, sleet or hail, rather than rain. Since the HOBO rain gauges do not have a heating mechanism, the solid precipitation became accumulated at the top of the rain gauge and did not get registered before it melted. However, some of the solid precipitation which will be accumulated at the top of the HOBO rain gauges in cold periods, may be blown away from the rain gauges or evaporate. Hail may experience outsplashing due to the protective grid. In a study described by Førland and Bjørbæk (1979) the evaporation from open snow

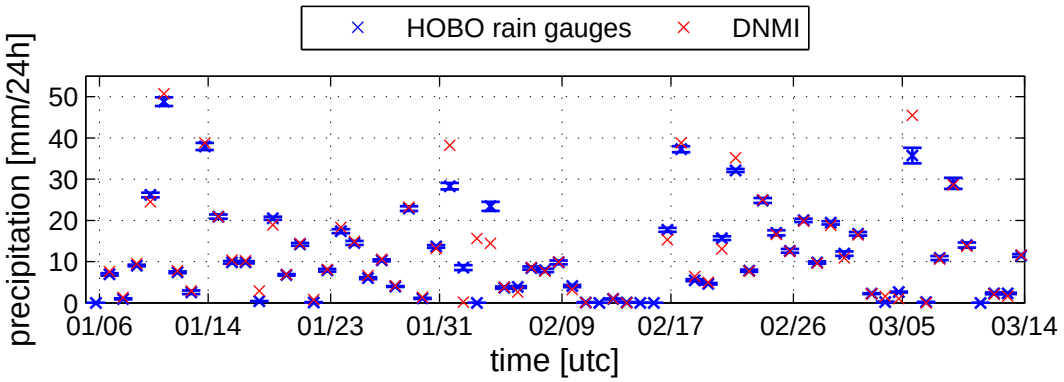

(a) The blue crosses give the 24 h mean value of the HOBO rain gauges with corresponding standard deviation. The red crosses give the 24 h precipitation measured by DNMI.

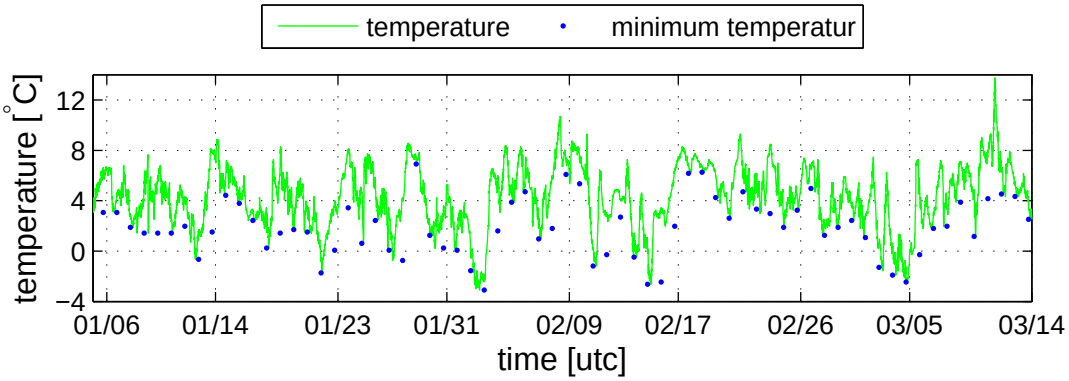

(b) The solid green line indicates the temperature measured by the weather station, while the blue dots give the minimum temperature during the 24 h period.

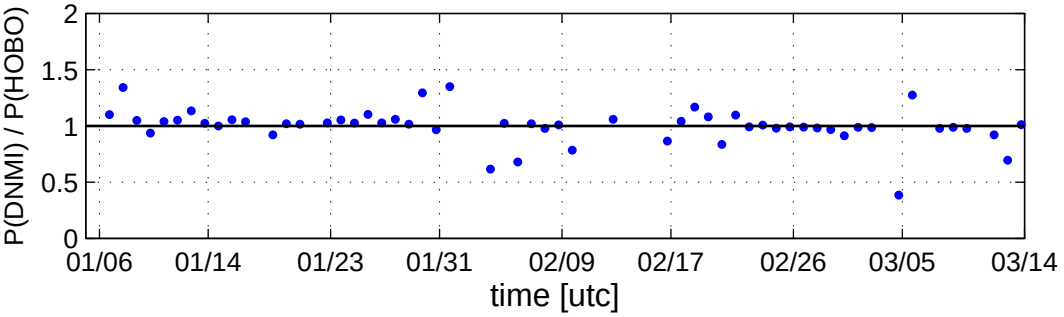

(c) Ratio between the 24 h precipitation observed at DNMI and the 24 h mean value of the HOBO rain gauges for precipitation values greater than 0.4 mm. Values above one indicate larger amounts of precipitation at DNMI compared to the HOBO rain gauges.

Figure 15: *An overview over precipitation measured by the HOBO rain gauges and the official precipitation registrations at Bergen-Florida and temperature measured by the Aanderaa weather station in the period from 6th of Januray to 14th of March 2008.*

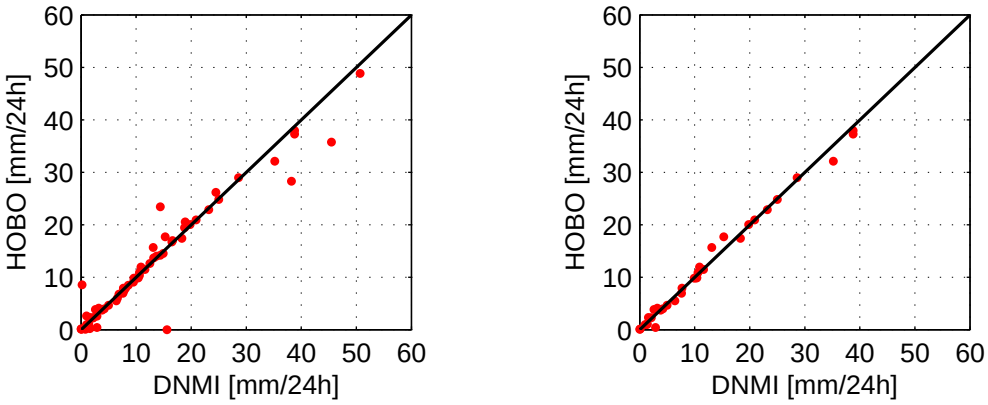

(a) All precipitation events.

(b) Events when there is not registered precipitation as snow, sleet or hail.

Figure 16: *Relationship between 24 h precipitaion at DNMI and the HOBO rain gauges for events with and without snow, sleet and hail.*

gauges was above 1.0 mm/24 h in over 50 % of the cases. Evaporation of accumulated snow will however not be addressed in this study. Both snow blowing away and evaporation of snow, sleet or hail from the top of the rain gauges lead to underestimation of the precipitation measured by the HOBO rain gauges. Therefore, based on information concerning the type of precipitation registered by DNMI, days with snow, sleet and hail registrations have been removed from the dataset. The relationship between DNMI and the HOBO rain gauges for days without solid precipitation is shown in Figure 16(b). Figure 16(a) shows all precipitation events regardless of type of precipitation. For the precipitation events when only rain is registered, the HOBO rain gauges are in average underestimating precipitation compared to the official registration by only 0.9 %.

Another error source that may influence the measurements is the wind. The HOBO rain gauges do not have any kind of wind shield, whereas the water collector maintained by DNMI is equipped with a funnel-shaped wind shield. This may cause a deficit in catch for the HOBO rain gauges. Figure 17 shows a histogram of the average hourly wind speed distribution at 4.05 meters above ground level (The wind speed measurement at 2.25 m contained missing data). The average hourly wind speed during the period is quite low, with the greater part of the values below 3.0 m/s and no values above 4.5 m/s. The HOBO rain gauges were in this experiment placed 180 cm above ground level, and therefore even lower wind speed values are expected here. Underestimation due to wind is therefore considered small in this experiment. However, the error source that the wind represents is always present in not calm conditions, and placing the HOBO rain gauges in a lower position could result in a less deficit in catch.

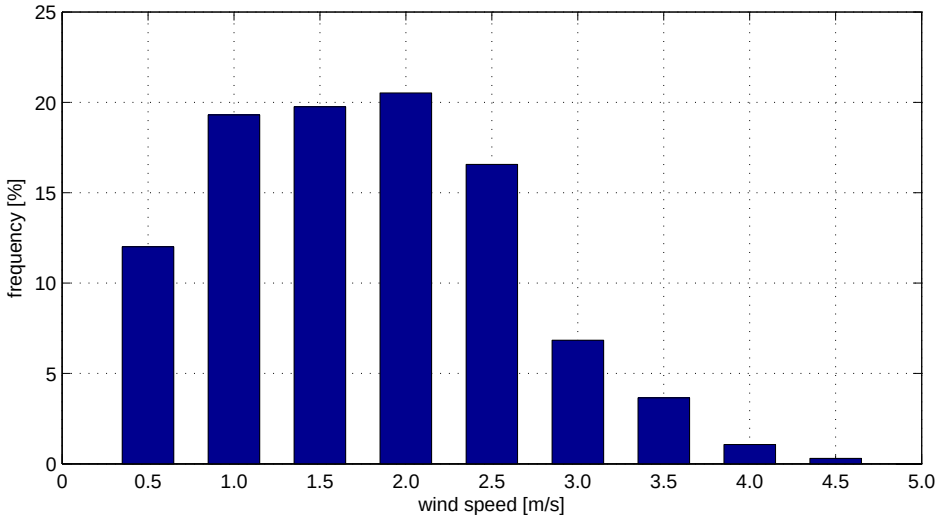

Figure 17: *Average hourly wind speed during the measurement period. Measurement height: 4.05 meter. Each bar represents wind speeds below the value given at the specific bar and above or equal to the former bar.*

4.4 Performed calibration of the HOBO rain gauges

Calibration of the rain gauges is important to achieve a result that is as accurate and certain as possible. This section gives an overview of the calibration done in connection with the experiments described in section 4.2 and 4.3, and the calibration of the HOBO rain gauges in connection with the Matre-project.

The HOBO rain gauges were, as described in section 4.2, calibrated in April 2008. At this time the rain gauges were tested only once, and the number of corresponding tips was presented in Table 4, section 4.2. If the calibration measurement showed less than 98 tips or more than 102 tips, the screws outside the rain gauge housing were adjusted until the number of tips was inside the desired interval. The number of tips after the adjustments performed in April 2008 is given in the second column of Table 5. The Matre campaign started in late April 2008, and lasted until late October 2008. All the rain gauges used in the Matre-project were once again calibrated in the laboratory after the measurement period. This calibration took place in January 2009, and each rain gauge was tested between three and six times. An overview of the number of tips achieved for each rain gauge during this calibration is given in Table 5. The rain gauges in the Matre-project with serial numbers starting with 21(xxx) were new before mounted in the field. New rain gauges are calibrated and adjusted by the manufacturer, and therefore assumed to be in the 100±2 tip range. Table 5 shows that some rain gauges have changed sensitivity compared to the calibration results of April 2008. A correction factor has been calculated for the rain gauges used in the Matre area. When calculating this correction factor, the number of tips after the adjustment in April 2008 is assumed to be 100. The same assumption is made for the new rain gauges with serial

numbers 21xxx calibrated by the manufacturer. The correction factor before the Matre campaign is ergo equal to 1. The correction factor in the last column of Table 5 has been determined by

$$\frac{1+\frac{100}{k}}{2}, \tag{4}$$

where k is the mean value of the number of tips for each particular rain gauge from the January 2009 calibration. This means that we assume a gradual linear change in sensitivity of the HOBO rain gauges with time. All data from the Matre-project have been multiplied by this correction factor.

The average number of tips from the January 2009 calibration is 97.3±3.4. After the adjustments performed in April 2008, the average number of tips was 100±2.0. This may indicate that the HOBO rain gauges, when situated in the field, gradually underestimate true precipitation. The repeated laboratory tests indicate an uncertainty of approximately ±4% for the HOBO rain gauges, which is used to describe the instrumental uncertainty when analysing the data from the Matre campaign. Other factors influencing the accuracy of precipitation measurements in the field are described in section 5.1.

HOBO	April 2008				January	2009				Correction
serial no.	Tested/not tested	# tips	# tips	# tips	# tips	# tips	# tips	# tips	k	factor
20545 ◇	Tested - Adjusted	101	Defect						-	-
20550∗◇	Tested - Adjusted	102	100	98	100				99.33	1.003
20551∗◇	Tested - Adjusted	101	99	101	97				99.00	1.005
20805 ◇	Tested - Adjusted	101	96	95	94	93	94	94	94.33	-
20806 ∗	Tested - Not adjusted	98	94	95	94				94.33	1.030
20818∗◇	Tested - Adjusted	98	97	100	97	95	97	99	97.50	1.013
20819∗◇	Tested - Not adjusted	100	89	90	88				89.00	1.062
20821∗◇	Tested - Not adjusted	99	96	94	95				95.00	1.026
20840∗◇	Tested - Adjusted	102	101	99	102				100.67	0.997
20856∗◇	Tested - Adjusted	101	105	104	104				104.33	0.979
20857∗◇	Tested - Not adjusted	99	104	102	101				102.33	0.989
21008 ∗	New rain gauge		94	98	97	97			96.50	1.018
21058 ∗	New rain gauge		96	96	96	96	96		96.00	1.021
21059 ∗	New rain gauge		101	102	102	102	101		101.60	0.992
21072 ∗	New rain gauge		100	101	100	101	100	101	100.50	0.998
21073 ∗	New rain gauge		96	96	96	96	98		96.40	1.019
21074 ∗	New rain gauge		94	96	97	96	97	96	96.00	1.021
21075 ∗	New rain gauge		98	99	98	99			98.50	1.008
21076 ∗	New rain gauge		96	95	95	94	95		95.00	1.026
21077 ∗	New rain gauge		99	100	99	101	100	101	100.00	1.000
21078 ∗	New rain gauge		99	95	93	95	95	94	95.17	1.025
21079 ∗	New rain gauge		93	91	92	93			92.25	1.042

Table 5: *Result from the calibrations in April 2008 and January 2009. The calibration in April 2008 was done after the measurement described in section 4.2 and 4.3 and before the Matre-project. The number of tips in column two is the number of tips after adjustment in April 2008. The correction factor in the last column is given only for the rain gauges used in the Matre-project. ∗: Rain gauges used in the Matre-campaign. ◇: Rain gauges used in the experiment described in section 4.2 and 4.3.*

4.5 Summary of field and laboratory test concerning the HOBO rain gauges

The following main results have been derived from the different field and laboratory tests performed as part of this thesis:

- For HOBO rain gauges out of level, the instruments tend to underestimate precipitation with increasing angle when the tipping bucket in the rain gauge is oriented parallel to the board. The maximum underestimation observed was around 10 % for a tilt angle of 6.3°. In the other cases when the tipping bucket is oriented perpendicular or 45° to the board, there were no clear effects of non-level mounting on the sampling efficiency.

- The total precipitation amount of the nine HOBO rain gauges in parallel setup in the field coincides within ±3.2 %. The corresponding number for the rain gauges after correction in accordance with the calibration was ±1.8 %.

- When comparing the HOBO rain gauges to the official precipitation registration, the mean accumulated precipitation from the HOBO rain gauges was underestimated by 2.6% during the entire period from 6th of January to 14th of March.

- For the precipitation events without snow, sleet or hail, the HOBO rain gauges underestimated precipitation compared to the official registration by 0.9 %.

- The calibrations indicate that HOBO rain gauges situated in the field, gradually underestimate true precipitation.

The results of this study show that thorough calibration of the HOBO rain gauges is important. In similar measurement campaigns in the future, multiple calibration of the rain gauges should be done both immediately before and after the measurement period. Maybe even a portable field calibration unit should be considered for longer deployment periods.

5 Field campaign

5.1 Error sources regarding precipitation measurements

Measurements by precipitation gauges suffer from inaccuracies and are subject to both random and systematic errors. The most important errors are summarized in short in this section.

Wind induced error: The wind induced undercatch generally represents the largest problem of rain gauge precipitation measurements. The rain gauge itself disturbs the wind field and deflects the trajectories of the particles around it. Due to this, the particles that should have reached the rain gauge will rather end up outside the gauge, causing deficits in catch. According to Førland (1981), during snowfall and with wind velocities larger than 5 m/s, rain gauges with a wind shield are measuring distinctly under 50 % of the true precipitation amount. For rain gauges without a wind shield the ability of interception is even lower. With precipitation in the form of rain the deficit was approximately 5 % with the mentioned wind velocity. In another study reported by Yang et al. (1998) the accuracy of standard 8" nonrecording precipitation gauges was addressed when precipitation was classified into snow, mixed, and rain. The beneficial effect of using a wind shield on gauge catch is clearly shown by the difference between the average catch ratios of the shielded and the unshielded gauges, as also seen in Larson and Peck (1974). In Yang et al. (1998), the difference between catch ratios ranged from 26 % for snowfall to 3 % for rainfall, and indicates the benefits of using a wind shield. It was also clear that gauge catch decreased with increasing wind speed for all types of precipitation, particularly for snowfall. For shielded and unshielded gauges, the catch ratios for rainfall and wind speed of 4 m/s were approximately 91 % and 88 %, respectively. For mixed precipitation with the same wind speed, the catch ratio was approximately 79 % for shielded and 67 % for unshielded gauges and for snow 66 % and 40 %. The HOBO rain gauges were mounted 64 - 120 cm above ground level in the Matre campaign to prevent undercatch caused by wind as far as possible.

Evaporation induced error: If all or part of the rainfall stored in a not full bucket inside a tipping-bucket rain gauge evaporates before the next tip, this amount of rainfall is unrecorded. This contributes to an error source, especially in warm weather. The protective grid on the HOBO rain gauges may contribute to increased evaporation of raindrops stuck on the grid, compared to other rain gauges. To eliminate water retention at the grid which could evaporate before being measured, the protective grid can be removed. However, the trade-off is that debris can get into the funnel and clog the orifice. Because of the absence of a heating mechanism in the HOBO rain gauges, snow can be accumulated at the top of the gauges in cold periods. As already mentioned, in Førland and Bjørbæk (1979), evaporation from open snow gauges (without funnel) was above 1.0 mm/day in over 50 % of the cases and above 0.3 mm/day in over 94 % of the cases studied. For Tretyakov, a non-recording precipitation gauge, Aaltonen et al. (1993) found from measurements in Finland that losses due to evaporation in

late spring and summer ware about 0.30 to 0.80 mm/day and in winter of 0.10 to 0.20 mm/day. Evaporation errors are difficult to correct because of its strong dependence on weather conditions and seasonal change.

Splashing error: If the catchment area of the gauge is too flat, large drops may splash out of the gauge, causing a sampling deficit. According to Sevruk (1982), splashing error depends on rainfall intensity, wind speed and the shape and depth of the gauge, and is typically of a magnitude of 1-2 %. This outsplashing effect may be somewhat increased for the HOBO rain gauges because of the protective grid. The outsplashing effect may be significant in hail showers, also due to the grid. The opposite effect, insplashing, will be assumed small because of the placement of the HOBO rain gauges away from objects like trees and buildings.

Site selection related errors: Objects close to the rain gauge may influence the amount of precipitation measured by the gauge. Generally, the rain gauge should be located at least as far from objects as 1-4 times the height of these objects. However, if the distance to nearby objects is too large, the location will often be wind exposed. The rain gauges used in the Matre-project are situated in the terrain with the desire to get the best possible location. However, because of practical considerations, all the rain gauge locations are not equally suitable.

Snow related errors: Precipitation in the form of snow is more difficult to measure than rain. As already mentioned, the undercatch due to wind is much higher for snow than for rain. Evaporation of accumulated snow at the top of a rain gauge also results in underestimation of the true precipitation amount. Accumulated snow at the rain gauge may experience blow-off, which also leads to an underestimation. In cold conditions, a common instrumental error is linked to frost and icing at the gauge.

Instrumental errors: Errors may occur due to incorrect use of the precipitation equipment such as setup at non-standard height above ground or oblique position of the rain gauges (see section 4.1). Errors due to sabotage and other unexpected influences may also be relevant.

5.2 The Matre catchment area

The measurement campaign described in the following is a cooperation between the Geophysical Institute and the power company BKK. BKK was established in June 1920, and is today among Norways bigger companies within production, wholesaling and transport of electrical power. BKK is owned by Statkraft and 17 counties between the Sognefjord and the Hardangerfjord. BKK owns and operates about 30 hydroelectric power stations.

The measurement campaign was performed in Western Norway in the Matre Hydro System (MHS), which is situated in a large mountain region at the border between the counties of Hordaland and Sogn og Fjordane (Figure 1). The westernmost part of the catchment area is about 40 km inland from the coast. The catchment area for MHS is about 200 km^2, including three power stations; Vestrebotn, Stordal and Matre (Figure 18). The normal annual precipitation for Stordal and Matre power station in the catchment area is 2750 mm and 2690 mm, respectively (Førland (1993)). For Takle, about 19.8 km northwest of Stordal, the normal annual precipitation is 3179 mm (Førland (1993)). MHS produces in the upper edge of 1 TWh yearly. An average family, two adults and two children, have an annual total consumption of roughly 25000 KWh. The power produced in this water system can thus, roughly calculated, cover the demand of electricity for 40000 average families. Figure 18 illustrates the catchment area, regulated reservoirs, waters, waterways (in the form of tunnels) and power stations in the hydro system. The catchment area of the Matre system has a brownish background color, the red rectangles denote power stations, the dark purple color are reservoirs, the light purple are unregulated waters and the dark purple lines denote waterways in the catchment area. The water is directed in a waterway from Store Fjellvatn to Fridalsvatn, and then further on to Vestrebotn power station and then to Krokevatn. Holmevatn, Kvanngrøvatn and Årnesstølsvatn is also directed in water tunnels to Krokevatn. From Krokevatn the water continues through Stordal power station to Stordalsvatn. Water from Årsdalsvatn and Stølsvatn (via Tverrvatn) is directed in waterways to Stordalsvatn. From Stordalsvatn, the water carries on to Matre power station, which is situated only a few meters above sea level. Figure 19 shows a cross-section of the MHS.

The ratio of reservoir suffuse[2] in this hydro system varies between 0.8 and almost 30, but is mostly between 1.5 and 5.0. This means that the annual precipitation broadly speaking is sufficient to fill a reservoir 1.5 to 5 times in a year. This denotes that some of the reservoirs in the hydro system get quickly filled, and the risk of flooding is present. Melting and extreme precipitation events may cause flooding in some areas, and a better understanding of the spatial precipitation distribution can reduce this risk.

In the measurement campaign, 20 HOBO rain gauges and two automatic weather sta-

[2]Ratio of reservoir suffuse; ratio between annual precipitation and reservoir size. Ratio of reservoir suffuse = afflux (precipitation in the catchment area) [M m^3] / reservoir size [M m^3]

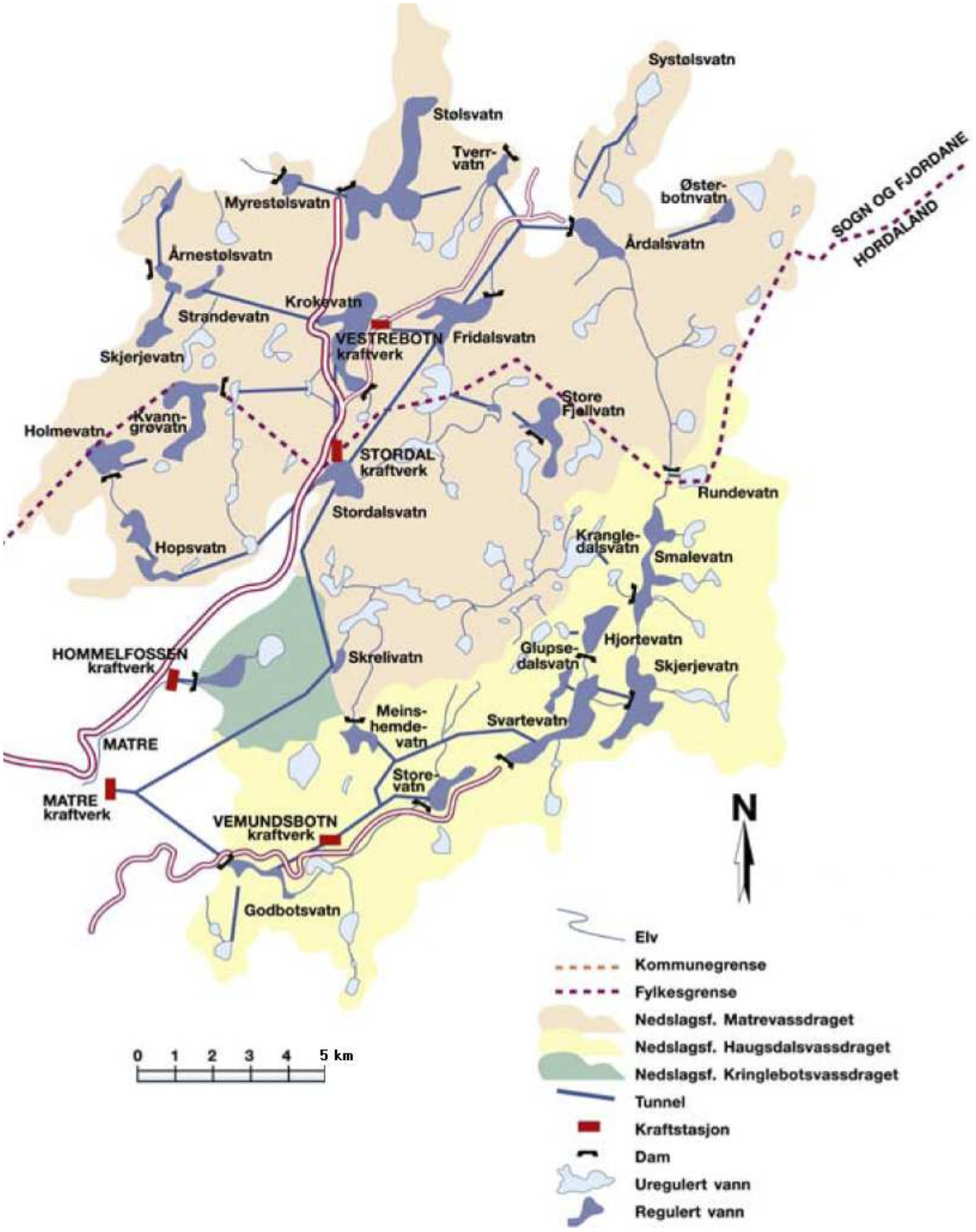

Figure 18: *The part of the figure with a brownish background gives an overview of waters, regulated reservoirs, water tunnels and power stations in the MHS. Figure from BKK (2009).*

Figure 19: *Overview of the elevation in the MHS and surrounding hydro systems. HOBO rain gauges were situated in the Førde and Matre hydro systems. Figure from BKK (2009).*

tions have been deployed in the Matre catchment area of BKK in the period from late April to October 2008. The catchment area in the MHS is large, and due to logistic reasons, it was impossible to place rain gauges in connection with every water or reservoir. Section 5.3 gives an overview of the finally realized instrumental setup.

5.3 Instrumental setup

During the measurement period 20 HOBO rain gauges (R1 - R20) and two automatic weather station (AWS 1 - AWS 2) were used.
The rain gauges R1 - R5 were mounted on the 22nd of April,
R6 - R15 and the two automatic weather stations on June 5th,
R17 on June 25th and the rest were mounted during the 29th of June.
Because of snow, parts of the measurement area were out of reach in April, causing the spread in mounting-time. The measurement period lasted until 29th of October. Site information and operating time concerning the rain gauges and automatic weather stations is given in Table 6. The distribution of the stations during the measurement period is presented in Figure 20.

Station no.	Location	GPS N	GPS E	GPS Elevation	Measurement-height	Serial no.	Start-date	End-date
R1	Matre power station	60.87562	5.58913	22 m	101 cm	20819	Apr 22nd	Oct 29th
R2	Stordal power station	60.96078	5.70367	481 m	109 cm	20818	Apr 22nd	Oct 29th
R3	Stordal river	60.96362	5.71132	480 m	64 cm	20551	Apr 22nd	Oct 29th
R4	Fosse	60.91328	5.63700	418 m	102 cm	20821	Apr 22nd	Oct 29th
R5	Skrikeberg	61.03163	5.48877	35 m	95 cm	20856	Apr 22nd	Sep 10th
R6	Blåfjell	61.00737	5.75353	898 m	105 cm	21079	Jun 5th	Oct 29th
R7	Årsdalsvatn	61.01828	5.81937	483 m	100 cm	21077	Jun 5th	Oct 29th
R8	Fridalsvatn	60.99747	5.74228	709 m	110 cm	21076	Jun 5th	Oct 29th
R9	Krokevatn	60.98452	5.71867	613 m	110 cm	21078	Jun 5th	Oct 29th
R10	Langevatn	60.97810	5.68937	651 m	120 cm	21074	Jun 5th	Oct 29th
R11	Stølsdalen	61.00650	5.70005	616 m	108 cm	21073	Jun 5th	Oct 29th
R12	Stølsvatn	61.03042	5.71025	571 m	108 cm	21072	Jun 5th	Oct 29th
R13	Gamle Stølsleitet east	61.01223	5.67707	767 m	102 cm	21059	Jun 5th	Oct 29th
R14	Skorvane	61.00965	5.68818	825 m	102 cm	21058	Jun 5th	Oct 29th
R15	Høgetjørnane	60.99095	5.66863	788 m	108 cm	21008	Jun 5th	Oct 29th
R16	Oppedal	61.06277	5.55925	60 m	92 cm	20857	Jun 25th	Oct 28th
R17	Gamle Stølsleitet west	61.01148	5.65885	656 m	81 cm	20550	Jun 29th	Oct 29th
R18	Hareheia	61.01200	5.63870	663 m	98 cm	20840	Jun 29th	Oct 29th
R19	Årnesstøl	61.01532	5.62775	702 m	82 cm	20806	Jun 29th	Oct 29th
R20	Hornsetvatn	61.02302	5.64953	622 m	86 cm	21075	Jun 29th	Oct 29th
AWS-1	Stordal	60.96362	5.71132	480 m	346 cm	-	Jun 5th	Oct 29th
AWS-2	Blåfjell	61.00737	5.75353	898 m	388 cm	-	Jun 5th	Oct 29th

Table 6: *Location of the measurement sites and data availability.*

Many of the rain gauges (R1,R2,R3,R4,R7,R8,R9) were placed in the terrain along the road from Matre and northeast to Årsdalsvatn, and were set nearby the waters and reservoirs in the area. Some rain gauges (R11,R13,R14,R17,R18,R19) were set in a west-east trace in the terrain, about 3 hours walk to the westernmost (R19) from the gravel road (R11). Two rain gauges were set north and south of this trace (R15,R20). R10 and R12 were placed nearby a small dam southwest of Krokevatn and nearby the reservoir Stølsvatn, respectively. Two other rain gauges were set at a lower elevation west (R5) and north (R16) of the main measurement area to look for west-east and north-south gradient and orographical differences. AWS-1 is placed by Stordalsvatn, not far from the rain gauge maintained by BKK. The other automatic weather station

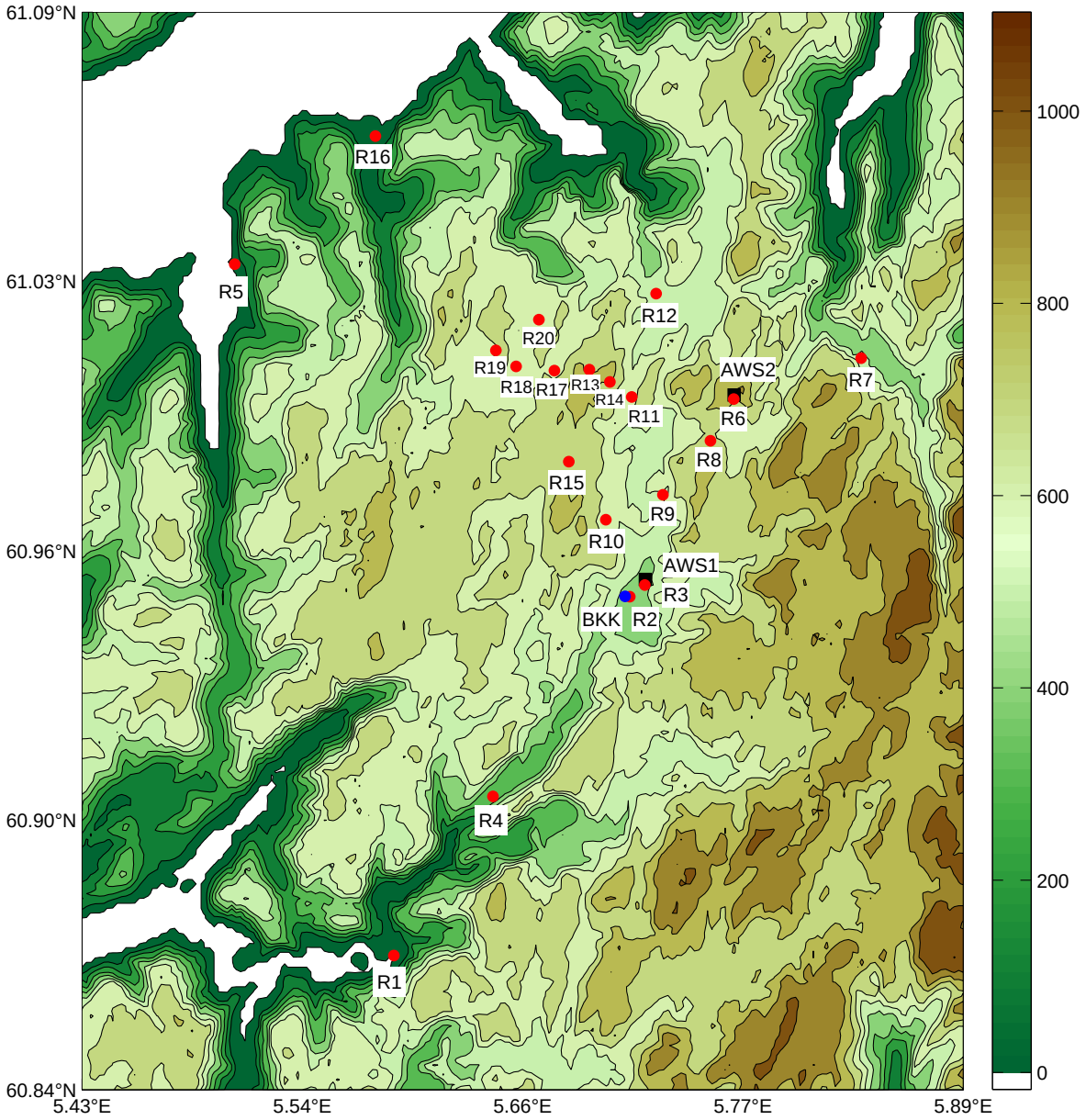

Figure 20: *Rain gauge and weather stations locations in the measurement area. The colorbar gives the elevation above sea level [m].*

is placed at Blåfjell, one of the highest points in the measurement area. This weather station was placed in this manner to get a picture of the large scale wind conditions and the minimum temperatures during precipitation episodes. R6 is placed next to AWS-2. All the stations are located as best as possible away from obstacles and tracks to minimize measurement errors and vandalism.

A short description of the measurement site for each rain gauge and weather station is given in the following.

R1 - Matre:
Southernmost station. Situated on a flat lawn at the bottom of a steep valley. The Matresfjord is on the western side. Mountains on the southern and eastern side. A valley in the northern direction.

R2 - Stordal power station:
Situated on a little hill in the northern part of Stordalsvatn. This rain gauge is situatued outside the fence at Stordal power station covering the rain gauge maintained by BKK and several power line poles. R2 is only a couple of meters away from RBKK. A cliff is located close to the power station on the western side. A picture of this rain gauge is given in Figure 21(b).

R3 - Stordal river:
Situated by the river north of Stordalsvatn, only about 500 meters northeast of R2. The rain gauge is situated in an open terrain with small bushes and ling.

R4 - Fosse:
Placed in a north-south valley nearby the road north of Matre and south of Stordal. A high mountain is situated somewhat to the west of the rain gauge. The rain gauge is situated in the terrain with bushes and ling.

R5 - Skrikeberg:
Westernmost station. This station is placed in a steep sloping terrain nearby the road E39 south of the tunnel of Skrikeberg. The valleyside is westward.

R6 - Blåfjell:
This is the highest station in the measurement campaign. There is another mountain top located east of Blåfjell, but except for this, the view is unobstructed for many kilometers. There is little or no vegetation in this area, and the site is assumed to be well exposed to all wind directions. The small amount of vegetation is visualized in Figure 5, which shows the weather station at this location.

R7 - Årsdalsvatn:
Placed in the terrain on the northwest side of Årsdalsvatn, close to the reservoir. There is a valley northwest of the rain gauge. Small bushes and trees in the area.

R8 - Fridalsvatn:
Situated at a flat area close to the road west of Fridalsvatnet. R6 Blåfjell is northeast of this station, and the ascent up to R6 Blåfjell starts here. Looking southwest we can see Krokevatn. Small bushes and ling in the area.

R9 - Krokevatn:
Mounted in an almost flat area on the peninsula in the dam. The area is covered with small trees, bushes and ling with a height of 10-100 cm.

R10 - Langevatn:
Situated at the end of a gravel road. The rain gauge is place by the small water in the valley. Ling is present in the area, but except for this the vegetation is considered to be low.

R11 - Stølsdalen:
The rain gauge is situated in a valley with high mountains on the westward and east-

ward side. Ling is present in the area.

R12 - Stølsvatn:

Placed in the terrain close to the weir by the reservoir Stølsvatn. This is the station with the strongest vegetation, both trees and bushes are present here. Figure 21(a) visualizes the vegetation in the area nearby the rain gauge.

R13 - Gamle Stølsleitet east:

Placed along the west-east trace in the terrain. The rain gauge is placed in the western side of an open valley. Low vegetation such as ling and small bushes in this area.

R14 - Skorvane:

Situated along the west-east trace in the terrain west of R11, but at a higher altitude. The rain gauge is situated on the mountainside. Vegetation as ling in the area.

R15 - Høgetjørnane:

Situated to the south of the west-east trace. Placed at a ridge west of a north-south dam. Ling is present in the area.

R16 - Oppedal:

Northernmost rain gauge. Placed at the lawn in the garden of Leiv O. Oppedal, on the southern valley side of the Sognefjord. Bushes near the rain gauge.

R17 - Gamle Stølsleitet west:

Situated on the west-east trace in the terrain. Placed in a valley, close to a dam. Open terrain in the north-northeast and south-southwest directions. Little vegetation close to the rain gauge.

R18 - Hareheia:

Situated in the west-east trace in the terrain. Placed on the western side of an open valley in an open terrain. Low vegetation as ling in the area.

R19 - Årnesstøl:

The westernmost station in the west-east trace in the terrain. Placed in a sloping terrain. A valley in the west-southwest direction. About 3 h walk from a gravel road. Little vegetation.

R20 - Hornsetvatn:

Situated north of the west-east trace. Placed in the valley north of Hornsetvatn. The valley narrows somewhat at this location. Bushes and ling in the area.

AWS 1- Stordal

The weather station was located by the river at Stordal, close to the rain gauge R3.

AWS 2- Blåfjell

This weather station was located at the top of the mountain Blåfjell. The rain gauge R6 was located next to the weather station. The mountain is one of the highest in the area, and therefore the wind direction measured is expected to be representative for the large scale situation. A picture of the weather station was given in Figure 5.

RBKK

RBKK denotes the SIAP rain gauge maintained by BKK (see section 3.3). This rain gauge is situated on the inside of the fence at Stordal power station. A cliff is located close to the power station and the rain gauge on the western side. Figure 21(b) shows the rain gauges RBKK and R2, and the cliff.

(a) Visualization of the vegetation at R12 Stølsdalen.

(b) The rain gauges at Stordal power station; R2 in front, RBKK inside the fence and the cliff in the background. View towards west. Stordalsvatn is situated southeast of the power station.

Figure 21: *a) The vegetation at R12 Stølsvatn. View towards south. b) R2, RBKK and Stordal power station. A cliff is situated in the background.*

Periodic controls of all the equipment took place on 27th of July and 13th and 14th of September. Control of three rain gauges was also done on 31st of August. At the control of the AWS, the logged data were collected and a new data storage unit was installed. When checking the rain gauges, all the observation data were downloaded from the recording system onto a temporary storage device. The level of each gauge was checked and the instrument, if necessary, adjusted. However, none of the rain gauges were noticeably oblique during the campaign.

On 15th of August a hiker informed that the lid of R20 was off, and that he had placed it back on again on this day. The incident is most probably caused by curious cows or sheep grazing in this area. When studying the data from this rain gauge it looks like it stopped recording the 10th of August and started again when the lid was put back on. Data missing for R20 in this period have been compensated for by using a correction factor in accordance with the nearby station R18. The rain gauge at Skrikeberg stopped recording, for an unknown reason, on the 10th of September. Data from this station are unfortunately not existing after this date. The rain gauge at Oppedal (R16) showed improbable large values at the end of the measurement period, and the last 24 h of data from this rain gauge have been removed from the dataset. No other problems concerning the rain gauges and the automatic weather stations have been detected.

5.4 Data description

Observation data: The raw data of the HOBO rain gauges consist of the time stamp of every single 0.2 mm precipitation amount. For further investigation, these data have been integrated to 1 h and 24 h sums. In the following chapters, corrected values in accordance with the calibration procedures described in section 4.4 will be used. The resolution of the weather station data is 10 minutes, which have been averaged over 1 h for the comparison with the precipitation data. Case study 2 (section 9.2) is an exception of this, where 10 minute values have been utilized. 10 minute values are also used in wind roses showing the overall wind distribution at AWS-1 and AWS-2 (section 6.3.1). Precipitation data from the SIAP rain gauge maintained by BKK enable 1 h resolution. As in chapter 4, 24 h precipitation assigned e.g. 24th of April has arrived between 00 UTC 23th of April - 00 UTC 24th of April. Analogous 1 hour precipitation events represent the sum over the hour ending with the report time.

ECMWF data: BKK uses an interpolated point forecast from the ECMWF model (European Centre for Medium-Range Weather Forecasts) at the location Stordal to estimate the amount of water expected in the hydrometric area. The current operational ECMWF forecast model is called TL799L91. The model utilizes a semi-Lagrangian numerical scheme. For the representation at the surface and for the model physics a grid point system is used. The model makes use of a so-called reduced Gaussian grid, which is almost regular in latitude. The average distance between the reduced Gaussian grid points is about 25 km in the current model version. The atmosphere is divided into 91 vertical layers up to 0.01 hPa. The vertical resolution is finest in the planetary boundary layer and coarsest in the stratosphere and mesosphere. More details concerning the model is availible in Persson and Grazzini (2007).

Stordal is located 480 meters above sea level, while it in the model-terrain is 671 meters above sea level. The data are corrected with respect to the altitude difference by a vertical precipitation gradient of 5 %/ 100 m (Villanger (2009)). The model runs twice a day, 00 and 12 UTC. The forecasts from the ECMWF model are available with 1 h resolution, and the data from forecast hour 06-18 are used in this thesis. Data from the ECMWF model are available from 22nd of April 2008.

6 Overall meteorological conditions

6.1 General overview

Figure 22 shows temperature, relative humidity, wind speed, wind direction and precipitation at Stordal and Blåfjell during the measurement period. Because of lack of own pressure observations, corresponding data from Fedje, a weather station maintained by DNMI southwest of the measurement area (see Figure 1), are used. Pressure observations are available every sixth hour.

DNMI is, based on observation from nearby weather stations, calculating percentage amount of precipitation and temperatures deviation out of the normal values for every month. According to DNMI (2008), for May 2008, the area where the HOBO rain gauges were operating experienced only 25-50 % of the normal precipitation amount, and the temperature was about 1.5-2 °C higher than normal. In June 2008, the Matre-area received about 125-150 % of the normal precipitation amount, with approximately normal temperatures. For both July and August 2008, only 50-75 % of the normal precipitation was achieved. In July, the temperatures were 3-4 °C above the normal temperature, while for August the corresponding number was 0.5-1.0 degrees above normal. For September, only 25-50 % of the normal precipitation amount was reported for the area, and the temperatures were 1.5-2.0 °C above normal. In October 2008, according to DNMI (2008), 150-175 % of the normal precipitation was reported for the area, and the temperatures were 1.0-1.5 °Cbelow normal. Because of this, snow was present in elevated areas.

Several high pressure situations have occurred during the measurement campaign, and the most dominant ones occurred around the 24th of July and 14th and 25th of September. The high pressure situations are characterized by weak wind and a large variation in day and night temperatures, particularly at Stordal. The most dominant convective precipitation case was an afternoon shower or thundershower which happened on the 30th of July about 14 UTC. This situation will be reviewed in more detail in section 9.2. Unluckily for a work of precipitation like this, only a relatively few strong frontal events happend during the summer 2008. Though, a warm and cold frontal passage from the 19th to 21st of June caused precipitation values up to 150 mm. Unfortunately, R16 - R20 was not yet operating during this period. A frontal passage occuring 15th of July will be investigated in section 9.1. Several frontal passages occurred during October. On the 25th of October precipitation amounts between 49.4 mm (R19) and 123.5 mm (R14) were measured within 24 h during a low pressure system. However, during October there were several events with low temperatures during precipitation, making the data in higher elevations hard to interpret. Before October, the temperatures during rainfall have been above freezing, except a minor episode on June 24th were the temperature at Blåfjell was about 0 °C for a couple of hours during precipitation.

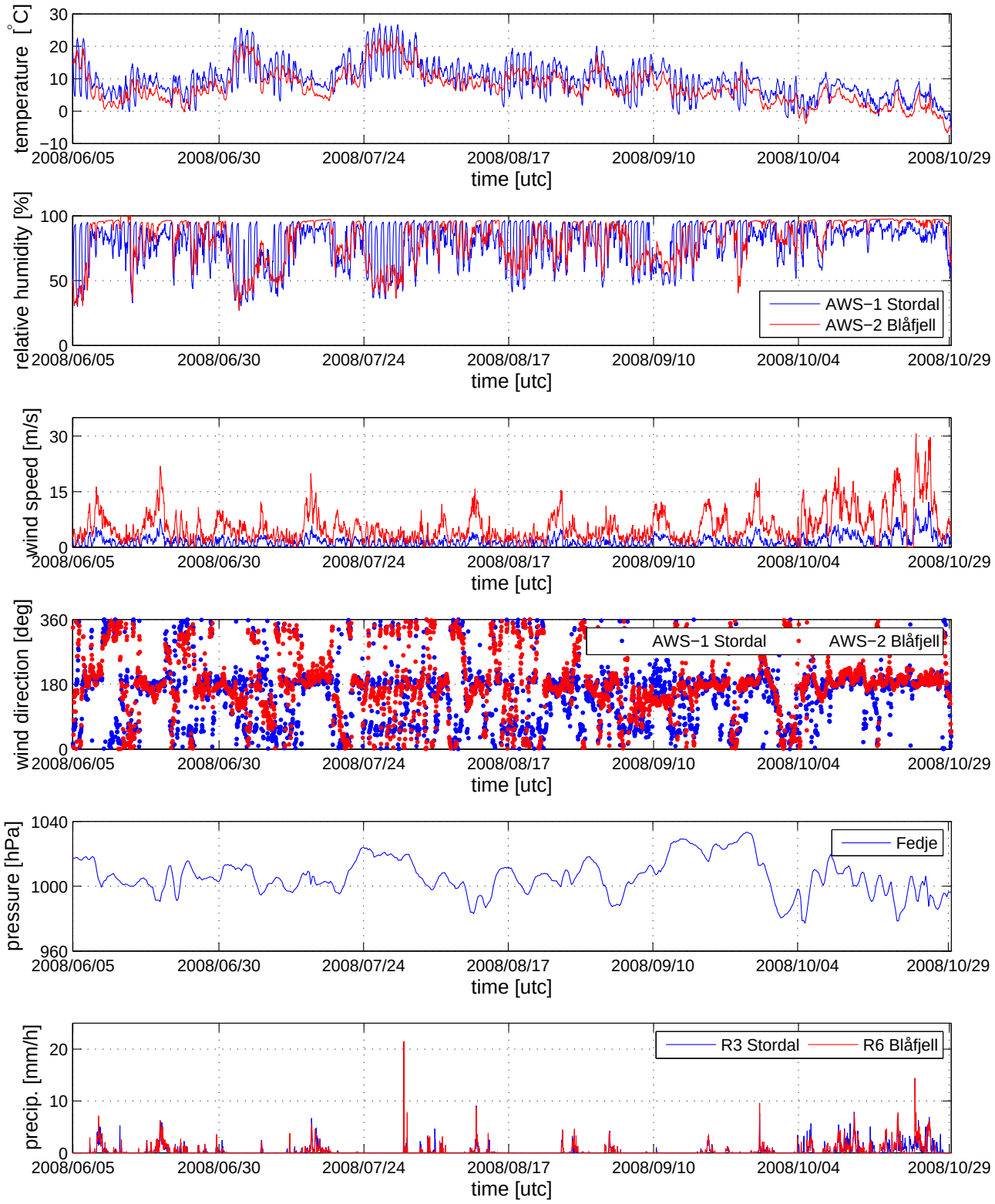

Figure 22: *Overview of the meteorological conditions for Stordal and Blåfjell during the field campaign. The pressure values from Fedje are measured four times per day. The other parameters are hourly values.*

6.2 Precipitation

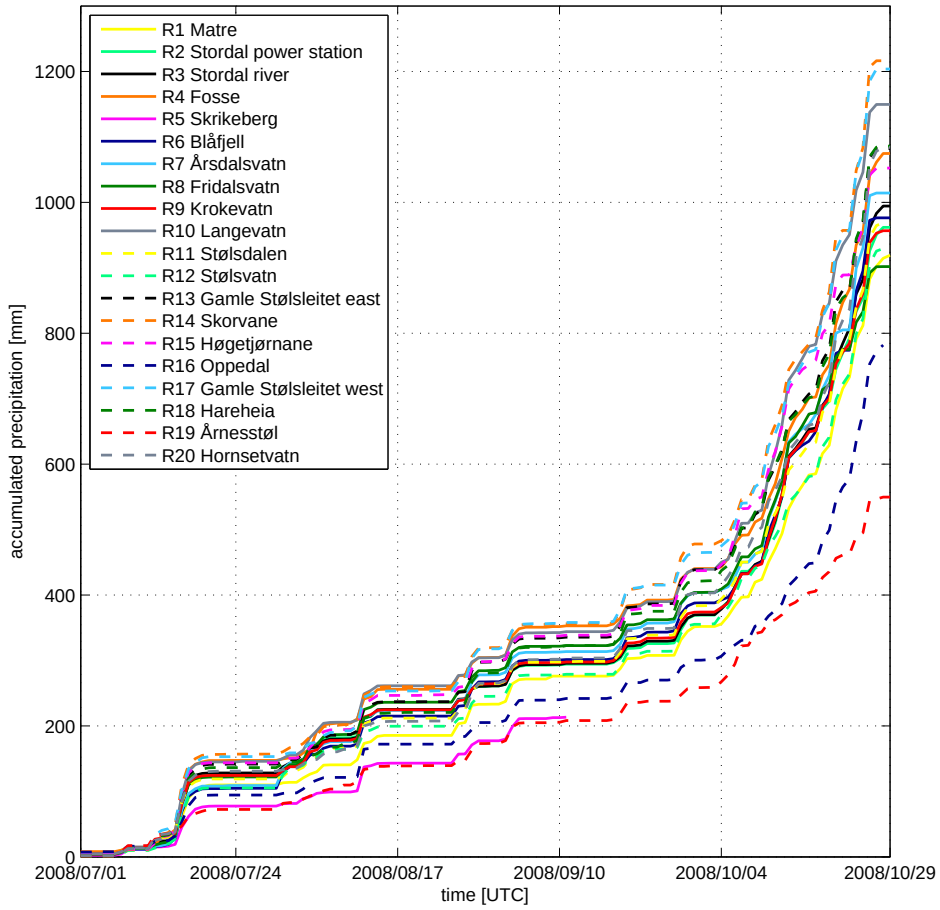

Figure 23: *Accumulated 24 h precipitation at the different rain gauge locations from 1st of July to 29th of October.*

Figure 23 shows the accumulated precipitation for all the locations from 1st of July to 29th of October. Precipitation amounts between approximately 550 mm and 1200 mm were measured in the period when all the stations were mounted. Rain gauge R14 recived the most precipitation, while R19 measured the minimum amount of precipitation during the campaign. For the rain stations in the MHS, the amounts are mainly between 900 - 1200 mm. Rain gauge R19 measured considerably smaller precipitation amounts compared to the nearby located gauges. A potential reason for this is poor rain gauge positioning. R16 measured second least during the campaign, which is expected to be due to its location in the lee of the mian wind direction.

6.3 Wind conditions

6.3.1 Stordal & Blåfjell: Wind observations

The weather station at the mountain Blåfjell, AWS-2, is situated almost 900 meters above sea level. The mountain is one of the highest in this area. Because of this location, the wind at Blåfjell is assumed to be rather representative for the large scale wind conditions. The weather station at Stordal, AWS-1, is situated 480 meters above sea level in a northeast-southwest oriented valley. The wind direction at Stordal is expected to be more influenced by the local topography. Close to AWS-1, rain gauge R3 is located, while R6 is located close to AWS-2.

Figure 24 and Figure 25 give the wind direction measured at AWS-1 and AWS-2, respectively. The graphs on the left hand side present the overall observed wind direction distribution during the campaign. The panels on the right give the percentage amount of precipitation related to the corresponding wind direction intervals. In both locations, the dominant wind direction when precipitation is observed is from S-SSW. From Figure 24(b), 68 % of the total precipitation amount at R3 is measured when the wind direction at AWS-1 is between 172.5° - 202.5°, a S - SSW wind direction. Approximately 7 % and 6 % of the total precipitation amount is registered for wind direction between 157.5°-172.5° and 202.5°-217.5°, respectively. Only minor amounts, 0.5 - 2 % of the total precipitation amount, are registered for other wind direction intervals. At Blåfjell, the main wind direction, regardless of precipitation, is from SE - SSW and from NW - NNE (Figure 25(a)). Figure 25(b) shows that for Blåfjell, 71 % of the total precipitation amount at R6 is measured when the wind direction at AWS-2 is between 172.5°-217.5°. In the wind direction intervals from 157.5°-172.5° and from 217.5°-232.5°, 5 % and 4 % of the total precipitation is registered, respectively. Only minor amounts are registered for the other wind directions. A large number of wind direction registrations at AWS-1 Stordal are from NNE - E. However, this wind direction is almost non-existing at AWS-2 Blåfjell, and might indicate a channeling effect at Stordal.

Figure 26(a) shows the wind speed at AWS-2 versus AWS-1 when precipitation is observed at the close by rain gauges. The wind speeds at Blåfjell are, as assumed, much higher than at Stordal. The highest average hourly wind speed at Blåfjell is 30.7 m/s, while at Stordal the corresponding number is only 12.1 m/s. The wind directions when precipitation is observed are depicted in Figure 26(b). The broader interval at AWS-2 for SSW wind directions is present, indicating a channelig effect at Stordal.

6.3.2 ECMWF model: Wind forecast

A single point forecast from the ECMWF model for the location Stordal is used. The wind direction forecasted at 850 hPa by the model is presented in Figure 27(a), and shows a broader distribution than observed at both Stordal and Blåfjell. Figure 27(b) shows the forecasted wind distribution when precipitation is forecasted. The main interval for forecasted precipitation is from 202.5 - 247.5 degrees, accounting for 47 %

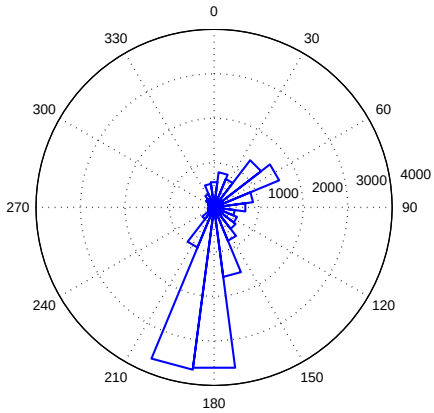

(a) All wind direction observed at AWS-1 Stordal.

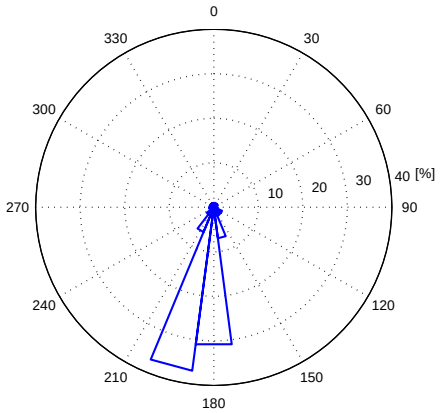

(b) Percentage amount of precipitation recorded by R3 based on wind direction at AWS-1 Stordal.

Figure 24: *Wind direction distribution at AWS-1 Stordal. The figures are based on 10 minute values.*

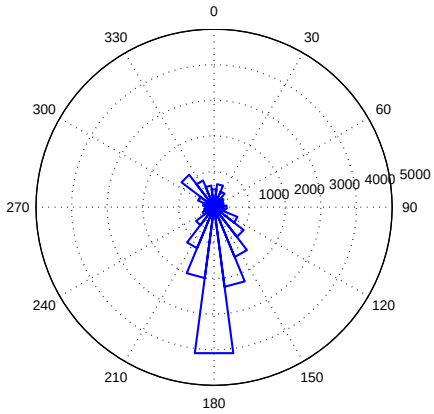

(a) All wind direction observed at AWS-2 Blåfjell.

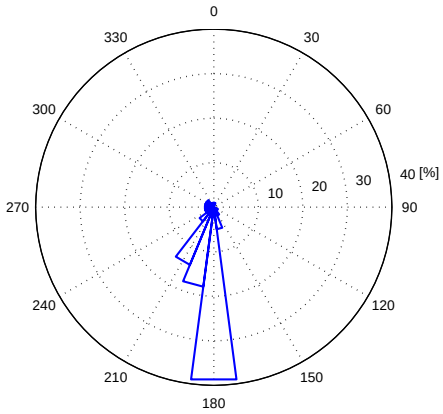

(b) Percentage amount of precipitation recorded by R6 based on wind direction at AWS-2 Blåfjell.

Figure 25: *Wind direction distribution at AWS-2 Blåfjell. The figures are based on 10 minute values.*

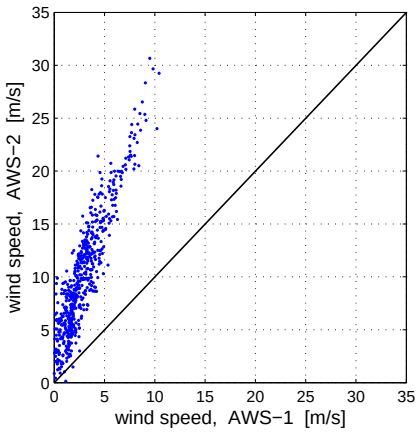

(a) Windspeed AWS-1 versus AWS-2.

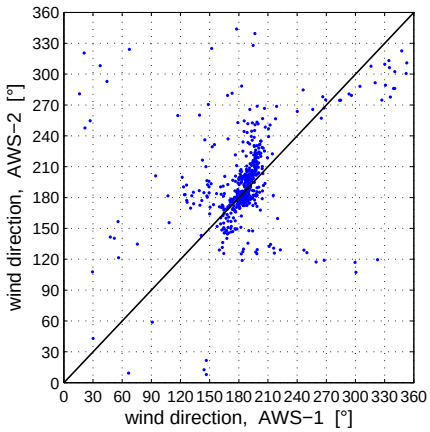

(b) Wind direction at AWS-1 versus AWS-2.

Figure 26: *Wind speed and direction at AWS-1 versus AWS-2 when precipitation is observed for both R3 (close to AWS-1) and R6 (close to AWS-2). The figures are based on 1 h values.*

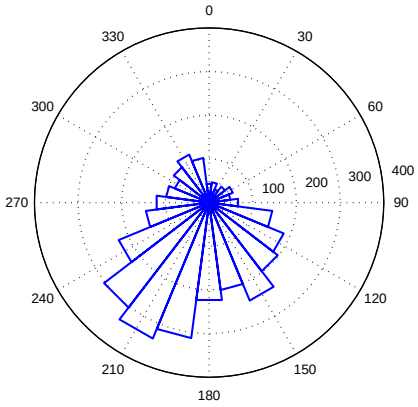

(a) All wind directions.

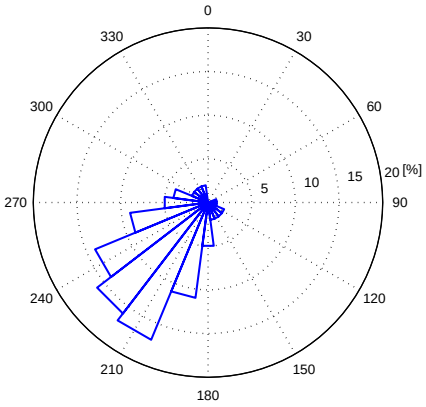

(b) Percentage amount of forecasted precipitation based on forecasted wind direction.

Figure 27: *Wind direction forecasted by ECMWF for the location Stordal. The figures are based on 1 h values.*

of the total amount. Altogether, for wind directions between 187.5-277.5 degrees, 72 % of the total amount of forecasted precipitation is registered. Respectively 5 % and 4% of the precipitation is forecasted for wind directions between 172.5 - 187.5 degrees and 277.5-292.5 degrees. Only minor amounts are registered for the other wind directions.

6.3.3 Wind forecast by the ECMWF model versus wind observations

The single point forecast for Stordal from the ECMWF model will be compared to both AWS-1 and AWS-2. For both Blåfjell and Stordal, the main wind directions when precipitation was observed were between 172.5-202.5 degrees. At Blåfjell, precipitation was also present in the interval from 202.5-217.5 degrees. In comparison, the ECMWF-model results show a broader wind direction distribution and more southwesterly wind directions when precipitation is forecasted (Figure 27(b)). Figure 28 shows the forecasted wind direction at 850 hPa versus the observed wind directions at the weather stations when precipitation is both forecasted and observed. The channeling effect for AWS-1 Stordal is clearly seen, as well as the more southwesterly wind direction forecasted by the model. Due to decreasing friction, the wind is rotating clockwise from the ground and upwards (Ekman spiral). The forecast at 850 hPa is analogous to approximately 1500 meters above sea level, while the weather stations are located at 898 and 480 meters above sea level, and the more southwesterly distribution from the model is expected to be due to this.

The wind speed forecasted by the ECMWF model versus observed wind speed at the weather stations when precipitation is both forecasted and observed, is seen in Figure 29. Figure 29(a) indicates a rather well agreement between the forecasted wind speed at 850 hPa and the observed speed at Blåfjell. Broadly speaking, the wind speed predicted is somewhat higher than observed. However, this seems reasonable when taking into consideration the height difference between the observations and the forecast height. The wind speed forecasted by the model at 10 meters level versus AWS-1 is seen in Figure 29(b). In particular for low wind speeds, the model shows a tendency to forecast higher speeds than observed at Stordal. However, the highest wind speeds observed at Stordal are not forecasted by the model.

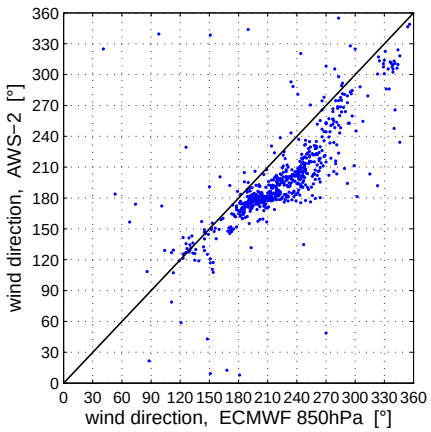

(a) Wind direction. ECMWF (850 hPa) versus AWS-2, when precipitation is forecasted by ECMWF and observed at AWS-2.

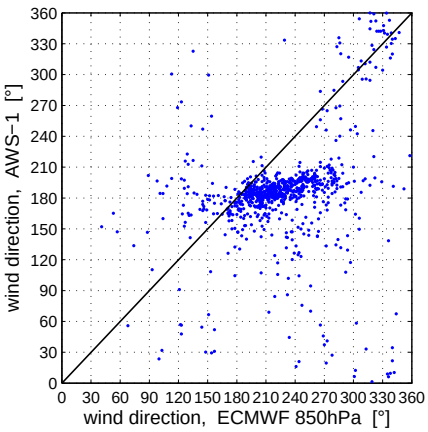

(b) Wind direction. ECMWF (850 hPa) versus AWS-1, when precipitation is forecasted by ECMWF and observed at AWS-1.

Figure 28: *Wind direction from the ECMWF model versus wind direction measured by the weather stations when precipitation is both forecasted and observed. The figures are based on 1 h values.*

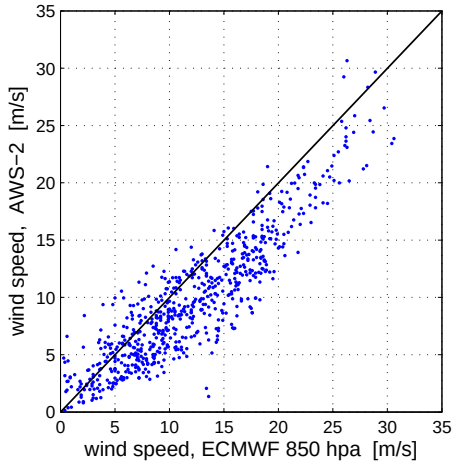

(a) Wind speed. ECMWF (850 hPa) versus AWS-2, when precipitation is forecasted by ECMWF and observed at AWS-2.

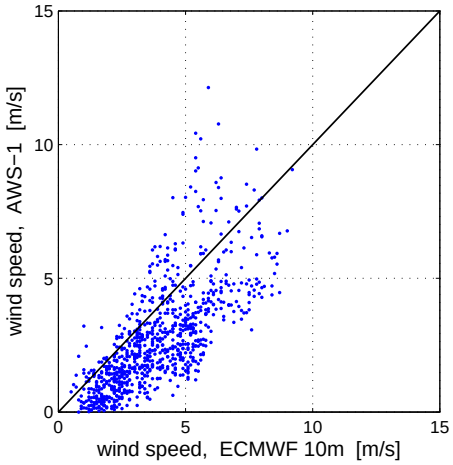

(b) Wind speed. ECMWF (10 m) versus AWS-1, when precipitation is forecasted by ECMWF and observed at AWS-1.

Figure 29: *Wind speed from the ECMWF model versus wind speed measured by the weather stations when precipitation is both forecasted and observed. The figures are based on 1 h values.*

7 Precipitation distribution at Stordal

The main source of information for BKK to describe the precipitation in the whole catchment area is one single SIAP rain gauge operated at Stordal power station. Consequently, Stordal will be used as reference station when comparing with measurements at other locations. This chapter presents a comparison between the HOBO rain gauges deployed at Stordal, R2 and R3, and the SIAP rain gauge maintained by BKK, RBKK. RBKK is situated inside the fenced area of Stordal power station, while R2 is situated just outside the fence, about 10 meters away from RBKK. At the western side of Stordal power station, a 15-20 meter nearly vertical cliff is located (see Figure 21(b)). To investigate if the cliff is influencing the measurements done nearby the power station, a second HOBO rain gauge, R3, was situated in an open terrain 520 meters northeast of the power station. The possible influence of the cliff is addressed in section 7.2.

7.1 Comparison: R2, R3 and RBKK

The accumulated precipitation of the three rain gauges through the entire measurement period is shown in Figure 30. R2 and R3 are almost equal during the period, with R3 slightly higher than R2. In the last days of the period, R2 and R3 differ more. The behavior of RBKK is changing throughout the period in relation to the other rain gauges. During the first part of the period (24th of April to 5th of June), RBKK measures approximately equal as the HOBO rain gauges. Thereafter, RBKK measures more than R2 and R3 until about 20th of July. Since then, the difference in accumulated precipitation between RBKK and the HOBO rain gauges decreases, and on 23rd of September

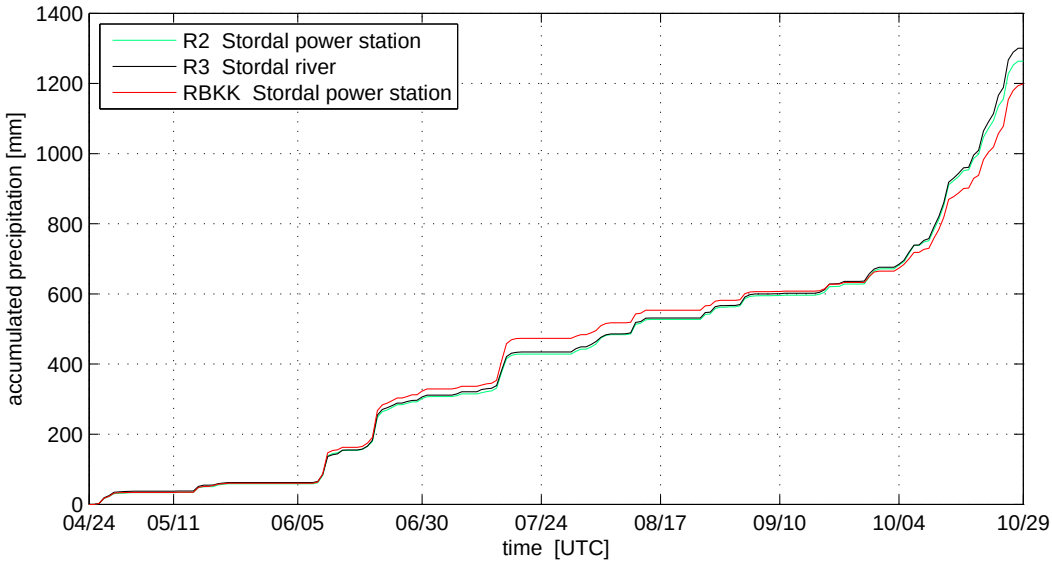

Figure 30: *Accumulated precipitation for the rain gauges at Stordal from 24th of April to 29th of October. Note the different accumulation period compared to Figure 23*

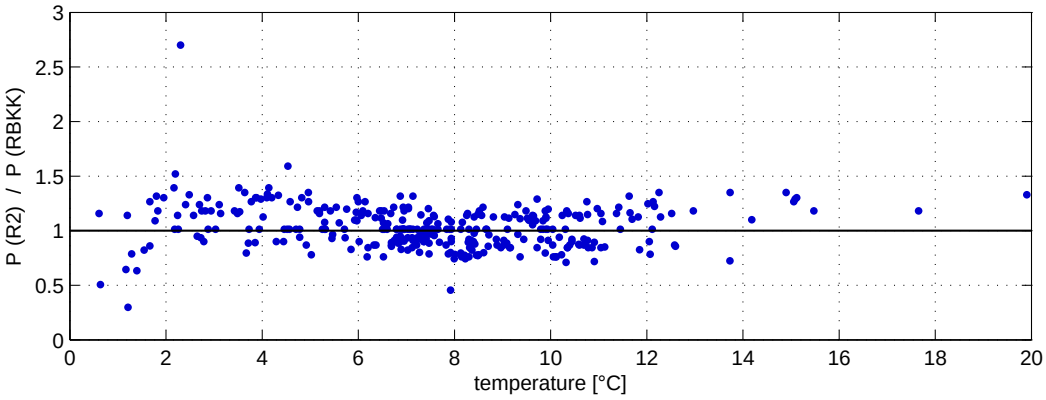

Figure 31: *Ratio between R2 and RBKK versus temperature. Only precipitation events when both R2 and RBKK are above 1 mm/h, are considered.*

the accumulated precipitation was equal for the different rain gauges. During the rest of the measurement period, R2 and R3 measured more precipitation than RBKK. The weather stations were mounted 5th of June, and only precipitation events after this are included when comparing with meteorological parameters measured by the weather stations. Figure 31 shows the ratio between R2 and RBKK (for precipitation values greater than 1.0 mm) in relation to temperature measured by AWS-1 at Stordal. As depicted in this figure, the variability in the ratio-values is largest at low temperatures. This is expected to be because RBKK is equipped with a heater, while the HOBO rain gauges are not. Because of this, in the rest of this chapter, only precipitation values when the measured temperature at AWS-1 is above 2°C, where the occurrence of solid precipitation should be minimized, are considered.

The change in range for the accumulated precipitation in Figure 30 for RBKK compared the HOBO rain gauges is investigated closer. Figures 32(a) and 32(b) show the ratio between R2 and RBKK, and R3 and RBKK with respect to time, for all hourly events with precipitation above 1.0 mm/h. In both figures, a sharp change in the ratio is seen between the precipitation episodes on 19th and 30th of July. The change is clearest in the ratio between R2 and RBKK (Figure 32(a)). This change in ratio found for both R2 and R3 when comparing with RBKK might indicate that something unforeseen has happened to the rain gauge maintained by BKK. Another possibility might be different weather situations in the first part of the measurement period compared to the last part, and that the location of the RBKK rain gauge compared to the other rain gauges is of vital importance at specific weather situations. The ratio between R2 and RBKK versus wind direction for the period before and after 24th of July is presented in Figure 33. The two periods are mainly containing the same wind direction when precipitation is present. In the period from 5th of June to 24th of July, by far the greatest number of values are below one, meaning RBKK is measuring more precipitation than R2. From 25th of July and on, the bulk part of the values are above one, meaning R2 measuring more than RBKK. The same pattern is present for the wind direction intervals when

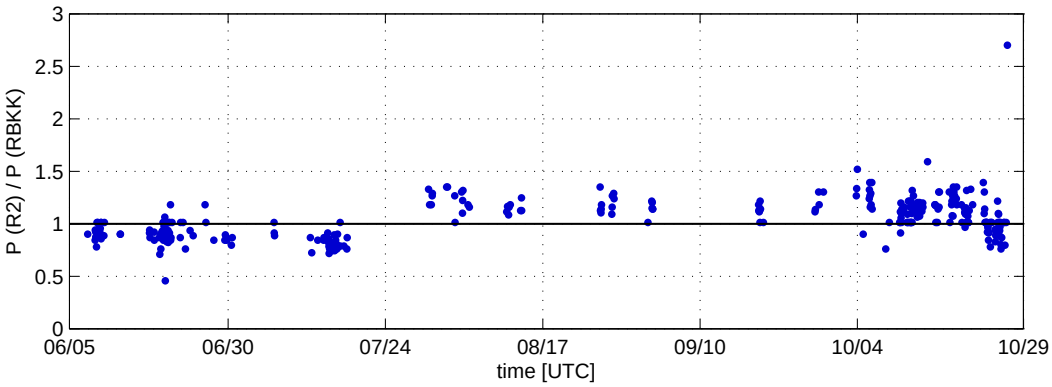

(a) P(R2) / P(RBKK)

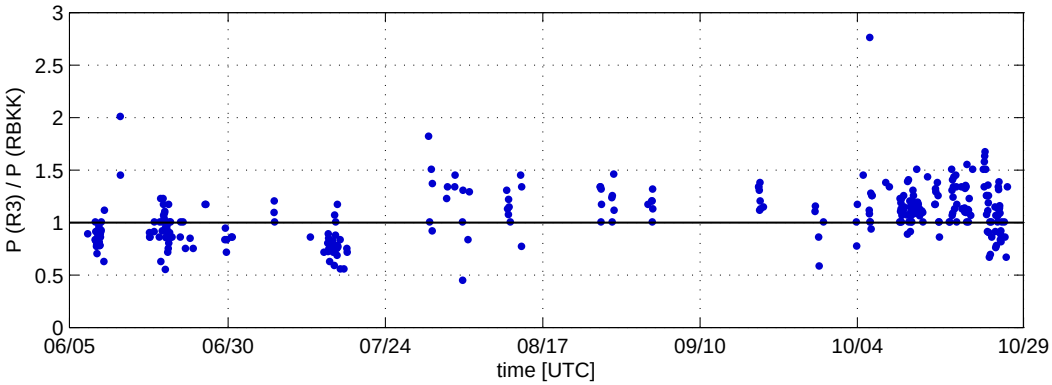

(b) P(R3) / P(RBKK)

Figure 32: *Ratio between R2 or R3 and RBKK versus time. Only precipitation events when both R2 or R3 and RBKK are above 1 mm/h, are considered.*

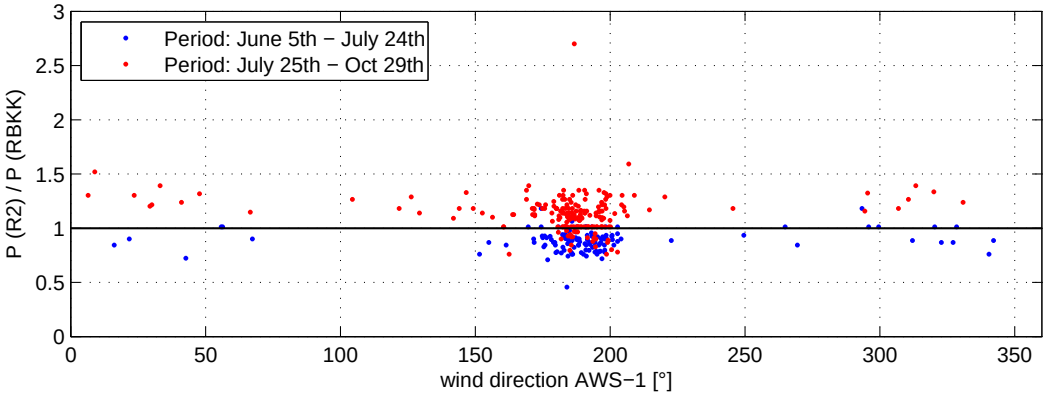

Figure 33: *Ratio between R2 and RBKK versus wind direction. Only precipitation events when both R2 and RBKK are above 1 mm/h, are considered.*

comparing R3 and RBKK (not shown). The same pattern as depicted in Figure 33 is highly present also when compared with wind speed and temperature (not shown). This unfortunate behavior of the RBKK rain gauge is inexplicable. The sudden change in ratio when divided into two periods for different meteorological parameters, indicates that something unforeseen has happened to the rain gauge maintained by BKK. RBKK was expected to be the reference station at Stordal when comparing with precipitation measurements at other locations, but because of the inexplicable change in ratio, the HOBO rain gauge R2 at Stordal power station is temporarily used as standard for the further investigations instead of RBKK.

7.2 Investigation of a potential influence caused by the cliff

A 15-20 meter high cliff is situated close to the Stordal power station, and might therefore influence the precipitation measurements here (see Figure 21(b)). Because of this, a second rain gauge (R3), was situated in an open terrain by the river 525 meters northeast of the power station. This set up enables the investigation of the potential influence of the cliff by a thorough comparison of the rain gauge data from R2 and R3. During the measurement period from April to October, the accumulated precipitation at R2 was 1263.7 mm, while for R3 the amount was 1300.5 mm (Figure 30). R3 therefore measured 2.9 % more than R2. Both instruments coincide well almost during the whole period, but at the end of the period the difference between the rain gauges increases to some extent. Nevertheless the difference is within the uncertainty level specified by the manufacturer as discussed earlier in section 4.4. R2 is situated on a little hill and mounted 109 cm above ground level, while R3 is situated in fairly open area which contains some bushes, and is mounted only 64 cm above ground. Rain gauge R2 is for this reason supposed to be more exposed to wind than R3. The last part of the measurement period contained snowfall, and the low catch ratio for snow might explain why the difference between the accumulated amounts increases in the last part of the period.

The ratio between measured precipitation at R3 and R2 for different wind directions at AWS-1 is shown in Figure 34(a). The colors denote different wind speeds at AWS-1. As seen in the figure, by far the greatest number of precipitation events occurred when the wind direction at Stordal was between SSE - SSW (150°-210°). Precipitation events when the wind speed is higher than 6.0 m/s almost only exists for wind directions between S - SSW. For these high wind speeds, R3 is measuring more compared to R2 in most of the cases. For wind directions between SSE and S (150°-180°), nearly only wind speeds below 6.0 m/s are present, and the majority of events have a ratio indicating larger amounts of precipitation at R3 than R2. Only a few precipitation events with low wind speed have occurred during northerly wind directions. Figure 34(b) shows the same precipitation events as in Figure 34(a), but compared with the wind direction measured at AWS-2 Blåfjell to avoid the channeling of the wind at Stordal. The colors denote the wind speed at AWS-1 Stordal. The greatest number of precipitation events occurred when the wind direction at Blåfjell was between SSE and SW (150°-240°).

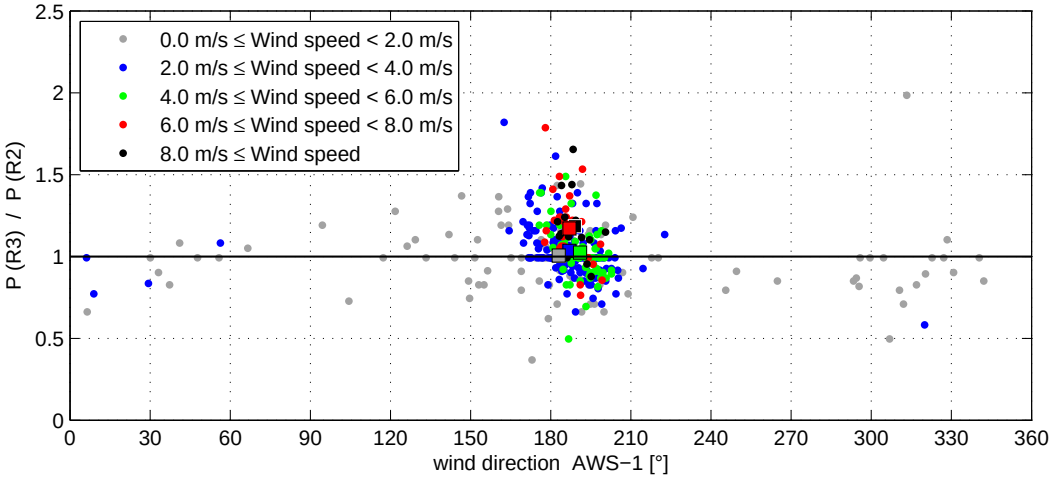

(a) Ratio of R3 and R2 compared to wind direction at AWS-1 Stordal.

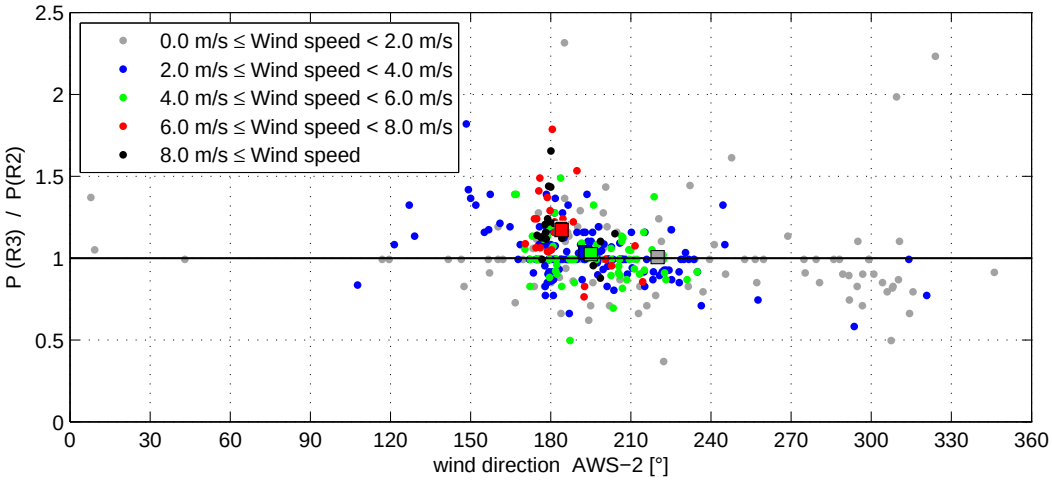

(b) Ratio of R3 and R2 compared to wind direction at AWS-2 Blåfjell.

Figure 34: *Ratio of precipitation measured at R3 and R2 compared as function of wind direction. The color of the dots denote the wind speeds at AWS-1. Only hourly precipitation events when both R2 and R3 are above 1.0 mm/h are considered. The squares denote the mean value of the events with corresponding color.*

Consequently, more southwesterly wind directions are present at Blåfjell than Stordal. An overview of the accumulated precipitation at R2-Stordal power station and R3-Stordal river for different wind directions at AWS-2 Blåfjell is shown in Table 7. The wind direction intervals are 15° for wind directions between 150°-240°, otherwise 30°. In the intervals from 120° - 195°, R3 is measuring more than R2, and from 195°-210° the rain gauges have measured the same during the measurement period. For the two intervals from 120°-165°, R2 has measured 23.5 % and 13.5 % less than R3, respectively. The average and maximum wind speed for these intervals are approximately 2 m/s and

Wind direction [°] AWS-2	# events	Acc. prec. [mm] R2	R3	Percentage R2 more/less than R3	ws AWS-1 [m/s] Average	Max
0 < wd ≤ 30	6	8.3	10.5	- 21.0%	0.9	2.1
30 < wd ≤ 60	4	4.1	3.8	+ 7.9%	0.5	1.0
60 < wd ≤ 90	1	0.2	0.2	0	0.9	0.9
90 < wd ≤ 120	11	8.5	7.8	+ 9.0%	1.6	2.3
120 < wd ≤ 150	59	30.0	39.2	- 23.5%	2.2	4.1
150 < wd ≤ 165	35	26.3	30.4	- 13.5%	2.1	3.7
165 < wd ≤ 180	181	231.5	253.9	- 8.8%	3.5	12.1
180 < wd ≤ 195	222	271.0	285.0	- 4.9%	2.9	10.4
195 < wd ≤ 210	150	233.7	233.8	0	2.9	9.8
210 < wd ≤ 225	77	128.6	118.6	+ 8.4%	2.6	7.8
225 < wd ≤ 240	34	46.6	45.0	+ 3.6%	2.3	4.3
240 < wd ≤ 270	50	37.5	40.0	- 6.3%	1.6	2.9
270 < wd ≤ 300	41	41.5	36.8	+ 12.8%	1.2	3.2
300 < wd ≤ 330	53	50.4	45.2	+ 11.5%	1.4	2.8
330 < wd ≤ 360	9	7.3	9.0	- 18.9%	0.7	2.5
SUM	933	1125.5	1159.2	2.9 % less		

Table 7: *Accumulated precipitation at R2 and R3 for different wind directions measured at AWS-2 Blåfjell. Only wind directions when the wind speed at AWS-2 is higher than 0.5 m/s are considered. The fifth column shows how many percent R2 is measuring more/less than R3. The two last columns denote the average and maximum wind speed, denoted WS, at AWS-1 when precipitation is present.*

4 m/s, respectively. However, the wind speed is measured close to R3, but 3.46 meters above ground level. Assuming a logarithmic variation of wind speed with height in the surface layer, the actual wind speed at the rain gauge R3 (0.64 meters above ground) will be distinctly lower. However, for this wind direction the wind speed at the measurement height is expected to be more representative for R2, because of the track the wind takes over open water with few obstacles. The highest wind speeds are existent for wind directions between 165°-195°, meaning that R2 probably experiences the highest undercatch in these directions. It is therefore uncertain whether R2 or R3 are measuring the highest true precipitation amount for this interval. For wind directions between 195°-210°, R2 and R3 have measured approximately the same. However, the maximum wind speed was 9.8 m/s, indicating that R2 might measure higher true precipitation than R3. In the intervals from 210°-240°, R2 has measured more than R3. A reason for this might be that the cliff located close by at the western and southwestern side of R2 is, to some extent, blocking the wind from this direction. R2 may because of this experience lighter wind, and therefore measure higher amounts than R3. In wind directions from 240°-270°, R3 is again measuring more than R2. When the wind has a westerly to north-northwesterly direction, R2 is measuring more than R3. However, the wind speed is small for these directions, and the precipitation is assumed to be

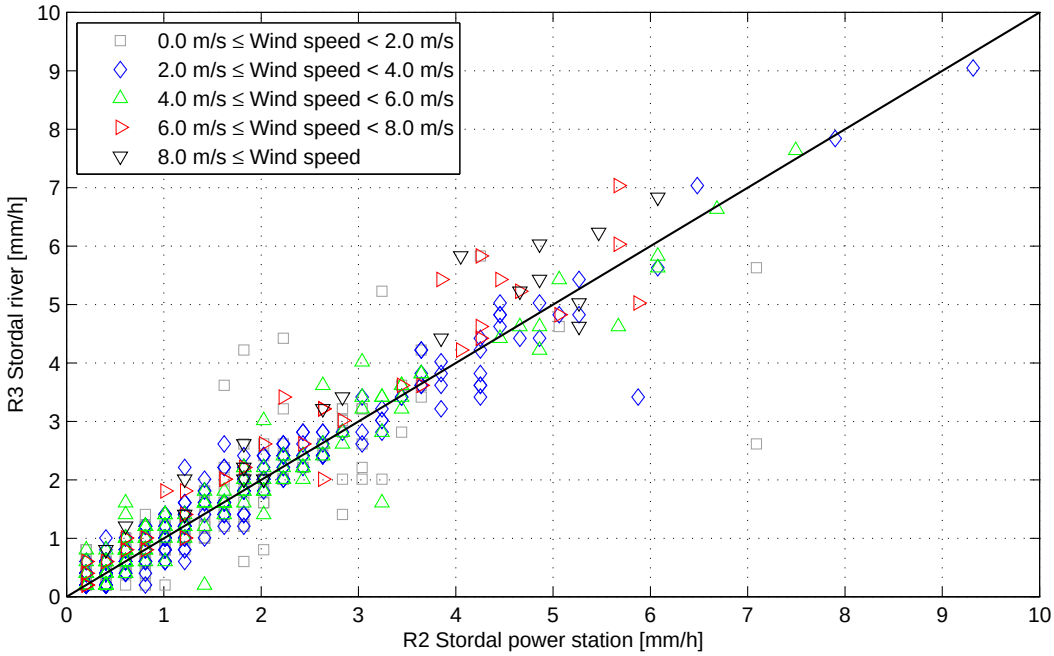

Figure 35: *R3 versus R2 for precipitation events above 0.0 mm/h at both stations. The colors denote the wind speed at AWS-1. The black line is the 1×1 ideal curve.*

wind speed (ws) interval	a	b	r	acc. prec. R2	acc. prec R3	# events
0.0 m/s ≤ ws < 2.0 m/s	0.87	0.12	0.88	325.1 mm	321.0 mm	324
2.0 m/s ≤ ws < 4.0 m/s	0.95	0.10	0.98	427.0 mm	435.4 mm	292
4.0 m/s ≤ ws < 6.0 m/s	0.94	0.13	0.97	211.5 mm	216.5 mm	126
6.0 m/s ≤ ws < 8.0 m/s	1.04	0.26	0.96	93.0 mm	106.5 mm	37
8.0 m/s ≤ ws	1.01	0.48	0.96	60.8 mm	70.5 mm	19

Table 8: *Linear regression (y=ax+b) for the different wind speed intervals in Figure 35. a = slope, b = value where the line crosses the y-axis, r = correlation coefficient. Column five and six contain accumulated precipitation for the different wind speed intervals for R2 and R3, respectively. The last column gives the number of events.*

from shower activity. For wind directions between 330° - 120°, only a few precipitation events with a small amount are measured. Undercatch due to wind can be neglected in these intervals.

Figure 35 shows a scatter plot of R3 versus R2 for precipitation events above 0.0 mm/h for both stations, divided into different wind speed intervals for AWS-1. Table 8 gives an overview of the best linear fit and the correlation coefficient for the different intervals. Because of different criteria, the sums are not consistent with Table 7. For wind speeds higher than 6.0 m/s, the best fitted line is situated approximately parallel, but

somewhat higher than the ideal curve. This indicates the tendency for R2 to measure smaller amounts than R3 for high wind speeds, and therefore R2 is assumed to experience undercatch due to wind. For wind speeds between 0-2 m/s, the slope is smaller than one, indicating a weak tendency for R2 to measure larger amounts than R3. For wind speeds between 2.0 m/s - 6.0 m/s, the best fitted line is approximately equal to the ideal line. The correlation, r, between R2 and R3 is especially good for wind speeds above 2.0 m/s, and somewhat lower for wind speeds between 0 - 2.0 m/s.

As stated in section 3.1, the accuracy of the HOBO rain gauges is ±2.0 % when doing tests in a laboratory. However, in the field the uncertainty increases (see section 5.1). Several of the intervals in Table 7 contain small amounts and few events, and a clear conclusion of the influence caused by the cliff will be difficult to achieve based on this short measurement period. R2 measured somewhat less than R3 in the wind direction interval 165°-195°. However, this interval contains the highest wind speed and for high wind speeds R2 is experiencing undercatch compared to R3. For wind between 210°-240°, the cliff might be blocking high wind speeds at R2, leading to higher precipitation amounts at R2 than R3. For wind speeds below 2.0 m/s and for wind directions between W-NW, R2 is showing a small tendency to measure larger amounts than R3. Altogether, not any large distinctions are found between the rain gauge located nearby the power station, R2 and the rain gauge at the river, R3, and the location of the RBKK rain gauge is therefore assumed representative for the Stordal area.

When further on comparing precipitation measurement at Stordal with other locations, the rain gauge R3, situated by the river at Stordal, will be used as a reference station. This rain gauge is decided to be best suited because of the expected lower undercatch due to wind, compared to R2.

7.3 Comparison: R3 and the ECMWF model

BKK uses a single point forecast from the ECMWF model interpolated to the Stordal location to estimate the expected precipitation in the catchment area. This section compares the ECMWF precipitation forecast and the observed precipitation at R3, Stordal river. Wind forecasts from the ECMWF model compared with observed winds at AWS-1 and AWS-2 have already been discussed in section 6.3.2 and 6.3.3.

Figure 36 shows the accumulated precipitation from the ECMWF model compared to the observed precipitation for R3. The figure shows that the forecasted precipitation is largely congruent with the observation, and during the measurement period from April to October 2008, the model forecasted in total 4.8 % more precipitation than observed. With a view to the fact that the HOBO rain gauges may underestimate precipitation in terrain compared to true precipitation (see section 5.1), this correspondence is very good.

In Figure 37, histograms for 1 h, 24 h and weekly precipitation amounts are presented. For hourly values, more dry events (0.0 - 0.1 mm) than forecasted are observed. However, in the three intervals from 0.1 - 2.0 mm, the model shows several more events compared to the observations. That means that the model predicts more hours with small precipitation amounts than observed. For hourly precipitation amounts above 2.0 mm, the model forecasts fewer events. This effect is also illustrated in Figure 38, which as an example indicates a smoothing by the model that neither captures the precipitation tops nor the short stops in rainfall. The same tendency is also seen for

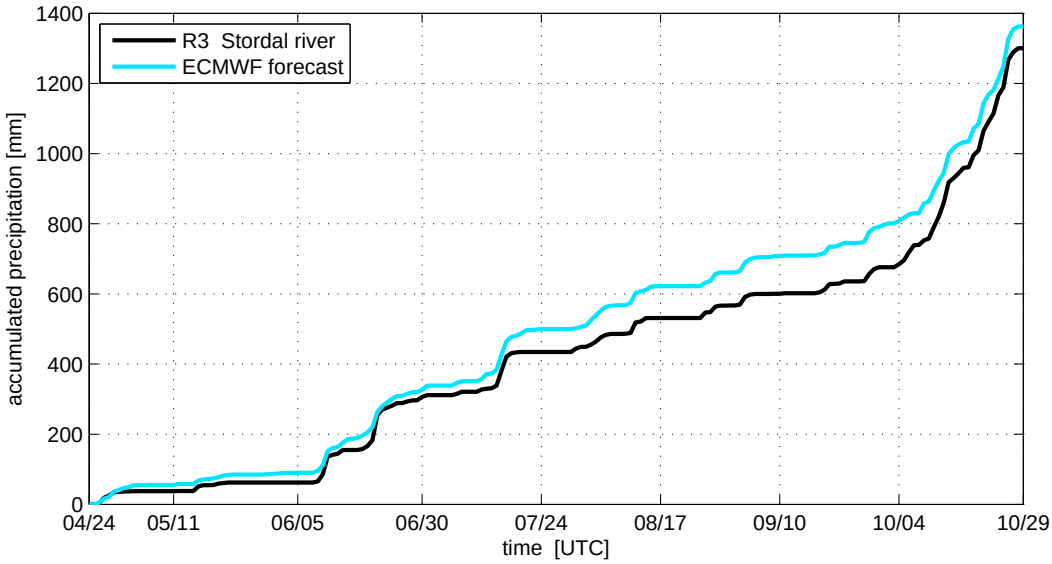

Figure 36: *Accumulated precipitation for R3 Stordal river and the ECMWF forecast in the period from April 24th to October 29th 2008.*

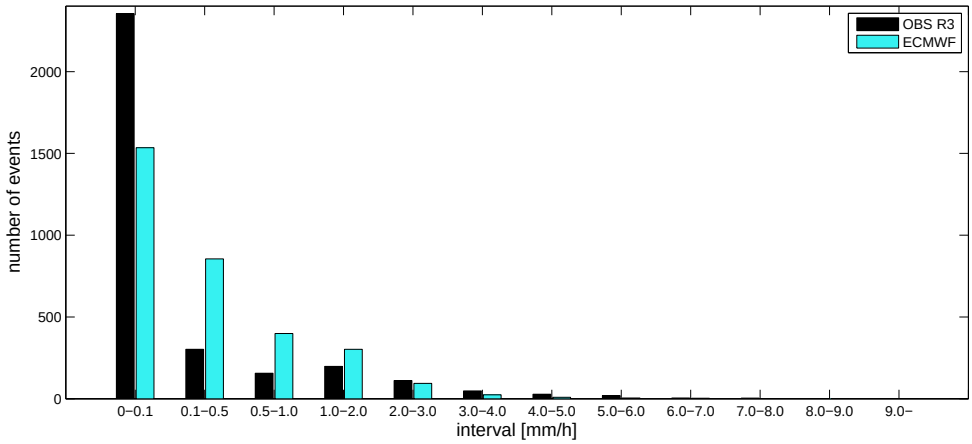

(a) Histogram. (mm/h)

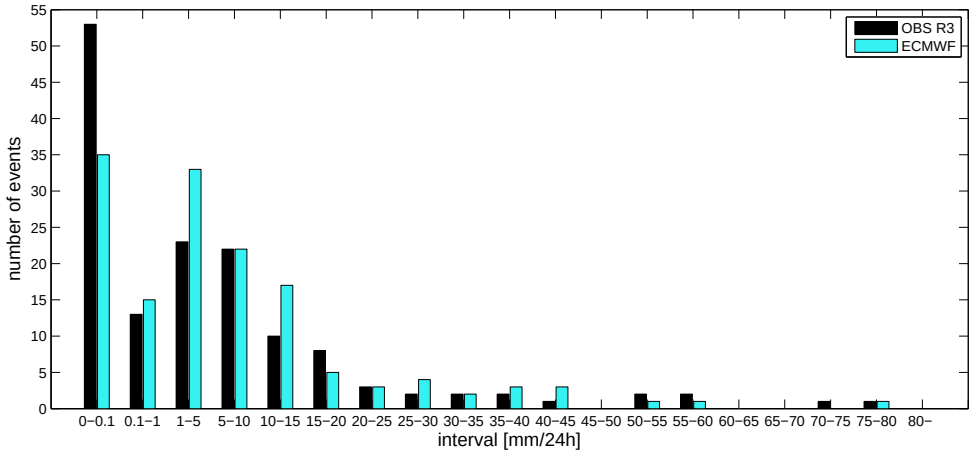

(b) Histogram (mm/24h)

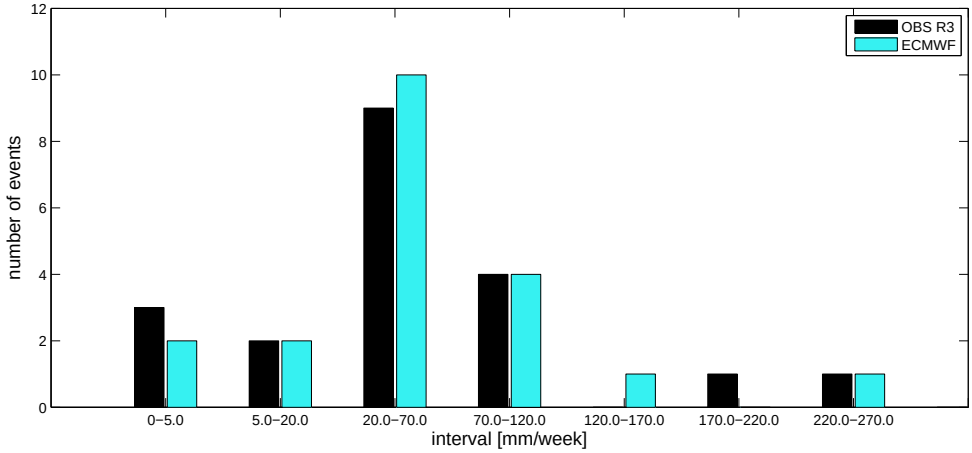

(c) Histogram (mm/week)

Figure 37: *Histogram for R3 Stordal river and ECMWF for 1 h, 24 h and weekly precipitation values. To reduce solid and mixed precipitation, hours when the temperature at AWS-1 is below 2 °C are omitted. These hours are also omitted when calculating 24 h and weekly values. The amount in an interval is higher or equal to the lower boundary, and lower than the upper boundary.*

24 h values for small amounts (Figure 37(b)). For intervals above 50 mm/24 h, the ECMWF model has fewer events, while in the intervals 30-45 mm/h the model has the most events. However, the total numbers of both observed and forecasted events above 30 mm/24 h in Figure 37(b) are equal (11 events). In Figure 37(c), histograms concerning the accumulated precipitation for a period of seven days are presented. This shows that when accumulating over a period of time, which is highly relevant for hydro power energy production issues, the ECMWF model is largely commensurate with the observed precipitation distribution.

Table 9 shows the accumulated precipitation at R3 and forecasted by the ECMWF model for different wind direction intervals observed at AWS-2 Blåfjell. The number of events is written in parenthesis in the table. An event is an hour when precipitation is observed or forecasted. As expected due to the smooth manner of the ECMWF model, the total number of events for the model is much higher compared to the observations. The solid lines in 39 visualize the main contents of the table. In the wind direction intervals at AWS-2 from 330°-120°, only few events and small precipitation amounts are present. However, the model has forecasted more precipitation than observed in all of these intervals. The model is also overestimating in the intervals from 120°-150°, 240°-270° and 300°-330°, but roughly speaking, the percentage is smaller than for the north-northeasterly intervals. For a north and northwesterly wind direction, precipitation in the form of showers is common. Due to the coarseness of the model, the precipitation in form of showers will be spread over a large area, while locally the shower might not hit the rain gauge. In the interval where most precipitation is observed (180°-210°), the model forecasted 100 % of the observed precipitation. Also in the intervals with the second most (150°-180°) and third most (210°-240°) precipitation amounts, the model is very good, with respectively 94 % and 98 % of the observed precipitation. This shows that the ECMWF model for the location Stordal performes especially good for the wind direction interval south-southeast to southwest, where the main precipitation is observed.

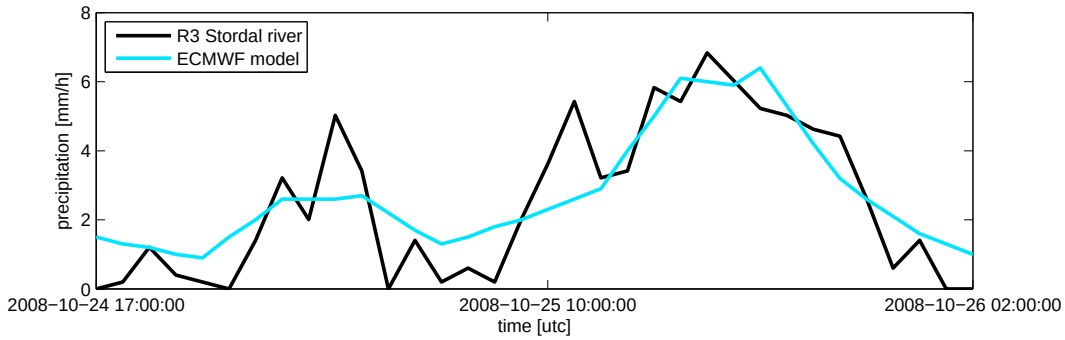

Figure 38: *Illustration of the smoothness of the ECMWF model. Precipitation event from 24th of October 17 UTC to 26th of October 02 UTC.*

Wind direction [°] AWS-2	Accumulated prec. [mm] R3	# events	ECMWF	# events	Percentage of R3 (%)
0 < wd ≤ 30	11	(5)	17	(57)	155 %
30 < wd ≤ 60	4	(2)	8	(21)	200 %
60 < wd ≤ 90	0	(1)	6	(12)	- %
90 < wd ≤ 120	8	(9)	16	(34)	200 %
120 < wd ≤ 150	39	(54)	68	(116)	174 %
150 < wd ≤ 180	284	(203)	268	(378)	94 %
180 < wd ≤ 210	519	(351)	517	(589)	100 %
210 < wd ≤ 240	164	(103)	161	(157)	98 %
240 < wd ≤ 270	40	(45)	51	(76)	128 %
270 < wd ≤ 300	37	(37)	31	(62)	84 %
300 < wd ≤ 330	45	(47)	52	(124)	116 %
330 < wd ≤ 360	9	(13)	22	(53)	244 %
sum	1160	(870)	1217	(1679)	105 %

Table 9: *Accumulated precipitation at R3 and forecasted by the ECMWF model for different wind directions intervals at AWS-2 Blåfjell. Column two and four denote the accumulated precipitation at R3 Stordal river and forecasted by the ECMWF model when the observed wind direction at Blåfjell is within the specific interval. Only wind directions when the wind speed at AWS-2 is higher than 0.5 m/s are considered. The last column gives the percentage amount of R3, rounded to the nearest integer.*

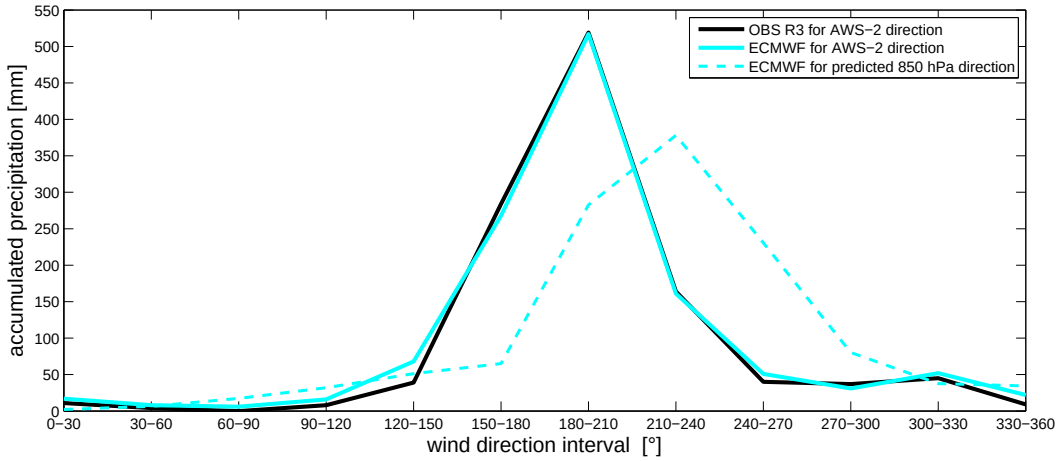

Figure 39: *The solid lines illustrate the accumulated amounts versus wind direction at AWS-2 from Table 9. The broken line shows the accumulated modeled amount with respect to the forecasted wind direction from the ECMWF model at 850 hPa (not shown in table).*

The broken line in Figure 39 gives the accumulated forecasted amount for the forecasted 850 hPa wind directions from the ECMWF model. As expected, on the basis of Figure 25(b), Figure 27(b) and Figure 28(a) in section 6.3, the average wind direction from the model is about 30 degrees clockwise and the distribution is wider compared to those based on the observed wind direction.

The ECMWF model appears as smooth, meaning that the precipitation gets apportioned over time. Fairly large deviations between observed and forecasted precipitation are seen in hourly histograms. For daily amounts this improves, and for weekly events the correspondence is good. The correlation coefficient for observations compared to forecast for 1 h, 24 h and weekly events are 0.73, 0.94 and 0.99, respectively. When verifying the model based on observed wind direction, very good correspondence for the accumulated precipitation was found in the intervals where the bulk precipitation is observed. This, and the fact that the model estimated only about 5 % more during the period, indicates that the models volume forecast is very good. Altogether, a single point forecast from the ECMWF model seems well suited to describe the major part of precipitation at Stordal. However, the representativeness of the observed and predicted precipitation at Stordal must be seen in relation to the observed precipitation at other locations in the MHS.

8 Precipitation distribution in the Matre Hydro System

This chapter deals with the investigation of the precipitation distribution in the Matre Hydro System (MHS) compared to the reference station R3 Stordal river. Local siting of the rain gauges, height gradients and potential horizontal gradients will be discussed. First of all an adjustment of the precipitation data set is presented.

8.1 Adjusted time series

In some periods towards the end of the measurement campaign, the temperatures were alternating above and below 0 °C, and periods of snow accumulating and melting occured. The main portion of the precipitation amount arrived during the last half of the measurement campaign. To minimize potential errors related to solid precipitation, an adjusted time-series of the precipitation has been derived.

Temperature measurements were performed at AWS-1 Stordal, situated 480 meters above sea level and at AWS-2 Blåfjell, situated 898 meters above sea level. Because of this, a temperature gradient between AWS-1 and AWS-2 has been calculated to give the other rain gauge stations an artificial temperature. The gradient has been derived as:

$$\Delta T = \frac{T(AWS2) - T(AWS1)}{z(AWS2) - z(AWS1)}, \tag{5}$$

where T denotes the temperature and ΔT the vertical temperature gradient, while z is the elevation above sea level. The temperature at a given elevation is therefore calculated as

$$T(Rx) = T(AWS1) + [z(Rx) - z(AWS1)] \times \Delta T, \tag{6}$$

where Rx denotes the different rain gauge locations specified in Table 6, when x is a number between 1 - 20 (except 3 and 6, which are the sites where the temperature measurements are performed).

To minimize effects of solid precipitation, only precipitation events when the calculated temperature is above 2 °C at each site are included in the adjusted time series.

8.2 Precipitation distribution

The adjusted precipitation distribution for the MHS during the period when all the rain gauges were operating, is presented in Table 10, and visualized in Figure 40. Only hourly values where the calculated temperature (see section 8.1) for all rain gauge locations has been above 2 °C, have been added up. In practice, due to decreasing temperature with height during precipitation events, it is reasonable that AWS-2 possesses the lowest temperature. This means that data from rain gauge stations lower than AWS-2 will most likely have temperatures higher than AWS-2. Due to this, solid precipitation is assumed tolerably well sorted out of the data material. In the following, the precipitation data presented in Table 10 will be discussed with the aid of scatter and ratio plots. A vertical gradient of precipitation will not be taken into account in this section.

Location	Acc. precipitation	% of R3	Height difference
R1 Matre	632.2 mm	91.6 %	-458 m
R3 Stordal,river	690.5 mm	100.0 %	0 m
R4 Fosse	774.2 mm	112.1 %	-62 m
R5 Skrikeberg[3]	213.5 mm	72.2 %	- 445 m
R6 Blåfjell	766.3 mm	111.0 %	+418 m
R7 Årsdalsvatn	579.6 mm	83.9 %	+ 3 m
R8 Fridalsvatn	683.7 mm	99.0 %	+ 229 m
R9 Krokevatn	686.8 mm	99.5 %	+ 133 m
R10 Langevatn	828.2 mm	120.0 %	+ 191 m
R11 Stølsdalen	664.4 mm	96.2 %	+ 136 m
R12 Stølsvatn	618.0 mm	89.5 %	+ 91 m
R13 Gamle Stølsleitet - east	797.8 mm	115.5 %	+ 287 m
R14 Skorvane	919.7 mm	133.2 %	+ 345 m
R15 Høgetjørnane	760.1 mm	110.1 %	+ 308 m
R16 Oppedal[4]	525.0 mm	76.0 %	- 420 m
R17 Gamle Stølsleitet - west	850.1 mm	123.1 %	+ 176 m
R18 Hareheia	776.2 mm	112.4 %	+ 183 m
R19 Årnesstøl	403.3 mm	58.4 %	+ 222 m
R20 Hornsetvatn	757.5 mm	109.7 %	+ 142 m

Table 10: *Accumulated precipitation from 00 utc 30th of June to 08 utc 29th of October 2008. Only precipitation hours when the calculated temperature (section 8.1) for all rain gauge stations has been above 2 °C are included. Column three contains the percentage of the reference station R3. The last column gives the height difference from R3.*

[3]Skrikeberg. Stopped measuring 10th of September 2008. The accumulated precipitation at R3 for the same period was 295.9 mm, and the percentage amount of R3 is calculated from this value.

[4]Oppedal. Stopped measuring 28th of October 2008. However, no precipitation is registered at any station in the last 24 h.

In Figure 41 - Figure 46 the adjusted time series described in section 8.1 are utilized. This means that only precipitation events when both R3 and the location that it is compared with have temperatures above 2 °C, are included. This means that the precipitation data set of R3 used is variable for each compared station. The Figures 41 - 43

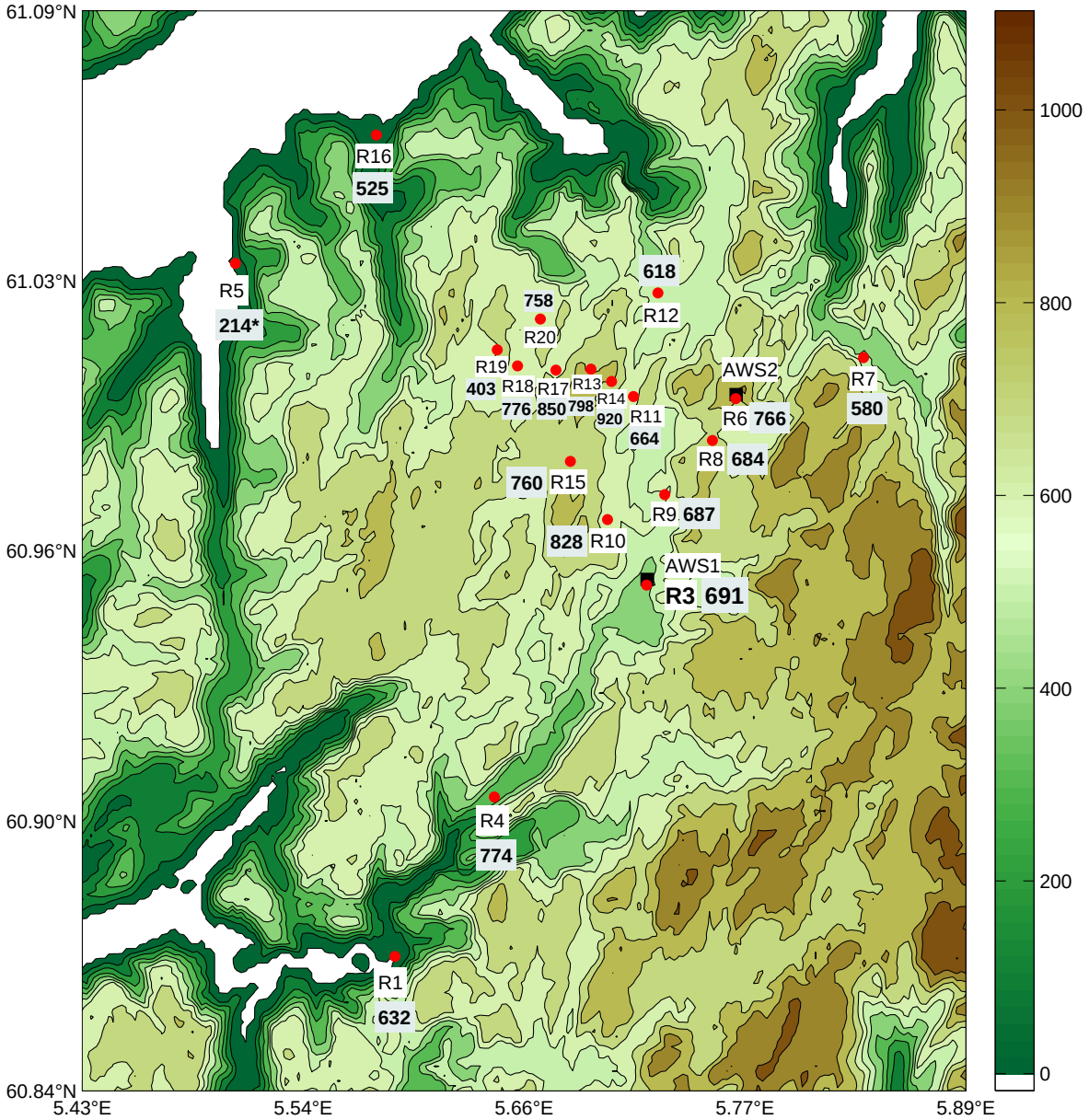

Figure 40: *Visualization of Table 10. Accumulated precipitation [mm] during the measurement period in the MHS when temperatures have been higher than 2 °C. *R5 Skrikeberg stopped measuring 10th of September. The accumulated precipitation at R3 for the same period was ≈ 296 mm. The colorbar denotes the elevation above sea level [m].*

show scatter plots for every location compared with R3 Stordal river for different wind speeds at AWS-2. For the scatter plots, 24 h values have been utilized. Only hours when both the locations have measured precipitation are added in the 24 h values, and only days when the precipitation amount is higher than 1.0 mm/24 h are included in the scatter plots. The wind speed is the average wind speed for the hours in the 24 h period which measured precipitation. The black thin line is the one-to-one ideal line and the thick black is the linear fit for events with speed $\geq$ 9.0 m/s. The grey dashed line gives the 10 % deviation from the ideal line. As seen in the Figures 41 - 43, the high precipitation amounts are almost always related to the high wind speeds (the black and grey dots), and low precipitation amounts to low wind speeds.

Ratio plots for every location compared with R3 for different wind directions and wind speeds at AWS-2 are presented in Figure 44-46. For the ratio plots, 1 h values are used to prevent smoothing of the wind direction. Only hours when the measured precipitation is above 1.0 mm/h are included in the figures. As seen from these figures, the highest wind speeds at AWS-2 Blåfjell is only present in a very narrow band around 180°. The accumulated precipitation for each rain gauge location, classified for different wind directions at AWS-2 Blåfjell, is seen in Table 11. In the table, only hourly values when the calculated temperature (see section 8.1) for all rain gauge locations has been above 2°C and the wind speed at AWS-2 above 0.5 m/s have been included. For the wind directions of main precipitation amount (165°-225°), the values larger (smaller) than R3 Stordal river have been highlighted in red (blue). The rain gauge locations will for the most part be discussed in ascending order based on the particular rain gauge number. However, rain gauges located close together will be discussed simultaneously.

Based on Table 10, Figure 43(e) and 46(e), the rain gauge located at Årnesstøl, R19, shows considerably smaller amounts than R3 and the other rain gauges. This rain gauge is, like the others, controlled in a laboratory after the field campaign (see section 4.4), and the data are adjusted based on the calibration results. No particular errors or defects were found. Therefore, the small precipitation amounts measured at this location are believed to be due to unfortunate rain gauge placing. When studying Figure 43(e), a tendency of points close to the ideal line for low wind speeds is seen, while for higher wind speeds, Årnesstøl measures much smaller amounts than Stordal. The rain gauge is located near the top of a steep slope, oriented towards the main wind direction. A local speed up of the vertical wind component close to the mountain top might explain the small amount measured at this station. No further interpretation of this rain gauge station will be performed.

R1 Matre is the southernmost rain gauge in the measurement area. The rain gauge is located at the farther end of a deep, narrow valley, surrounded by high mountains in every direction, except on the western side where a fjord comes in. R1 has measured approximately 92 % of the amount at R3. When studying Figure 44(a), R1 Matre shows a tendency to measure higher amounts than R3 for a wind directions between 135°-165° (Also seen in Table 11). For the main wind directions between 165°-225°,

R3 measures more than R1 (Table 11). R4 Fosse is located in a southwesterly position in the measurement area, with higher terrain on the western side. R4 has measured approximately 12 % more than R3 during the time considered in Table 10. R4 has measured more than R3 in most of the wind directions intervals, except for northerly directions (315°-15°) (Table 11), however, only small amounts are registered from this direction. R5 Skrikeberg was the westernmost rain gauge station in the campaign. Unfortunately this rain gauge stopped measuring on the 10th of September. However, for the period that data are available, R3 has measured about 28 % more than R5. According to Table 11, R5 has measured less or approximately the same as R3 for all wind directions. Because of the shortened time series for R5, the rain gauge station is omitted when considering height and horizontal gradients.

R6 Blåfjell has measured about 111 % of the amount at R3. The vegetation around R6 is low or almost non-existing, and the rain gauge is therefore well exposed to wind. The wind speed at AWS-2 has during the measurement campaign been significantly higher than AWS-1 (Figure 22). Undercatch when high wind speeds are present is very likely at this station. Still, when considering Figure 41(d), R6 shows a tendency to measure higher amounts than R3 when high wind speeds are present. For the wind direction interval from 165°-195°, R6 has measured more precipitation than R3. In the direction from 195°-225°, larger amounts are found for R3 (Table 11). This tendency of shift for wind directions from south to southsouthwest is seen in Figure 44(d). R6 has measured higher amounts than R3 for westerly to northwesterly directions (Figure 44(d)). However, only small amounts are present for these directions (Table 11).

R7 Årsdalsvatn is the easternmost station, and has measured only 84 % of the amount achived at R3. R3 has measured more than R7 in most of the wind direction intervals, except in the northern interval. However, a great part of the precipitation from 345°-15° is expected to have happened during a convective case situation (see section 9.2). Approximately the same preciptiation amounts are measured at R8 Fridalsvatn and R3. For high wind speeds, mainly from a southerly direction, Figure 41(f) and 44(f) show that R3 measures higher amounts than R8. For a westerly to northerly direction, R8 has measured higher amounts than R3 (Table 11). The corresponding figures for R9 Krokevatn show the same tendency as for R8.

R10 Langevatn is located northwest of R3, somewhat southwest in the main measurement area, and has measured about 20 % more than R3. When studying the observed precipitation at this location, R10 has measured higher amounts than R3 in almost all of the registered 24 h events (Figure 42(b)), regardless of wind speed. A clear tendency for this is also seen when studying the 1 h events (Figure 45(b)). R15 Høgetjørnane is located not far from R10, and has measured overall approximately 110 % of the amount of R3. Figure 46(a) shows that when hourly wind speeds above 20.0 m/s are present, R3 measures more compared to R15. For 24 h values (Figure 43(a)), the high speed events are located closer to the 1-to-1 ideal line than at R13, R14, R17, R18 and R20 (discussed later), where R3 measures considerably smaller precipitation amounts for

high wind speeds. When studying Table 11, it is clear that R15 has measured almost the same as R3 for wind directions between 165°-195°, while for directions between 195°-225°, R15 has measured more. R15 is situated almost at the mountain top, but with a little elevation nearby at the western side, and the rain gauge is therefore well exposed for wind directions from south. R15 is therefore believed to experience, as R19 Årnesstøl, undercatch when high wind speeds are present. The true precipitation amount at this location is assumed to be somewhat higher.

R11 Stølsdalen and R12 Stølsvatn have received 96 % and 90 % of the amount at R3, respectively (Table 10). When comparing R12 and R3, higher amounts are present at R3 for the main wind direction (165°-225°). In the interval from 195°-225°, R3 measured more, and the deviation between the amount measured at R12 and R3 is much larger. This is the same tendency as seen for R6 Blåfjell, and is also present for R11. The Figures 45(c) and 45(d) illustrate this. From a westerly to northwesterly wind direction, higher amounts are present at R11 and R12 than R3.

The rain gauges R13 Gamle Stølsleitet east, R14 Skorvane and R17 Gamle Stølsleitet west are located fairly close, with about 0.7 km between R14 and R13, and 1.0 km between R13 and R17. These rain gauge stations have measured higher amounts than R3. However, the rain gauges are located at a much higher altitude than R3. When studying the scatter and ratio plots for R13, R14 and R17 (Figure 42(e),42(f), 43(c)), 45(e),45(f) and 46(c)), it is clear that the high wind speed events give greater amounts at these locations than at R3. R13 shows a tendency to measure smaller amounts than R14 and R17. The location of R13 is not believed to be more exposed for wind than the two others, and this local variability is hard to explain. Also for these stations, a higher amount of precipitation is present compared to R3 for the southern wind direction interval. R3 has measured more than R13 and R17 for directions between 195°-225°. This lower percentage amount of the R3 value in this direction is also present for R14 (Table 11). R18-Hareheia and R20-Hornsetvatn have measured about 10 % more than R3. However, like R13, R14 and R17, when high wind speeds are present, higher amounts are registered for R18 and R20 compared to R3. The tendency of shift in precipitation amounts from 165°-195° to 195°-225° compared to R3 is seen in the ratio plots for these locations. When studying the rain gauges R13, R14, R17, R18 and R20 in Table 11, a clear tendency for lower amounts at R3 is present for southwesterly to northwesterly wind directions.

R16 Oppedal is located at the northern side of the elevated main area. This station is therefore not freely exposed to the main wind direction, and measures smaller amounts than R3 for these directions. For wind directions between 255° and 315°, R16 measures higher amounts than R3 (Table 11).

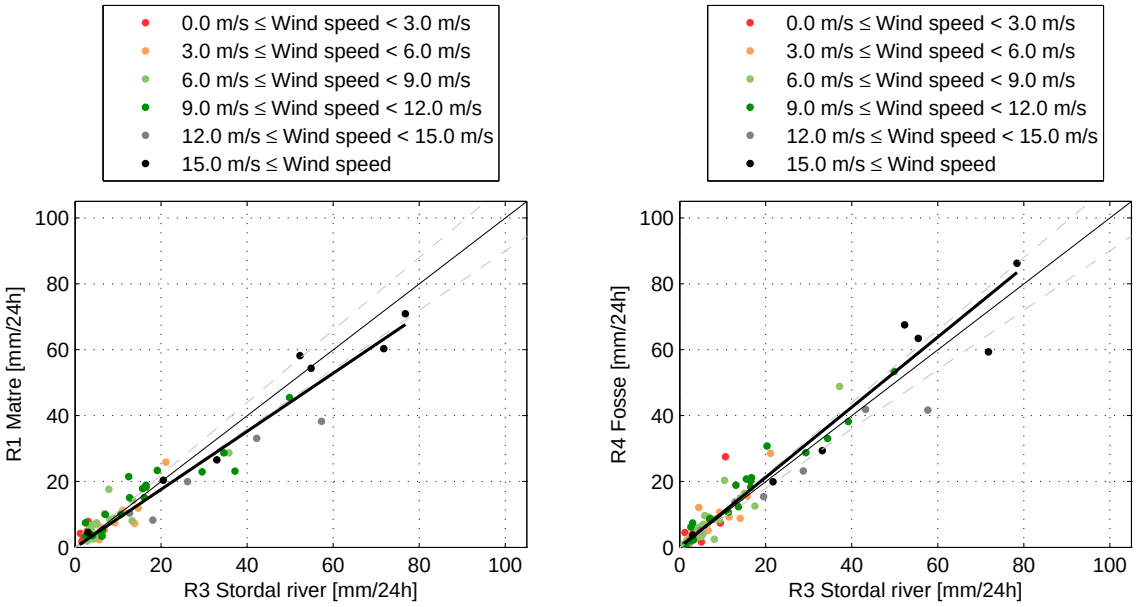

(a) R1 Matre versus R3 Stordal river.

(b) R4 Fosse versus R3 Stordal river.

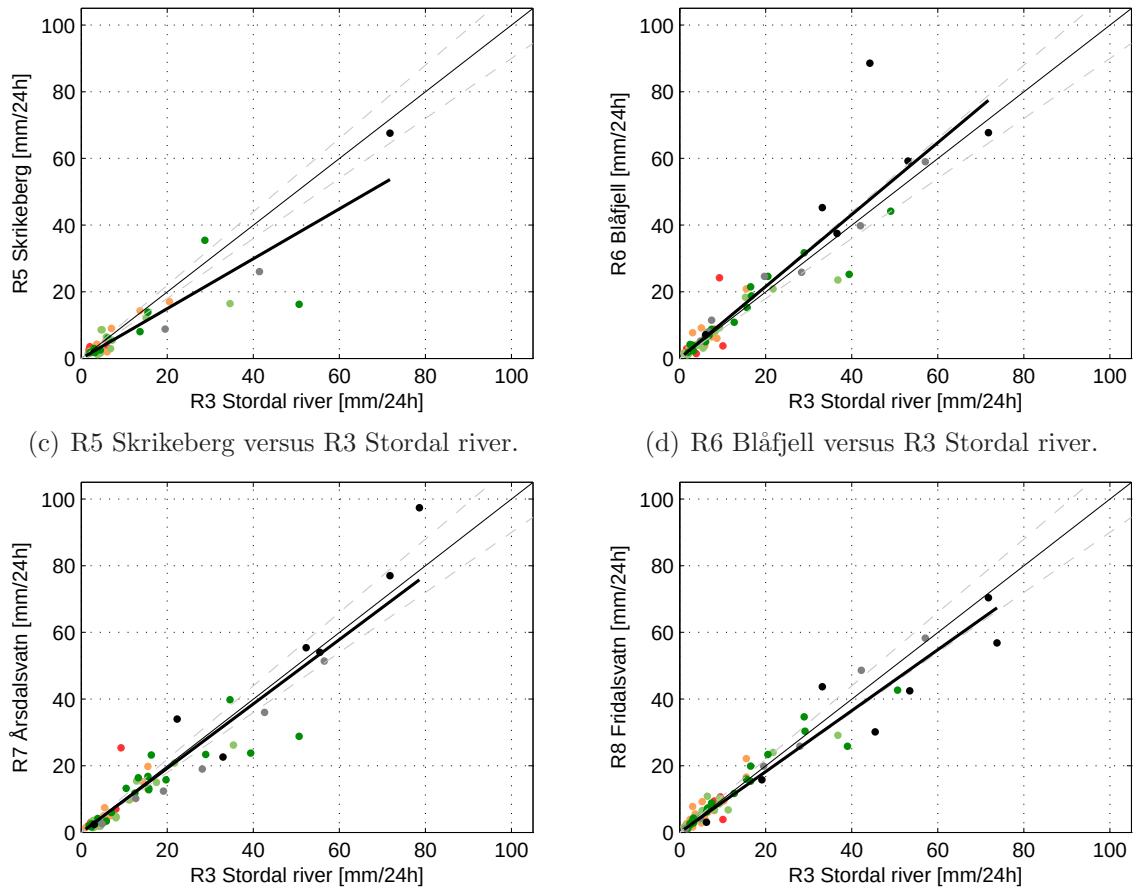

(c) R5 Skrikeberg versus R3 Stordal river.

(d) R6 Blåfjell versus R3 Stordal river.

(e) R7 Årsdalsvatn versus R3 Stordal river.

(f) R8 Fridalsvatn versus R3 Stordal river.

Figure 41: *Scatter plots of R1, R4, R5, R6, R7 and R8 versus R3-Stordal river. 24 h data from the adjusted time series are utilized.*

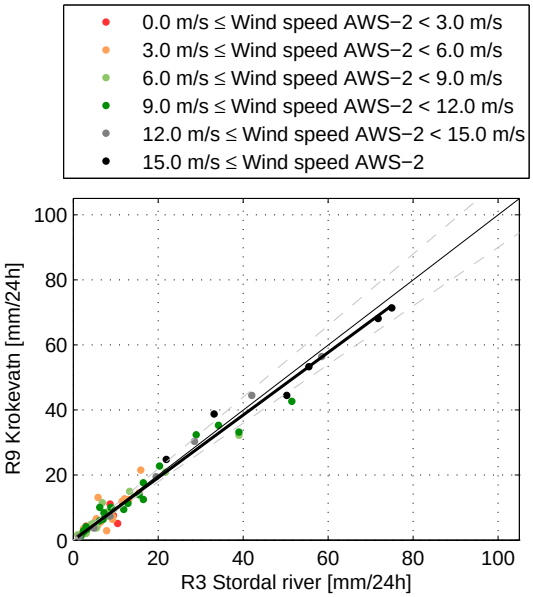

(a) R9 Krokevatn versus R3 Stordal river.

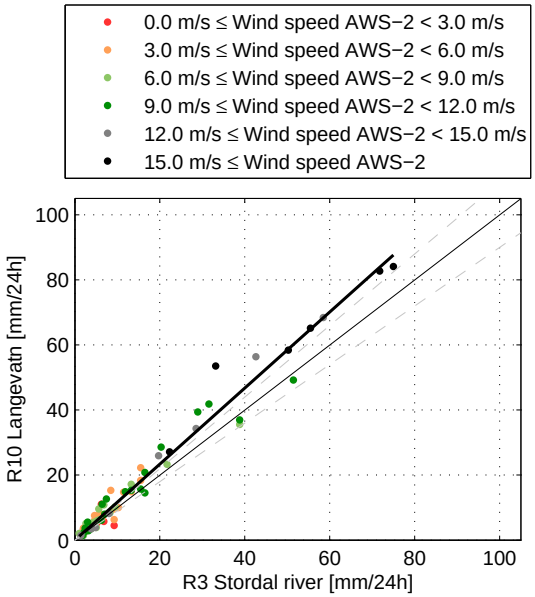

(b) R10 Langevatn versus R3 Stordal river.

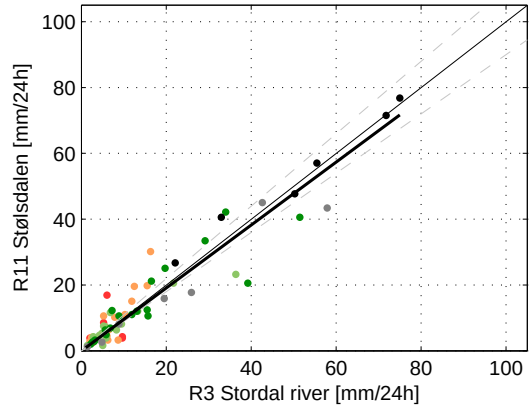

(c) R11 Stølsdalen versus R3 Stordal river.

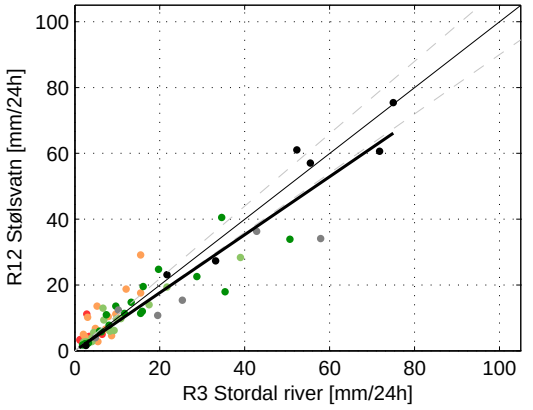

(d) R12 Stølsvatn versus R3 Stordal river.

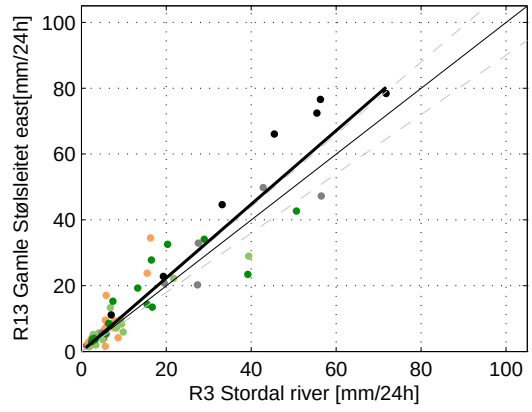

(e) R13 Gamle Stølsleitet east versus R3 Stordal river.

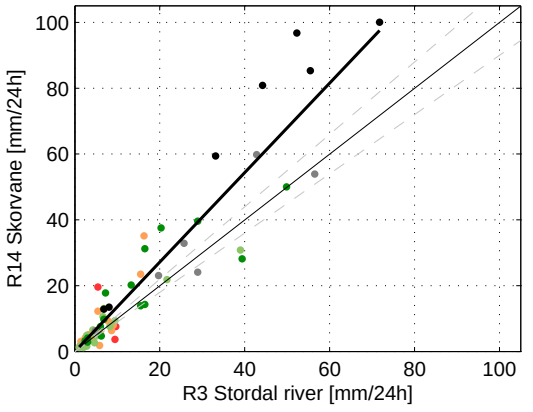

(f) R14 Skorvane versus Stordal river.

Figure 42: *Scatter plots of R9-R14 versus R3-Stordal river. 24 h data from the adjusted time series are utilized.*

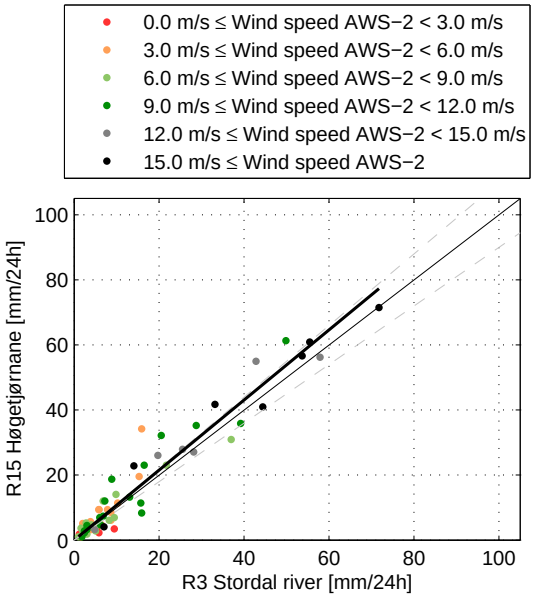

(a) R15 Høgetjørnane versus R3 Stordal river.

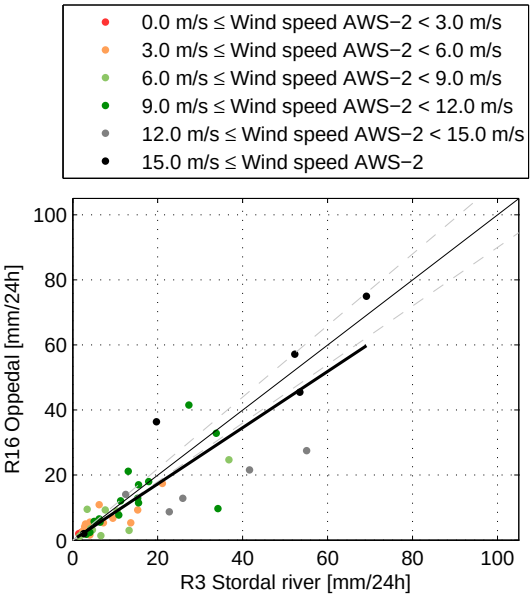

(b) R16 Oppedal versus R3 Stordal river.

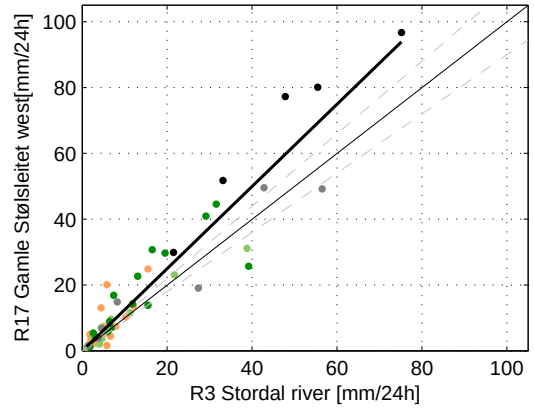

(c) R17 Gamle Stølsleitet west versus R3 Stordal river.

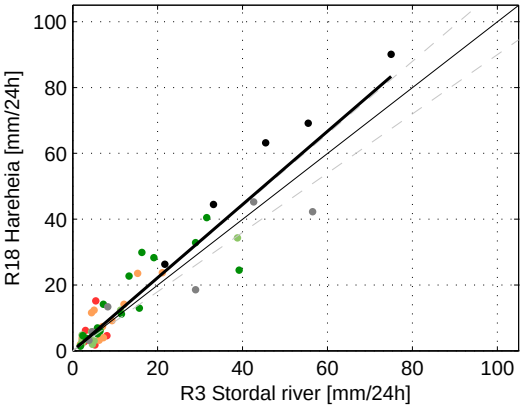

(d) R18 Hareheia versus R3 Stordal river.

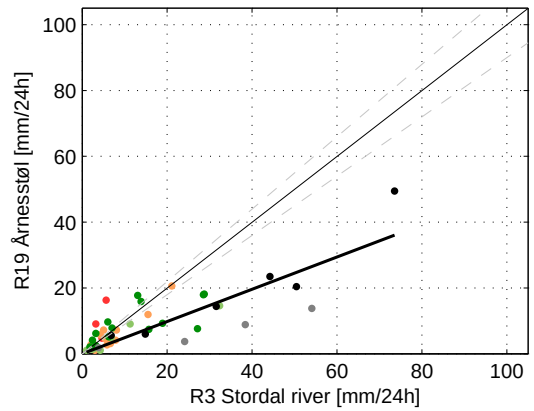

(e) R19 Årnesstøl versus R3 Stordal river.

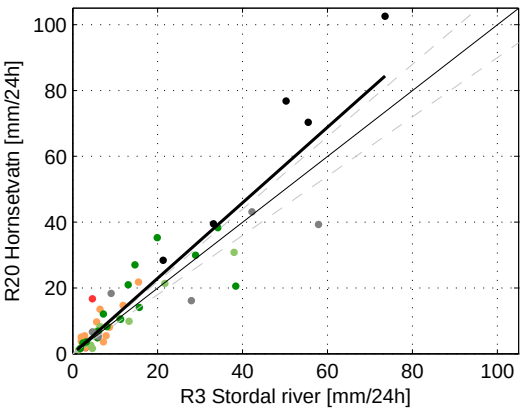

(f) R20 Hornsetvatn versus R3 Stordal river.

Figure 43: *Scatter plots of R15-R20 versus R3-Stordal river. 24 h data from the adjusted time series are utilized.*

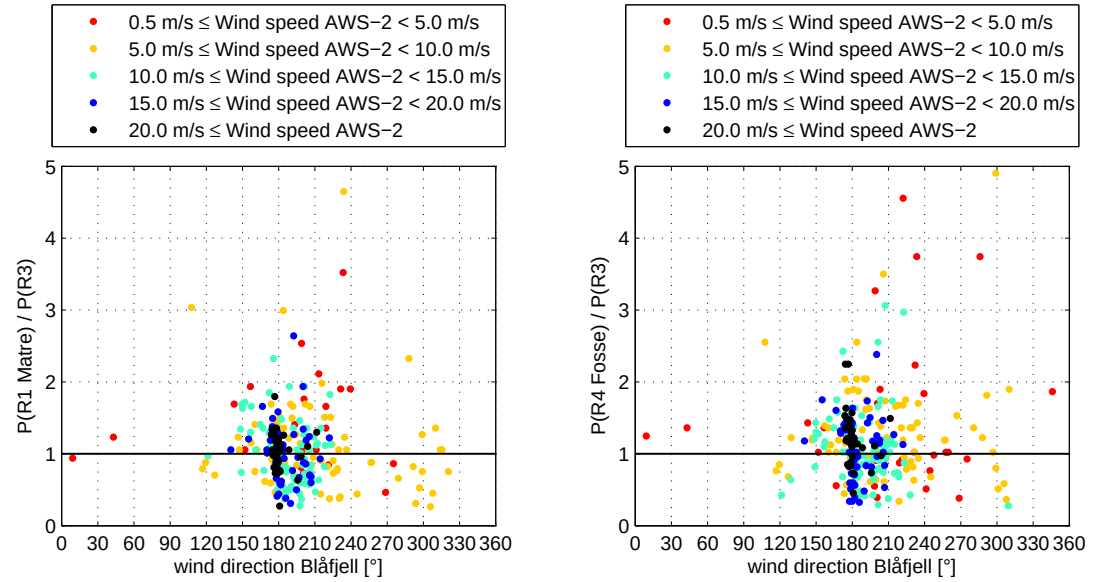

(a) Matre / Stordal river.

(b) Fosse / Stordal river.

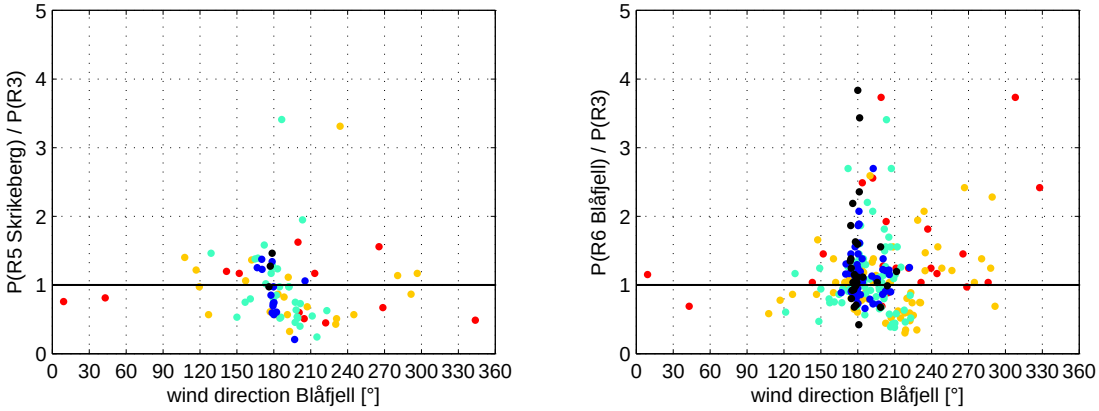

(c) Skrikeberg / Stordal river.

(d) Blåfjell / Stordal river.

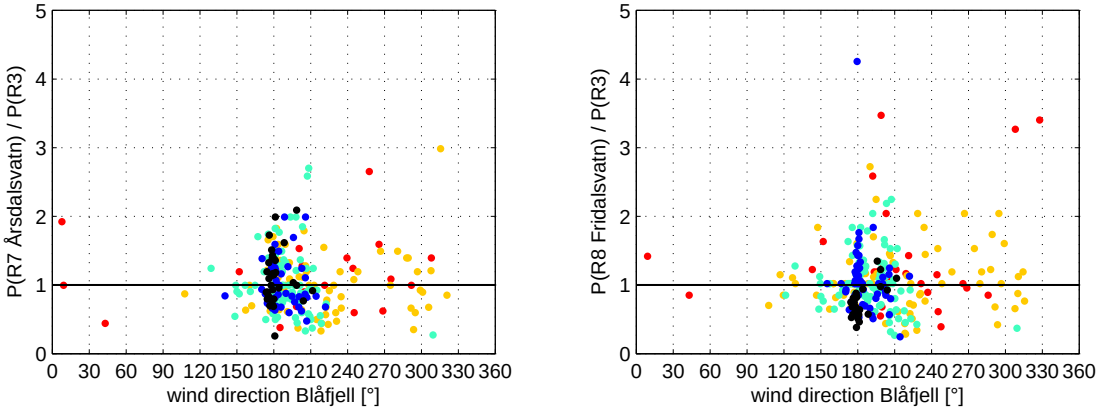

(e) Årsdalsvatn / Stordal river.

(f) Fridalsvatn / Stordal river.

Figure 44: *Ratio plots of R1-R8 (except R2) compared to R3 Stordal river. Hourly data from the adjusted time series are utilized. Only hours when the precipitation at both locations is above 1.0 mm/h are included.*

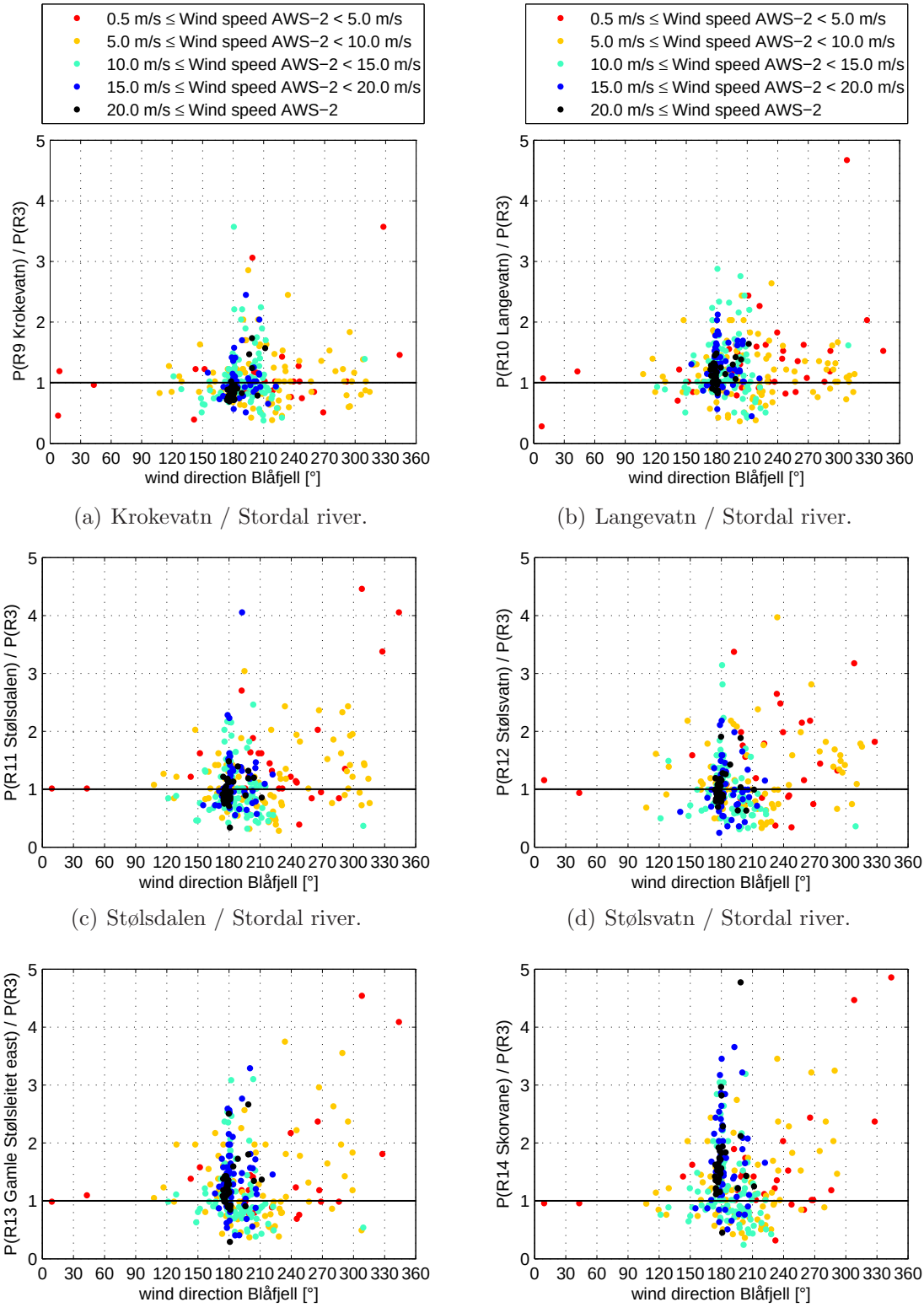

(a) Krokevatn / Stordal river.

(b) Langevatn / Stordal river.

(c) Stølsdalen / Stordal river.

(d) Stølsvatn / Stordal river.

(e) Gamle Stølsleitet east / Stordal river.

(f) Skorvane / Stordal river.

Figure 45: *Ratio plots of R9-14 compared to R3-Stordal river. Hourly data from the adjusted time series are utilized. Only hours when the precipitation at both locations is above 1.0 mm/h are included.*

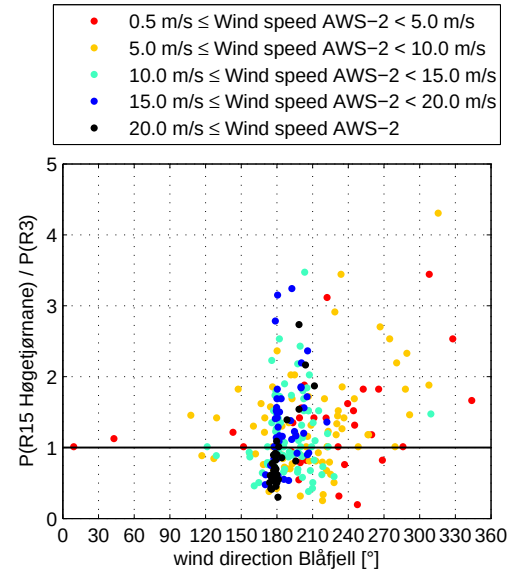

(a) Høgetjørnane / Stordal river.

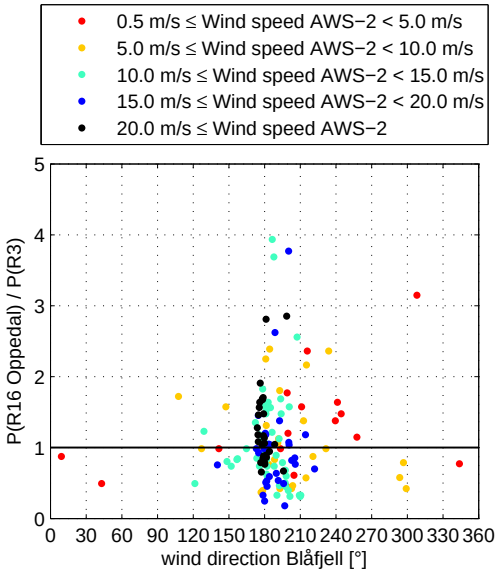

(b) Oppedal / Stordal river.

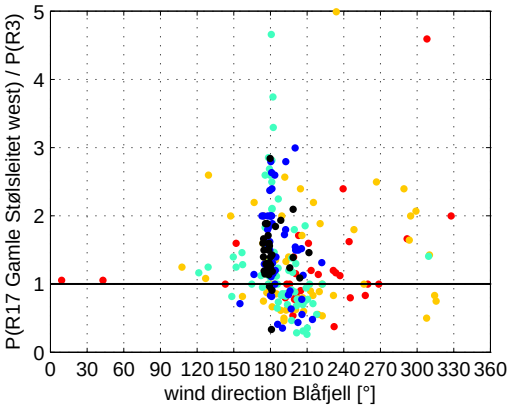

(c) Gamle Stølsleitet west / Stordal river.

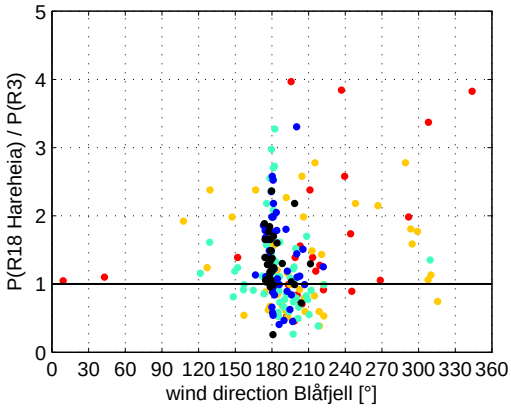

(d) Hareheia / Stordal river.

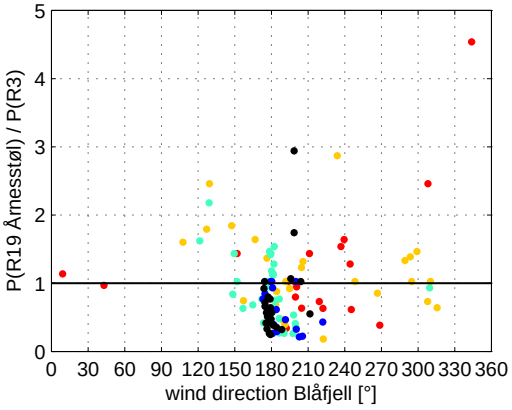

(e) Årnesstøl / Stordal river.

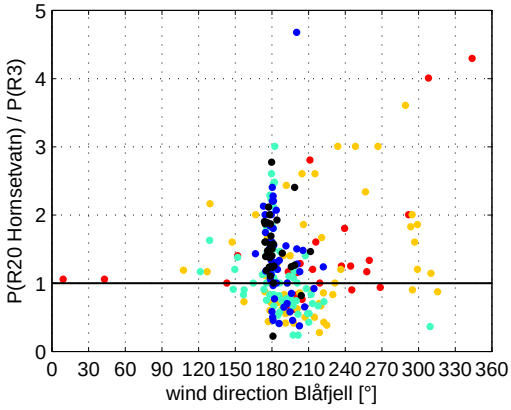

(f) Hornsetvatn / Stordal river.

Figure 46: *Ratio plots of R15-20 compared to R3-Stordal river. Hourly data from the adjusted time series are utilized. Only hours when the precipitation at both locations are above 1.0 mm/h are included.*

AWS-2	R1	R3		R4	R5[5]	R6	R7	R8	R9	R10	R11	R12	R13	R14	R15	R16	R17	R18	R19	R20
345 < wd ≤ 15	5	15	(15)	14	4	28	29	23	15	10	8	9	5	6	6	4	5	4	5	4
15 < wd ≤ 45	6	4	(4)	11	3	3	2	4	4	4	4	3	4	4	5	2	4	4	4	5
45 < wd ≤ 75	1	0	(0)	0	0	0	1	0	0	0	0	0	0	0	0	2	0	0	0	1
75 < wd ≤ 105	1	1	(1)	1	1	0	0	1	1	0	1	0	0	0	1	1	0	1	0	0
105 < wd ≤ 135	23	18	(18)	21	18	14	14	17	17	19	16	16	19	16	19	20	24	28	33	23
135 < wd ≤ 165	52	31	(22)	42	21	23	24	28	26	34	27	24	33	33	25	32	39	35	32	33
165 < wd ≤ 195	277	316	(105)	342	89	396	251	310	309	390	328	302	403	486	325	269	443	391	169	392
195 < wd ≤ 225	225	255	(100)	268	57	237	207	239	254	303	206	186	247	282	294	146	244	227	105	213
225 < wd ≤ 255	27	27	(13)	40	8	25	23	22	24	28	24	30	28	32	35	21	32	34	17	27
255 < wd ≤ 285	13	12	(8)	22	7	19	19	17	13	19	19	20	23	25	17	18	23	21	12	26
285 < wd ≤ 315	0	4	(4)	9	4	12	7	10	12	9	13	9	16	15	12	9	12	12	7	14
315 < wd ≤ 345	2	7	(7)	5	3	6	2	9	12	12	19	18	19	21	20	3	25	18	20	20
sum total	632	690	(295)	774	213	762	579	680	686	828	664	618	797	919	759	525	849	776	403	757
sum 165 < wd ≤ 225	502	571	(295)	610	146	632	458	550	563	692	535	488	650	768	619	414	687	619	273	757
sum(165-225)*100% / sum(total)	79%	83%	(69%)	79%	68%	83%	79%	81%	82%	84%	80%	79%	82%	84%	82%	79%	81%	80%	68%	80%

Table 11: *Precipitation amount [mm] at the different rain gauge locations when the temperatures at all locations are above 2 °C and the wind speed at AWS-2 is above 0.5 m/s. Because of the wind speed criterion, the sums differ somewhat from Table 10 and Figure 40. The second last row gives the sum for all wind directions between 165°-225°. The last row gives the percentage amount of precipitation for wind directions between 165°-225°. For the wind directions of the main precipitation amount (165°-225°), the values larger (smaller) than R3 Stordal river have been highlighted in red (blue).*

[5]R5 Skrikeberg stopped measuring 10th of September, 13 UTC. The numbers in parenthesis for R3 is for the same period as R5.

8.3 Vertical precipitation gradient

This section deals with the investigation of the altitude dependency of precipitation in the MHS. Figure 47 shows a scatter plot of the accumulated precipitation from Table 10 during the measurement period versus the measurement altitude. As already stated in the previous section, neither R5 Skrikeberg nor R19 Årnesstøl will be included in the calculations due to missing data and unfortunate rain gauge positioning. The corresponding regression line shows the following relation between precipitation amount, P and height above sea level, z:

$$P(z) = 556.7 + 0.289 \times z \tag{7}$$

This results in an average precipitation increase with height of $\gamma = 5.2\ \% \ / \ 100$ meters for the MHS. This value will be used further as the average vertical precipitation gradient in the MHS when investigating potential horizontal gradients.

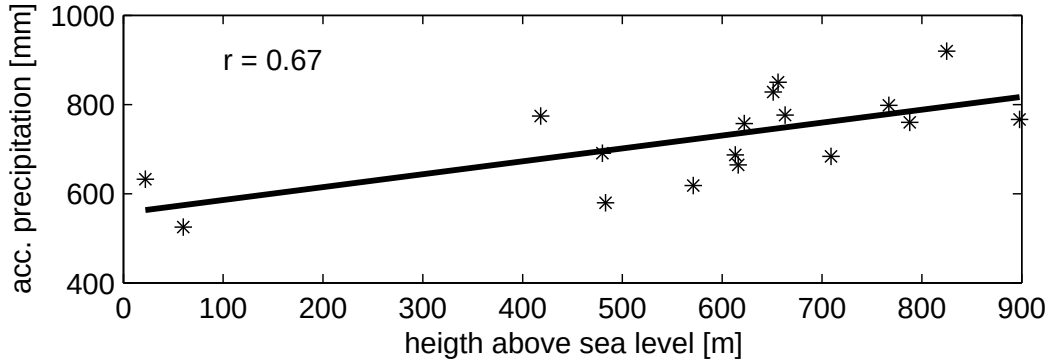

Figure 47: *Scatter plot of accumulated precipitation amounts versus elevation above sea level for the different rain gauge locations.*

8.4 Horizontal precipitation gradient

For the investigations of horizontal gradients in the MHS, the following formula is used to normalize the amounts of precipitation of all measurement sites to the altitude of R3 Stordal river:

$$P(Rx, z(R3)) = \frac{P(Rx, z(Rx))}{1.052^{\frac{z(Rx)-z(R3)}{100}}} \tag{8}$$

In the formula, Rx denotes the different rain gauge locations specified in Table 10, when x is a number between 1 and 20 (except R5, R19). P denotes the accumulated precipitation from Table 10, and z the altitude above sea level for the particular rain gauge.

This formula normalizes the precipitation amounts from Table 10, to the precipitation amount at the level of R3 (480 meters above sea level) when using the average vertical gradient of 5.2 % increased precipitation / 100 meter rising for the MHS. P(Rx,z(R3)) is in the following referred to as the normalized precipitation at the level of R3. The normalized precipitation values at the level of R3 are given in Table 12. In Figure 48, the percentage values with respect to R3 are presented. In the Figures 49 - 51, the values have been normalized with the aid of equation 8. Otherwise, the criteria are similar to Figures 41 - 43. If the precipitation amount is described by the vertical precipitation gradient, the regression line should be equal to the 1-to-1 ideal line. If the regression line differs from this, other mechanisms have to be considered as explanation.

Both R1 Matre and R4 Fosse now show considerably higher overall precipitation values, about 115 % of the value at R3 Stordal river, when adjusting to R3-level. Because of the higher elevation particularly on the western side of R4 Fosse, a spill over effect might be present for this area for westerly winds directions. However, lack of precipitation measurements in the nearby western area makes it hard to conclude on this. For R6 Blåfjell the regression line indicates lower normalized amounts at R6 compared to R3 (Figure 49(c)). The normalized value for R6 Blåfjell is about 10 % lower than the value for R3. As already discussed, R6 is well exposed to wind, and the true precipitation

Location	normalized accumulated prec.	% of R3
R1 Matre	797.4 mm	115 %
R3 Stordal river	690.5 mm	100 %
R4 Fosse	798.9 mm	116 %
R6 Blåfjell	620.0 mm	90 %
R7 Årsdalsvatn	578.7 mm	84 %
R8 Fridalsvatn	608.8 mm	88 %
R9 Krokevatn	642.0 mm	93 %
R10 Langevatn	759.4 mm	110 %
R11 Stølsdalen	620.1 mm	90 %
R12 Stølsvatn	590.1 mm	85 %
R13 Gamle Stølsleitet east	689.8 mm	100 %
R14 Skorvane	772.1 mm	112 %
R15 Høgetjørnane	650.2 mm	94 %
R16 Oppedal	649.6 mm	94 %
R17 Gamle Stølsleitet west	777.5 mm	113 %
R18 Hareheia	707.4 mm	102 %
R20 Hornsetvatn	704.9 mm	102 %

Table 12: *The table gives the precipitation amounts for each rain gauge location normalized to R3-level when using equation 8. The last column contains the percentage of the reference station R3.*

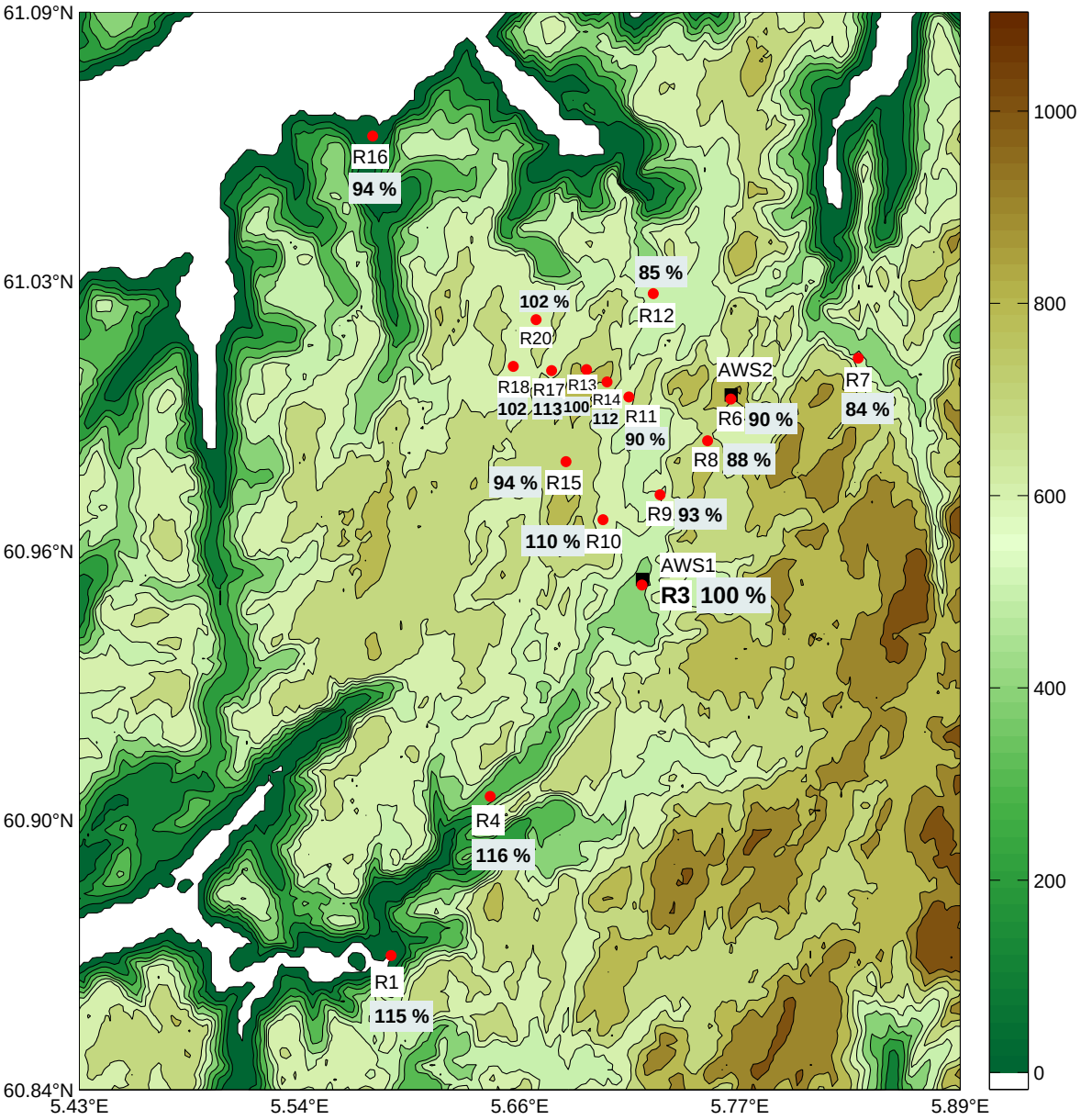

Figure 48: *Percentage of the normalized precipitation values refered to the reference station R3. The values are given in Table 12. 100 % at R3 ≈ 691 mm. The colorbar denotes the elevation above sea level [m].*

amount is therefore assumed to be somewhat higher.

The normalized amount of R7 Årsdalsvatn is only 84 % of the R3 value (Table 12), and therefore makes it the location with the lowest normalized amount. The normalized precipitation amount in Figure 48 for R8 Fridalsvatn is approximately 12 % less than the value for R3. This is also evident in Figure 49(e). As stated in section 8.2, R8 shows a tendency to measure lower amounts of precipitation when strong winds are

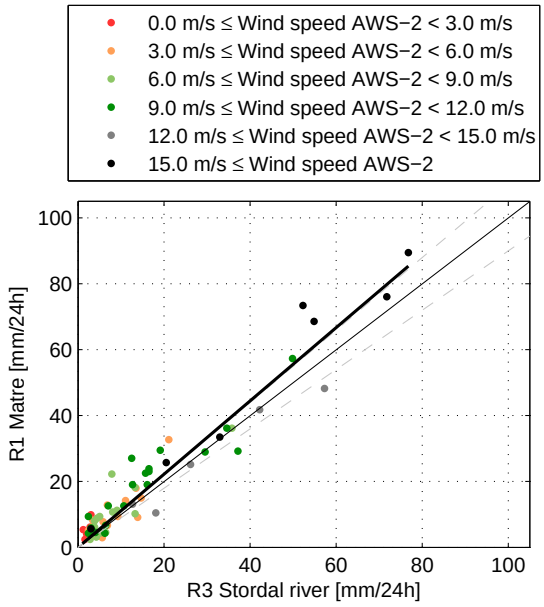

(a) R1 Matre versus R3 Stordal river.

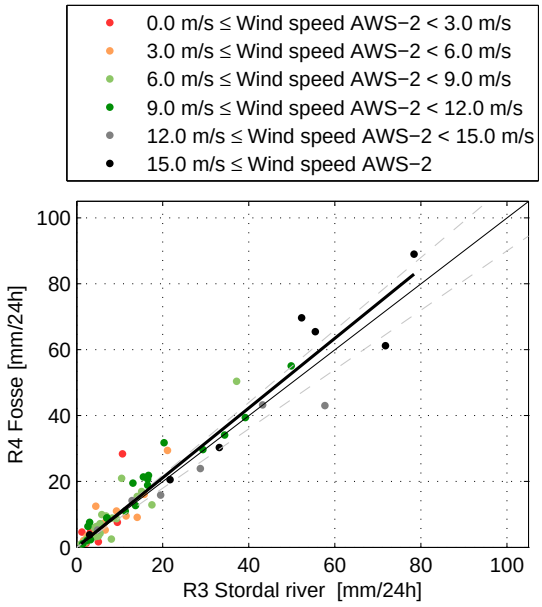

(b) R4 Fosse versus R3 Stordal river

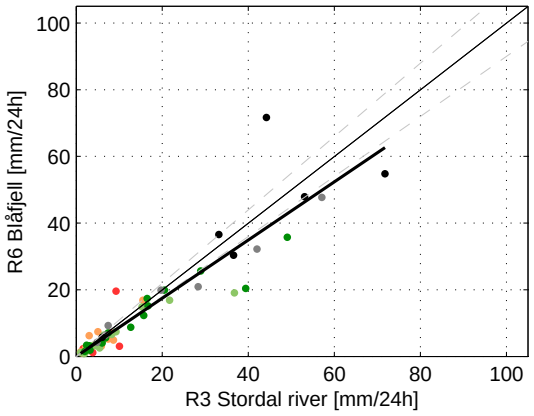

(c) R6 Blåfjell versus R3 Stordal river

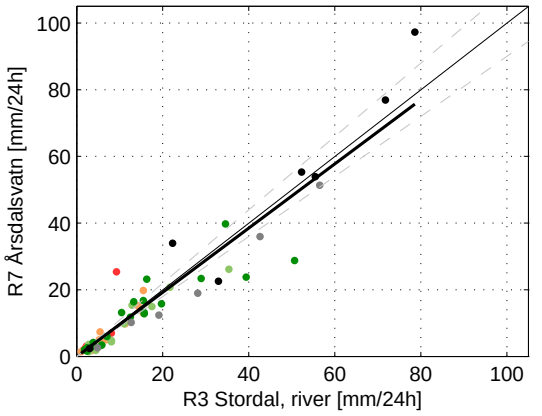

(d) R7 Årsdalsvatn versus R3 Stordal river

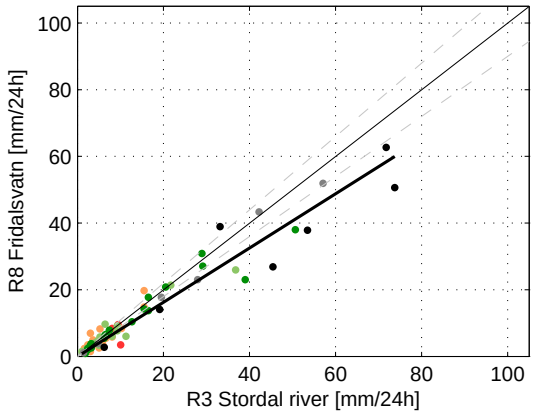

(e) R8 Fridalsvatn versus R3 Stordal river

Figure 49: *Scatter plots of R1, R4, R6, R7 and R8 versus R3-Stordal river. 24 h data from the adjusted time series are utilized. The data are normalized to the level of R3 by equation 8.*

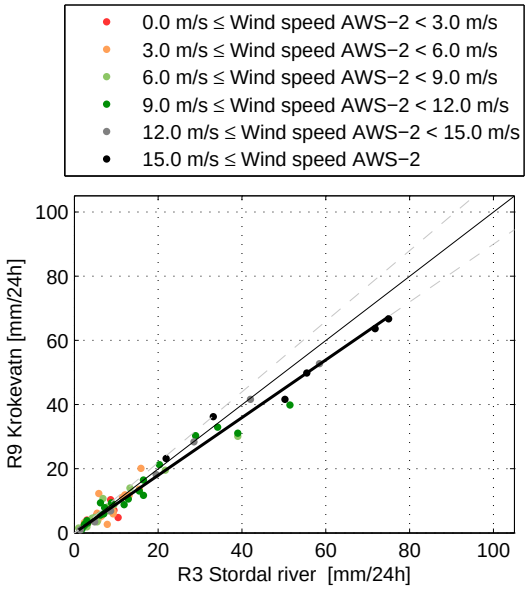

(a) R9 Krokevatn versus R3 Stordal river

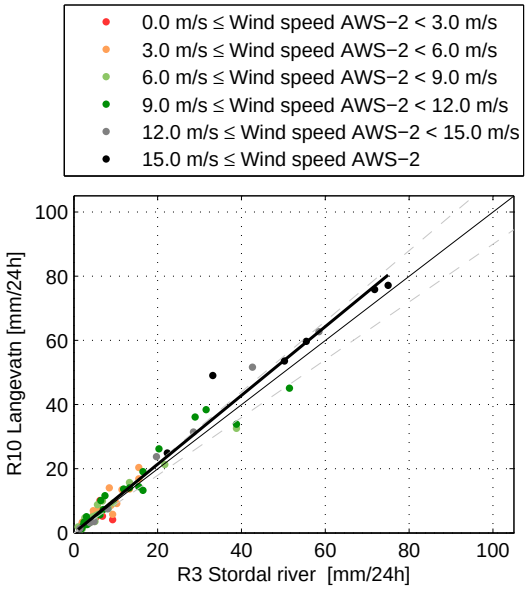

(b) R10 Langevatn versus R3 Stordal river

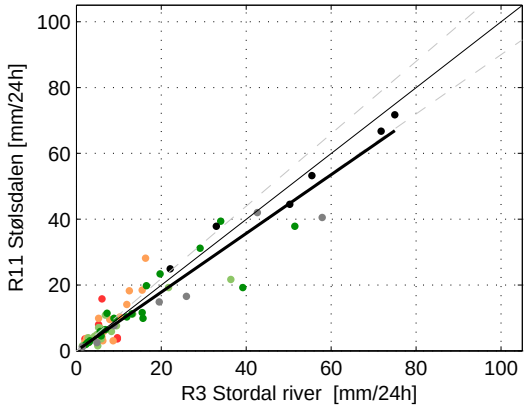

(c) R11 Stølsdalen versus R3 Stordal river

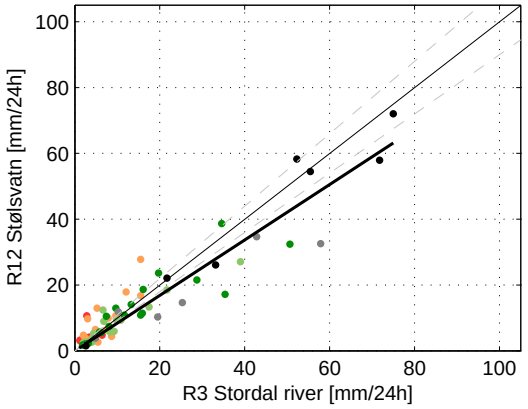

(d) R12 Stølsvatn versus R3 Stordal river

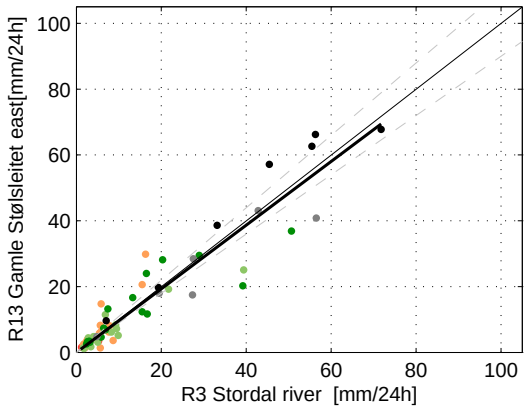

(e) R13 Gamle Stølsleitet east versus R3 Stordal river

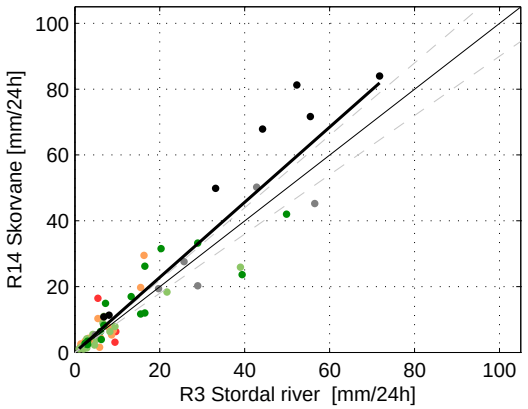

(f) R14 Skorvane versus Stordal river

Figure 50: *Scatter plots of R9-R14 versus R3-Stordal river. 24 h data from the adjusted time series are utilized. The data are normalized to the level of R3 by equation 8.*

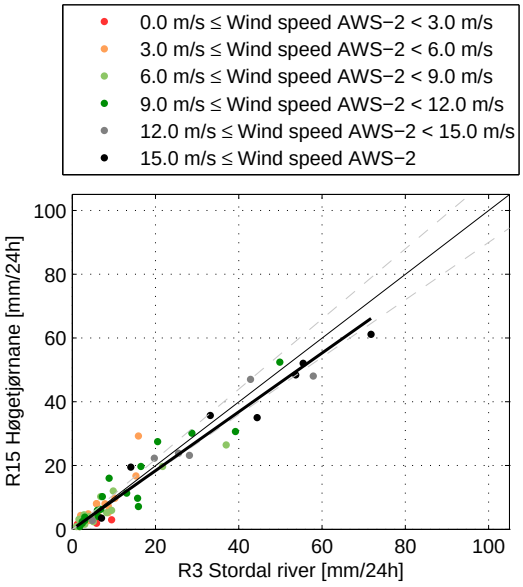

(a) R15 Høgetjørnane versus R3 Stordal river

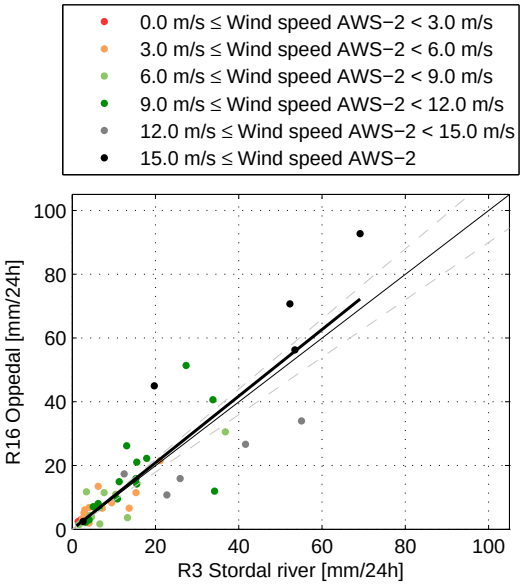

(b) R16 Oppedal versus R3 Stordal river

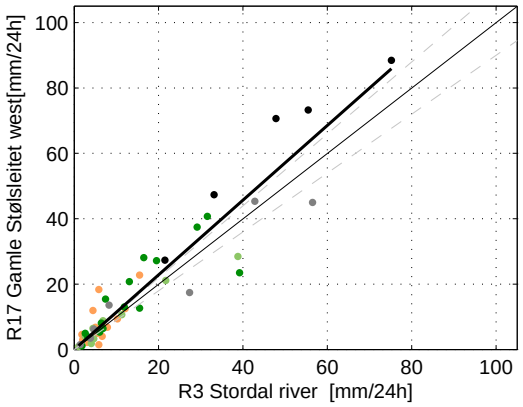

(c) R17 Gamle Stølsleitet west versus R3 Stordal river

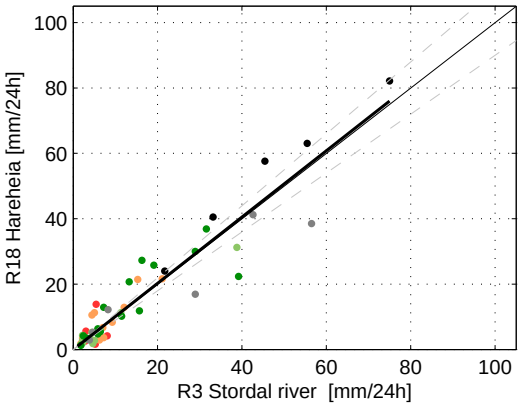

(d) R18 Hareheia versus R3 Stordal river

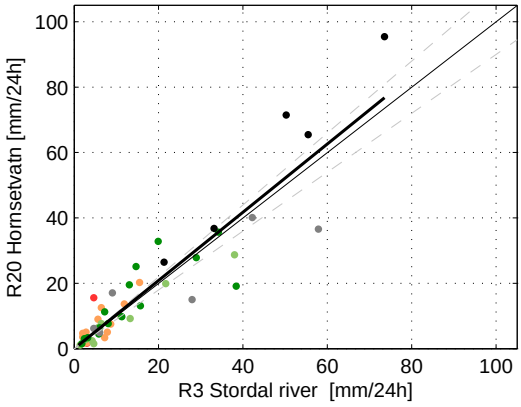

(e) R20 Hornsetvatn versus R3 Stordal river

Figure 51: *Scatter plots of R15, R16, R17, R18 and R20 versus R3-Stordal river. 24 h data from the adjusted time series are utilized. The data are normalized to the level of R3 by equation 8.*

present. However, there is no reason for a larger influence at R8 than R3, and this difference is believed to be caused by a horizontal gradient. The normalized overall amount for R9 Krokevatn is about 93 % of the R3-value, and Figure 50(a) shows the same tendency as for R8 Fridalsvatn. R9 Krokevatn is surrounded by moderate vegetation, and is therefore not expected to experience a notable loss of precipitation due to wind induced undercatch, and the lower normalized amount can be explained by a horizontal gradient.

The normalized amount at R10 Langevatn is about 10 % higher than at R3 (Figure 48). The regression line in Figure 50(b) is also indicating higher amounts at R10 than R3 for high wind speeds. As discussed in section 8.2, R15 Høgetjørnane is believed to experience strong undercatch due to wind, and the normalized percentage amount is therefore believed to be somewhat higher than 94 % (Figure 48).

For the investigation of horizontal gradients, both R11 Stølsdalen and R12 Stølsvatn show a lower normalized value for the level of R3 than R3 itself. This is clear from the regression lines in Figure 50(c) and 50(d). Because of the relatively strong vegetation near R12 (see Figure 21(a)), this rain gauge is not believed to experience any notable loss of precipitation due to undercatch, and the differences in amount are explained by a horizontal gradient. Neither R11 is believed to be influenced by strong undercatch, and the value for this station is also belived to be caused by a horizontal gradient.

The normalized values for both R14 and R17 are considerably higher than R3, while R13 is well in accordance with the utilized vertical gradient (Figure 48 and 50(e)). There is no evident reason for these differences, but the local positioning and local wind field for each rain gauge might play a crucial role. However, not any of the rain gauges are believed to experience a larger loss due to wind induced undercatch than the others. The calibration tests in section 4.4 indicated an instrumental uncertainty for HOBO rain gauges used in fieldwork of approximately ± 4 %, and this must be taken into consideration when great differences are discovered in such a limited area. An average value of these stations will therefore be utilized in this horizontal gradient evaluation. Both R18 Hareheia and R20 Hornsetvatn are in considerable accordance with R3 when normalizing using the average vertical gradient (Figure 48). This is also evident when studying the regression lines for high wind speeds when the amounts are normalized in Figure 51(d) and 51(e). Either R18 or R20 are believed to experience larger loss due to wind induced undercatch than R13, R14 or R17, which is located relatively close. When normalized to the level of R3, R16 Oppedal shows approximately 94 % of the value of R3. R16 is located northwest of the main measurement area, on the southern side of the Sognefjord, not freely exposed to the main wind direction when precipitation is present.

In the following, an generalized precipitation gradient will be considered. Based on the evaluation for the rain gauge stations from Figure 48-51, Table 12 and the explanations given in this section, roughly estimated gradient lines for the MHS are drawn in Figure 53. After the calibration test in January 2009, the HOBO rain gauges indicated an aver-

age instrumental uncertainty of approximately ±4% (section 4.4). In addition, because of uncertainties concerning local wind fields in consequence of rain gauge location, and evaporation- and outsplashing errors, the uncertainty is higher. Because of this, where the local differences in the field is found to be large, an average value of the nearest gauges is considered when making the gradient lines.

In general, lower normalized precipitation amounts are detected in the northeastern and eastern measurement areas, while higher normalized amounts are observed in south and southwest. A bending of the gradient lines seems to be present in the northwestern part of the area. However, this is somewhat uncertain due to the high variability in the area. When comparing these results to the distribution found by Skaar (1976) in Figure 4, the gradient lines show, in broad outline, the same pattern. However, when calculating from the figure of Skaar (1976) (Figure 4), the gradients found by Skaar (1976) are stronger, indicating in the lower edge of 140 % of the Stordal value at Matre in southwest, and about 70-80 % around Årsdalsvatn in northeast. In the distribution of annual precipitation amounts in 1966, which Skaar (1976) referred to as a year with approximately normal conditions, roughly calculated, the gradient lines showed from 120 % and higher of the Stordal value at Matre, and about 85 % around Årsdalsvatn. This is in accordance with the values found in this section, particularly for the northeastern area. Similar tendencies were found for 1964 and 1965, a 'wet' and a 'dry' year respectively. However, in the area around the Sognefjord studied by Skaar (1976), great local variability was seen. This is also the case in the MHS, for instance between R13, R14 and R17. Figur 52 shows the percentage of the normalized precipitation amount of Stordal-level (Table 12) versus the distance normal to the blue line in Figure 53. The correlation is r = -0.72, accordingly 52 % of the variance explained. When averaging the closly located gauges which show a large variability (R13, R14, R17 and R18), approximately 70 % of the variance is explained when utilizing the same method (not shown).

Table 11 shows that for every rain gauge location included in this section, from 79 % to 84 % of the total amount of precipitation when the temperatures are above 2 °C, are

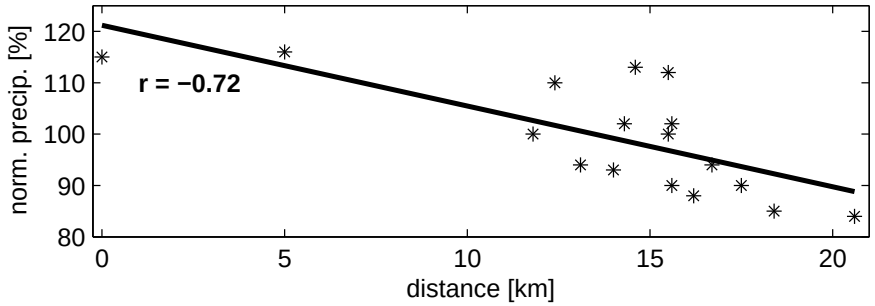

Figure 52: *The percentage of normalized accumulated precipitation [mm] at the level of R3 versus distance from the blue line in Figure 53.*

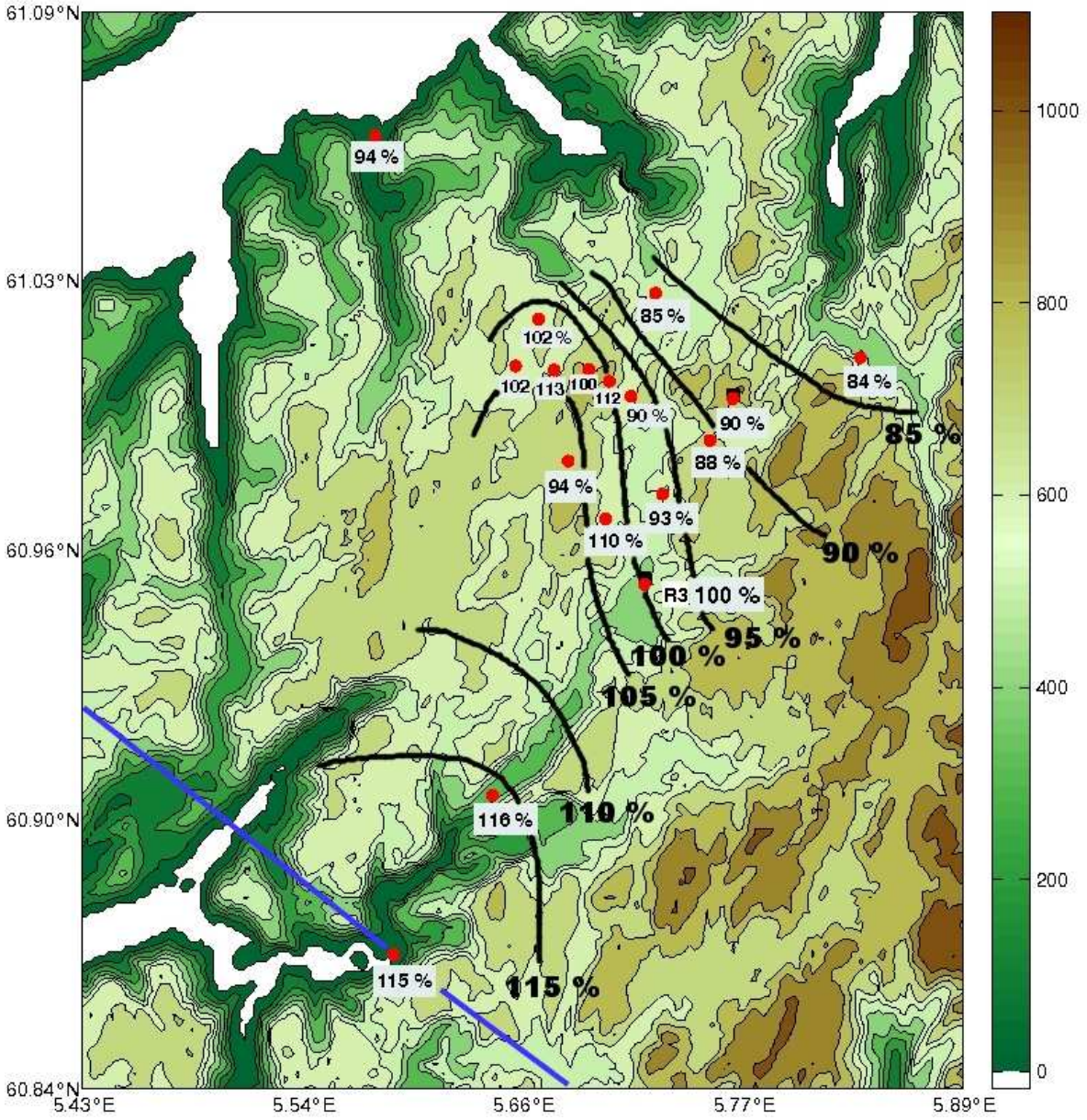

Figure 53: *Rough estimates gradient lines for the MHS when all the stations are adjusted to the R3-level. The colorbar denotes the elevation above sea level [m]. The blue line is not included in the gradient lines, but is used in connection with Figure 52.*

present for wind directions between 165°-225°. The generalized horizontal precipitation gradient in the MHS found in this section is therefore expected to be highly connected to these wind directions where the main part of the precipitation is present, due to a typical low pressure pattern towards the coast of Norway. The gradient is therefore expected to be common in this area during front passages. However, relatively small changes in the wind direction within this interval may change the distribution for parts of the area. Table 11 shows that six of the stations switch the sign in difference to R3 for the two main precipitation intervals (denoted by the different colors). A more detailed investigation with smaller wind direction intervals has been performed and is presented in Appendix A. It indicates a slight tendency of falling ratio with respect to R3 for wind directions changing from SSE to SSW for some of the rain gauge locations in the northwestern area.

In periods or years when a lot of the precipitation arrives from a northwesterly direction, the precipitation distribution may differ considerably. In this measurement period, only small amounts arrivied from this direction, but an indication of lower amounts at R3 compared to several rain gauge locations is present for wind directions between west and north. It must also be taken into consideration that the main horizontal gradient, principally caused by frontal precipitation, may be blurred by convective precipitation events (see section 9.2).

8.5 Run-off

This section contains a rough comparison of the normal run-off for the MHS and the normalized precipitation gradient given in Figure 53. Run-off is described as the number of cubic meter of water reaching a reservoir during a normal year. Because of snow melting in the beginning of the measurement period and snowfall in periods in the end, run-off data from the measurement period are unsuitable for direct comparison. Therefore, annual normal run-off data normalized to Stordal are used in this section.

Table 13 gives the run-off data in percent for a normal year, normalized to Stordal location, for different reservoirs in the MHS. The normalized precipitation amount, estimated on basis of the gradient lines in Figure 53, is also given in Table 13. The run-off data for the MHS are divided into catchment areas for the different reservoirs, and the different catchment areas have a different height distribution. Figure 18 shows the location of the different reservoirs. Nordgjelsvatn and Nedre Mosedalsvatn are not named in this map, but are located approximately at Hopsvatn. Nordgjelsvatn is located west of Nedre Mosedalsvatn. A study of local maps show that the average height distribution of the catchment areas for Holmevatn and Kvanngrøvatn differs by only ∼50 meter from Stordalsvatn. This means that the normalized values for these reservoirs will not differ much when adjusted to the level of Stordalsvatn. Except for Store Fjellvatn, Fridalsvatn and Hommelvatn (written in bold), and Holmevatn and Kvanngrøvatn with approximately the same catchment elevation, the height distribution of

	norm. run-off	norm. prec. from gradient lines
Fridalsvatn	**90 %**	**90 %**
Holmevatn	95 %	109 %
Hommelvatn	**113 %**	**115 %**
Krokevatn	95 %	95 %
Kvanngrøvatn	95 %	107 %
Nedre Mosedalsvatn	103 %	110 %
Nordgjelsvatn	104 %	112 %
Stordalsvatn	**100 %**	**100 %**
Store Fjellvatn	**90 %**	**91 %**
Stølsvatn	69 %	85 %
Tverrvatn	90 %	84 %
Årsdalsvatn	90 %	84 %

Table 13: *Normalized run-off for a normal period and normalized precipitation estimated from the gradient lines in Figure 53.*

the catchment area for each reservoir is not adjusted to the level of Stordalsvatn. Because of this, and the fact that the numbers in the columns do not represent the same period, a direct comparison is not possible. However, a tendency of correspondance is seen. For both Fridalsvatn and Krokevatn, the normalized gradient precipitation shows a clear connection to the run-off. This tendency is also seen for Store Fjellvatn, Tverrvatn and Årsdalsvatn. For Stølsvatn, BKK seems to be operating with apparently low values compared to the normalized precipitation at R3-level for the Stølsvatn location. For a normal period, both Holmevatn and Kvanngrøvatn show considerable lower run-off compared to the normalized precipitation. Taking into account that these two resevoirs have approximately the same catchment height as the Stordal reservoir, data are indicating that BKK operates with too low run-off for these catchment areas. Higher normalized run-off values are present also for Nedre Mosedalsvatn and Nordgjelsvatn. Hommelvatn in the southwestern part of the area, where the run-off data are adjusted to Stordal-level, shows good correspondence with the normalized precipitation.

The gradient indication found in section 8.4 is to a large extent present when comparing normalized run-off data for a normal year and normalized precipitation based on the gradient lines from the Matre campaign. Well agreement is seen for reservoirs were the height distribution of the catchment area is adjusted to reference level. An indication of underestimation of the run-off is present for Stølsvatn, Kvanngrøvatn and Holmevatn. However, it must be taken into consideration that the project period may differ from a normal period, and in addition the rain gauge measurements contain uncertainties.

9 Case studies

This chapter contains two case studies; a frontal system passage and a convective situation.

9.1 Case study 1 - Frontal

A case study is performed for the HOBO rain gauges situated in and close by the MHS. The case which will be investigated in this section, lasted from 00 UTC 15th of July to 12 UTC 17th of July 2008. A frontal system with warm front, cold front, trough and following occlusion with subsequent showers passed the western coast of Norway during this period. This situation is chosen on the basis of temperatures above 2.0 °C and because R5 Skrikeberg was still operative during this period. Figure 54(a) shows an analysis map from the 15th of July 06 UTC, when the warm front of the low pressure system has reached the west coast of Norway. Figures 55(a) and 55(b) show the hourly precipitation for all the rain gauges. The precipitation forecast from the ECMWF-model is included in Figure 55(a). Meteorological parameters such as temperature, relative humidity, wind speed, wind direction and pressure are shown in Figure 56. The most intensive precipitation in this case period occured between 03-12 UTC on July 15th. The cold front is expected to have passed the area about 08 UTC 15th of July, indicated by the thereafter decreasing temperature and rising pressure (due to pressure data only every sixth hour, the pressure is believed to start rising somewhat later than indicated in Figure 56). According to analysis maps, the following trough was located between Great Britain and the Faroe Islands, but west of the Shetland Isles at 18 UTC the 15th of July. The pressure observed at Fedje decreases (Figure 56), and the precipitation intensity increases from approximately 20 UTC. The trough is located at the

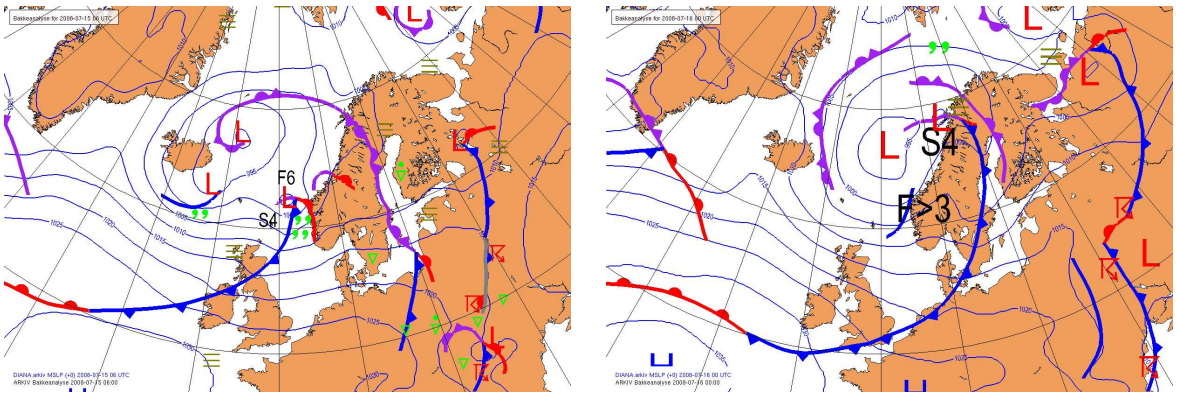

(a) Synoptic situation 06 UTC 15th of July

(b) Synoptic situation 00 UTC 16th of July

Figure 54: *Analysis maps of the synoptical situation 06 UTC July 15th and 00 UTC July 15th 2008. The maps are from DIANA (DIgital ANAlysis), a 2D visualization and production system for meteorological and oceanographic data.*

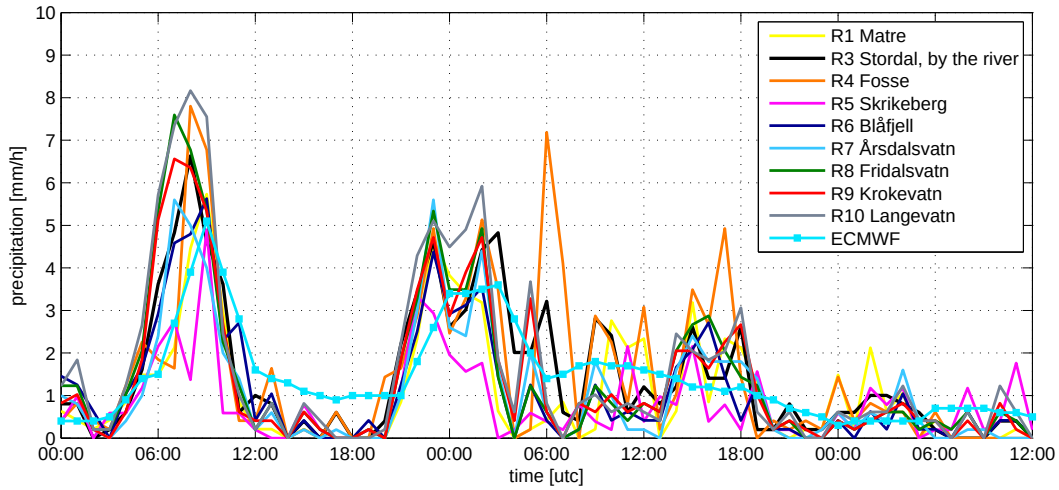

(a) 15th of July 00 UTC - 17th of July 12 UTC. Rain gauge station R1-R11 (except R2) + ECMWF.

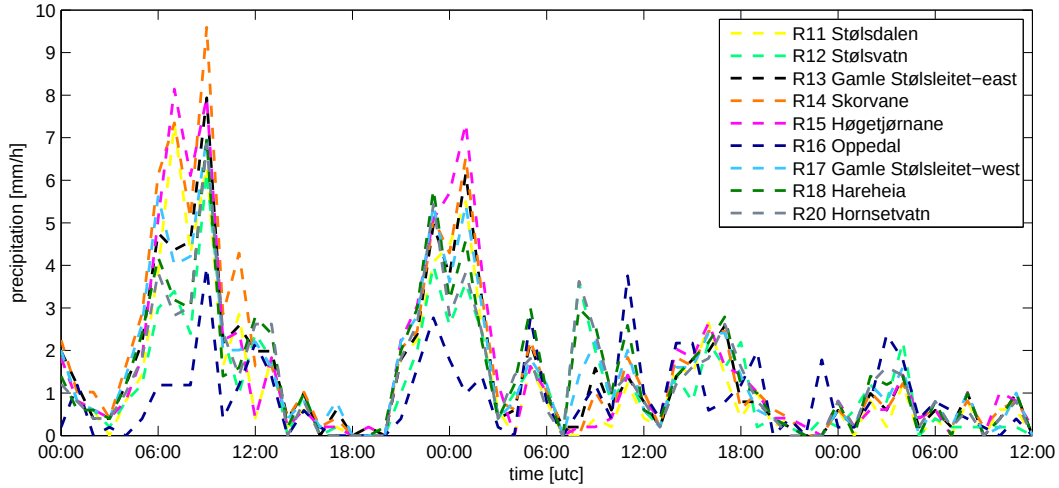

(b) 15th of July 00 UTC - 17th of July 12 UTC. Rain gauge station R12-R20 (except R19).

Figure 55: *Precipitation intensity for each rain gauge station during the case study from 15th of July 00 UTC - 17th of July 12 UTC 2008. Each time grid line on the x-axis represents six hours, starting at 00 UTC the 15th of July 2008.*

coast of Norway approximately 00 UTC 16th of July, see Figure 54(b). An occlusion is present at the coast of Norway approximately twelve hours later. Subsequent showers are dominating the second part of the case period.

The wind direction during the period is mostly S-SSW. In some parts of the period the wind direction, especially at AWS-2 Blåfjell is more westerly. The accumulated precipitation during the case period is shown in Figure 57. R14 Skorvane measured the most during the period, 101.5 mm, closely followed by R11 Langevatn (99.8 mm). Also

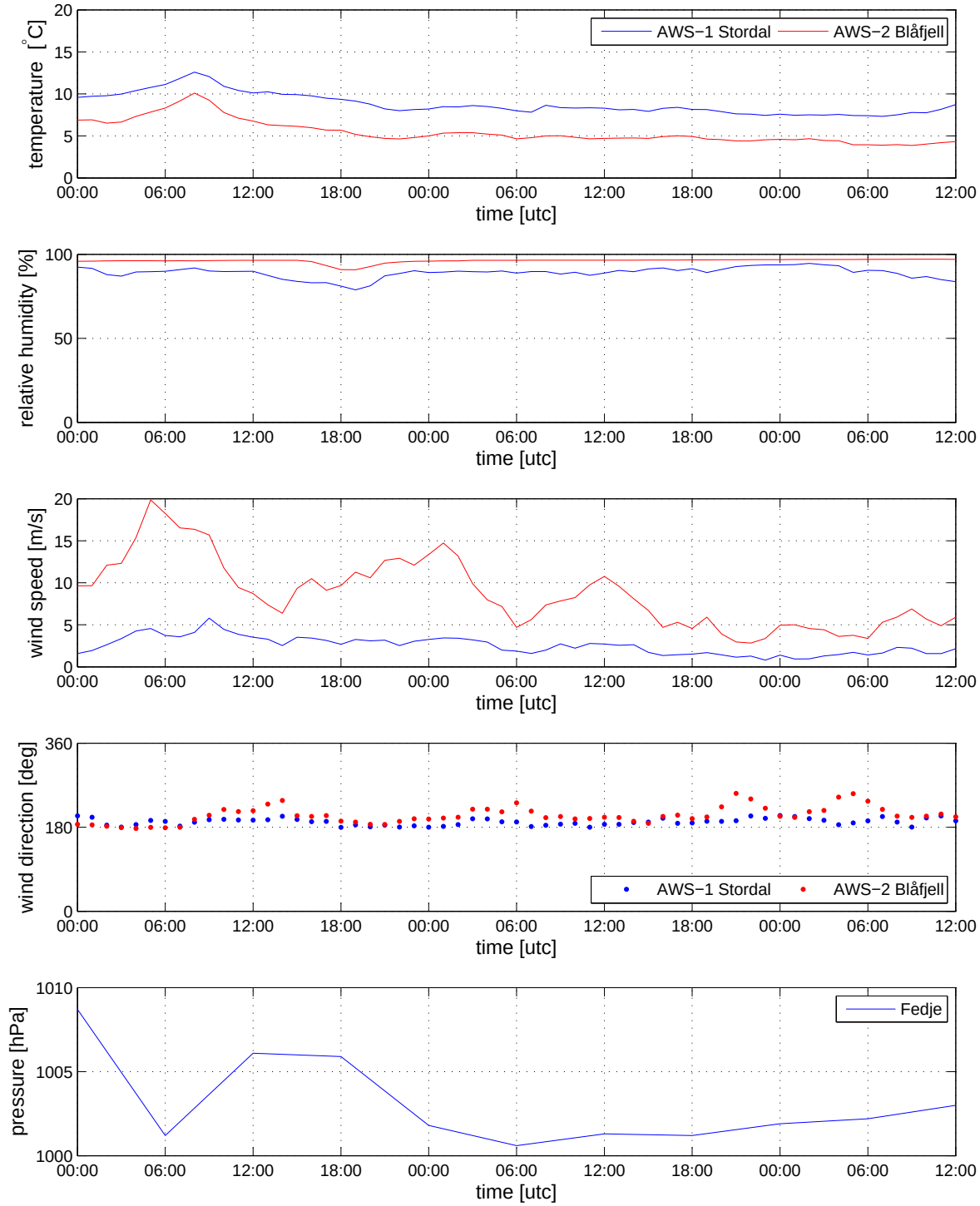

Figure 56: *Meteorlogical parameters during the case. Each time grid line on the x-axis represents six hours, starting at 00 UTC the 15th of July 2008.*

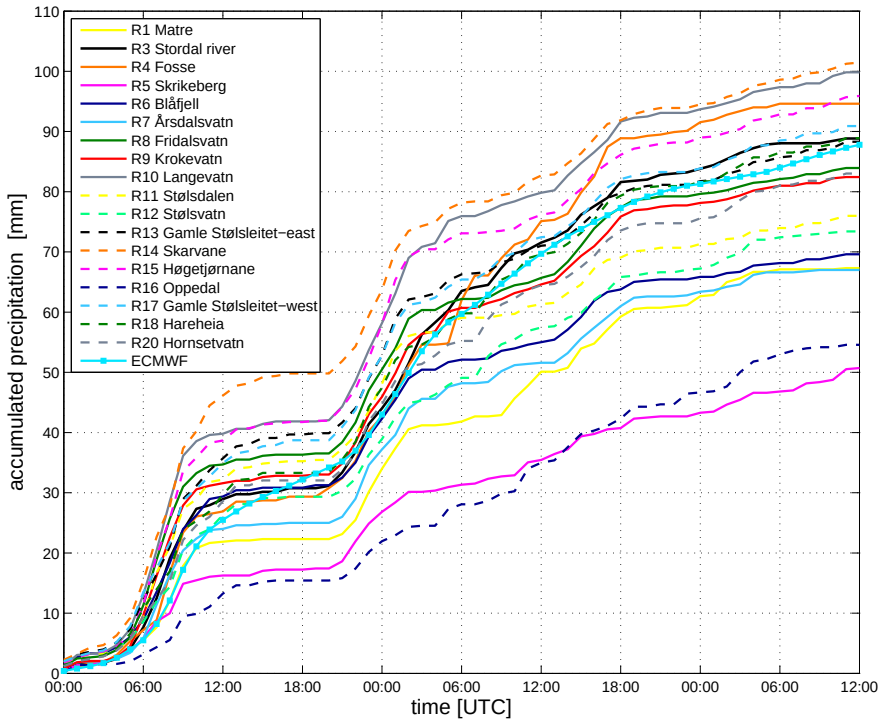

Figure 57: *Accumulated precipitation for the different rain gauge locations. The ECMWF forecast is alo included in the figure. Each time grid line on the x-axis represents six hours, starting at 00 UTC the 15th of July 2008.*

R4 Fosse and R15 Høgetjørnane measured high amounts of precipitation. The reference station, R3 Stordal river, measured 88.8 mm. R1 Matre measured considerably more than the other rain gauge stations close to the sea level. Table 14 shows the percentage amount of R3 in this case study compared to the entire measurement period (not normalized) earlier shown in Table 10. Table 14 is visualized in Figure 58. The percentage amounts in this case study are not normalized to the same level, and a direct comparison to Figure 53 is therefore not reasonable. In this case, smaller percentage amounts of R3 compared to the entire period is present for the gauge locations, indicating a relatively large amount of precipitation at R3 Stordal river during this frontal passage. The wind direction is mostly above 180 degrees, and as discussed earlier a tendency of falling ratio between some of the rain gauges and R3 is seen for wind direction changing from SSE to SSW. This is in well agreement with earlier results. The figure indicates, with a correlation coefficient between percentage amount of R3 in the measurements campaign and the case study of 0.87, that the precipitation distribution in the case study is considerably well in accordance with the overall distribution found in section 8.2. The vertical precipitation increase with height for this case is found to be 6.3 % / 100 meter, which is fairly well in accordance with the average gradient of 5.2 % / 100 meter found in section 8.3.

	% of R3 in campaign	% of R3 in case study 1
R1 Matre	91.6 %	75.7 %
R3 Stordal river	100.0 %	100.0 %
R4 Fosse	112.1 %	106.5 %
R5 Skrikeberg	-	57.1 %
R6 Blåfjell	111.0 %	78.4 %
R7 Årsdalsvatn	83.9 %	75.4 %
R8 Fridalsvatn	99.0 %	94.5 %
R9 Krokevatn	99.5 %	92.8 %
R10 Langevatn	120.0 %	112.4 %
R11 Stølsdalen	96.2 %	85.5 %
R12 Stølsvatn	89.5 %	82.6 %
R13 Gamle Stølsleitet east	115.5 %	99.4 %
R14 Skorvane	133.2 %	114.2 %
R15 Høgetjørnane	110.1 %	107.9 %
R16 Oppedal	76.0 %	61.4 %
R17 Gamle Stølsleitet west	123.1 %	102.3 %
R18 Hareheia	112.4 %	100.1 %
R20 Hornsetvatn	109.7 %	93.5 %

Table 14: *Percentage of accumulated precipitation at R3 for the case study and for the measurement campaign (given in Table 10).*

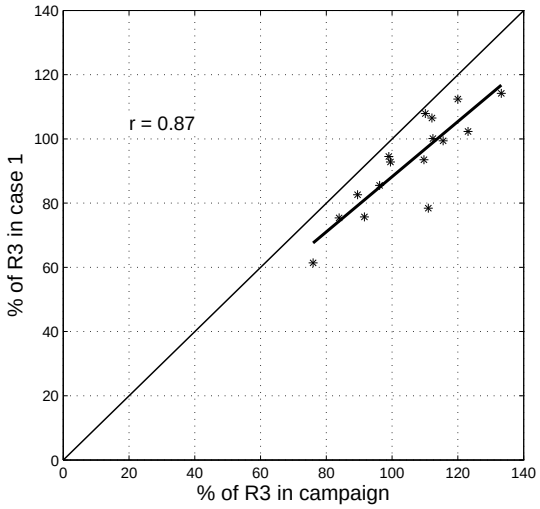

Figure 58: *Visualization of Table 14. Percentage amount of R3 in the measurement campaign versus percentage amount of R3 in case study 1.*

As illustrated in Figure 38 and also seen in this case study (Figure 55(a)), the ECMWF-model does not manage to forecast the top of the highest precipitation intensities, nor the temporary stops or very low intensities of precipitation. However, the total amount of forecasted compared to observed precipitation is extremely good. The accumulated forecasted precipitation is 87.8 mm, while the observed precipitation for R3 Stordal river is 88.8 mm. R3 Stordal river thus observed only 1.1 % more than forecasted.

9.2 Case study 2 - Convective

In this section a convective case which lasted from 13 - 20 UTC 30th of July 2008 will be studied. Because of the short time period for this case, 10-minute values for the rain gauges and weather stations are utilized. However, the ECMWF prognosis enables only a 1 h resolution. The synoptical situation is shown in Figure 59. A high pressure system is situated over southern Norway, Sweden and Finland, with its center over the Baltic Sea. The high pressure has moved somewhat to the east from 12 UTC to 18 UTC. A weak cold front is situated over the western coast of Norway.

The pressure at Fedje during the case event was gently rising. At 12 UTC on the 30th of July, the pressure at Fedje was 1017.6 hPa. Six hours later, 18 utc, the pressure had risen to 1018.9 hPa, and at 31th of July 00utc, the pressure was 1019.6 hPa. Several official weather stations in the district reported heavy showers and thunderstorms. At 30th of July 18 UTC, Førde and Modalen reported showers and thunder since the last observation (locations visualized in Figure 1). Førde also reported rainshowers and thunder in the period between 18 UTC the 30th of July to 06 UTC 31st of July. Bergen-Florida experienced thunder between 18 UTC 30th of July - 00 UTC 31st of July. Takle, on the other hand, did not report thunder. The local variability is therefore expected to be large.

Figure 61 shows the precipitation intensity for all the HOBO rain gauges and the prognosis of the ECMWF model. As seen in the figure, precipitation occured in two intervals from approximately 13-16 UTC and from 17-19 UTC. The accumulated precipitation amounts are seen in Figure 62. Temperature, relative humidity, wind speed and wind direction at both AWS-1 Stordal and AWS-2 Blåfjell are shown in Figure 60. The temperatures at both AWS-1 and AWS-2 are relatively high, but gently decreasing through-

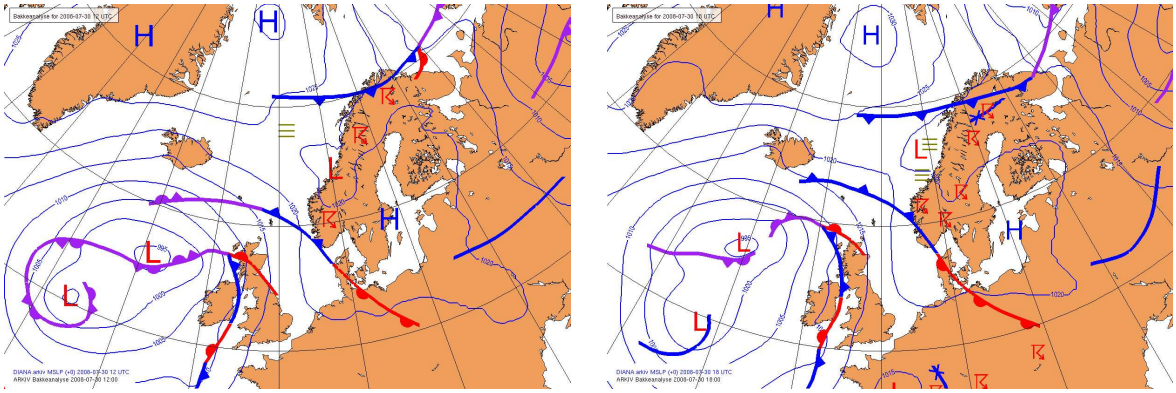

(a) Synoptic situation 12 UTC 30th of July

(b) Synoptic situation 18 UTC 30th of July

Figure 59: *Analysis maps of the synoptical situations 12 and 18 UTC 30th of July 2008. The maps are from Diana (DIgital ANAlysis).*

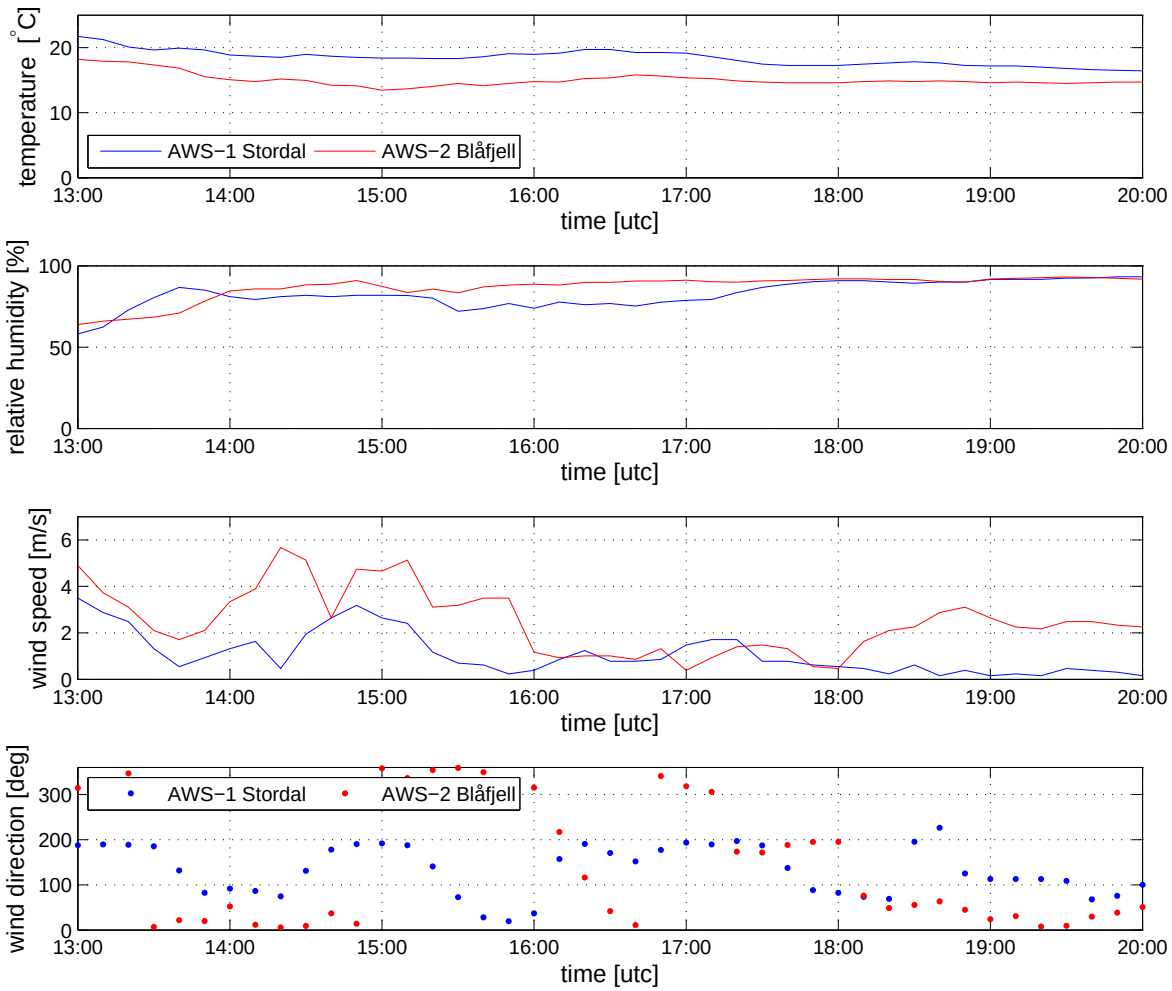

Figure 60: *Temperature, relative humidity, wind speed and wind direction during case study 2 from 13-20 UTC July 30th 2008.*

out the case period. The wind direction during the first precipitation episode in the case differs when comparing the two weather station locations. The wind direction at Blåfjell fluctuates between NNE to NNW, while Stordal mostly experiences wind from E and SSW. The wind speed at Blåfjell is generally somewhat higher than Stordal. The highest wind speed for both locations are occuring during the first precipitation episode.

As seen in Figure 61, precipitation occured in two intervals from approximately 13-16 UTC and from 17-19 UTC. R7 Årsdalsvatn had three intense precipitation periods in the time between 13 and 16 UTC, the first one starting at about 13 UTC. Precipitation was also present at R3 Stordal river, R9 Krokevatn and R10 Langevatn before 14 UTC, however with lower intensity than R7 Årsdalsvatn. At approximately 14 UTC the rain intensity increased strongly at R6 Blåfjell, and the highest amount for this station during the case and even the whole measurement campaign, 9.0 mm/10 min, was measured.

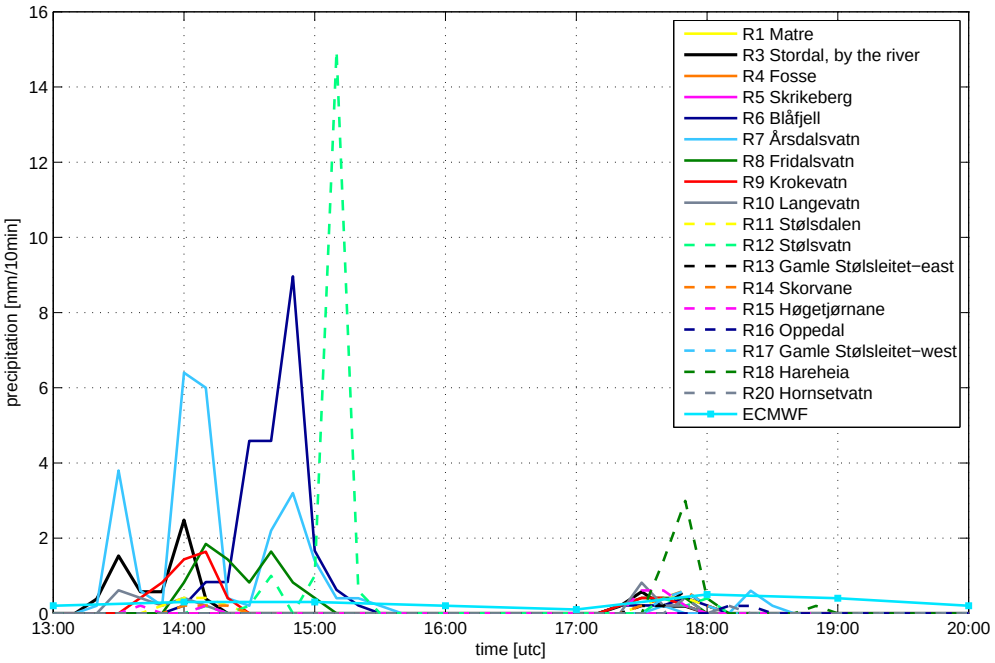

Figure 61: *Precipitation intensity for each rain gauge station during the case study from 13-20 UTC, 30th of July 2008. ECMWF forecast is also included.*

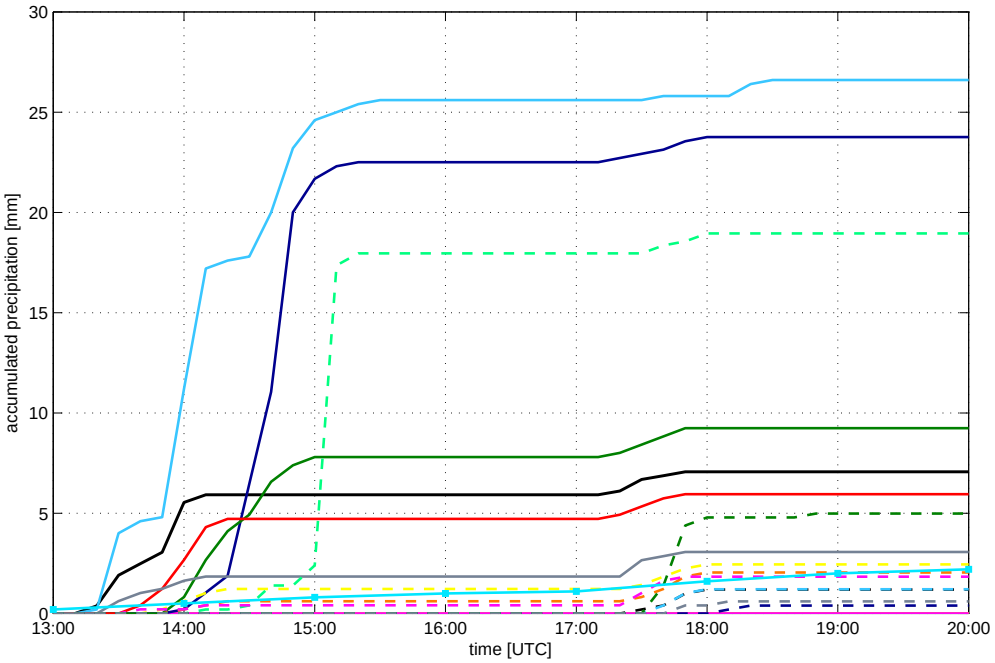

Figure 62: *Accumulated precipitation for each rain gauge station during the case study from 13-20 UTC, 30th of July 2008. ECMWF forecast is also included.*

In the period between 14 UTC and 15 UTC, R6 Blåfjell received 21.5 mm. R8 Fridalsvatn also measured precipitation between 14 and 15 UTC. At 15 UTC the precipitation intensity increased strongly at R12 Stølsvatn, which experienced 15.0 mm/10 minutes. This is the highest intensity measured during the campaign, irrespective of rain gauge location. The other locations measured small or no amounts of precipitation during the first precipitation interval. In the second precipitation interval, smaller amounts of precipitation were measured compared to the first period. The showers at R3 Stordal river are badly forecasted by the model. However, this was expected due to the smoothness of the model seen in e.g. section 7.3. The accumulated precipitation for the model in this convective case study is 2.2 mm, while the total amount at R3 Stordal river is 7.1 mm. The model is however well in accordance with e.g. R14 Skorvane. This means that the ECMWF model, due to its coarse resolution, is not suited for a point forecast for local showers, but the amount might be seen as an average for the area considered.

The accumulated precipitation for this case seen in Figure 62 is on the whole not corresponding to the overall precipitation distribution seen in section 8.2. R7 Årsdalsvatn and R12 Stølsvatn, which in the frontal case measures relatively small amounts, here measures the highest amounts. R6 Blåfjell, which in the overall situation shows small amounts compared to the height above sea level, shows in this case study high values. For instance, the accumulated amount at Årsdalsvatn in this case study, is approximately 5 % of the total amount of Årsdalsvatn in Table 10. The current problem is also present for Stølsvatn and Blåfjell. If removing the amounts in this case for Årsdalsvatn and Stølsvatn from the total amount, the normalized amounts would have been about 80 % and 83 %, respectively, and the gradient lines therefore stronger. In addition, this might explain some of the differences between normalized run-off and precipitation seen for Stølsvatn in section 8.5. Locations which usually experience high precipitation amounts during frontal cases, e.g. R14 Skorvane and R10 Langevatn, experienced small amounts during this convective situation. Typical winter precipitation is connected to frontal situations, and the amount of convective precipitation will yearly be relatively small compared to the campaign period. Convective situations like case study 2 are therefore contributing to a blurring of the main gradients in the field seen for low pressure passage, and a stronger horizontal gradient is assumed to be present in the MHS if a longer period would have been investigated.

10 Model comparison

A comparison between the observation at Stordal (R3) and the single point forecast from the ECMWF model with a resolution of 25 km was discussed in section 7.3. This comparison showed that during the measurement period from April-October 2008, the model forecasted in total less than 5 % more precipitation than observed, and that the model highly corresponds to the observations when comparing precipitation per week. This chapter investigates the performance of two other models with higher horizontal resolution. For this purpose, the observation at R3 Stordal river will be compared with MM5- and HIRLAM4-model forecasts. The ECMWF model will also be included when comparing single point forecasts for the Stordal location. In addition, a short investigation of the MM5's and HIRLAM4's ability to indicate the gradient found in section 8.4 will be carried out. The ECMWF model will not be included in this gradient investigation due to the coarseness of the model. First of all, a description of the two models and output data will be presented. The corresponding description of the ECMWF model was already given in section 5.4. Statistics used in this chapter are described in short in Appendix B.

10.1 Data description: MM5 and HIRLAM4

MM5: The PSU/NCAR mesoscale model, known as MM5 (Mesoscale Model 5), is a limited-area, nonhydrostatic, terrain-following sigma-coordinate model designed to simulate or predict mesoscale and regional-scale atmospheric circulation (Grell et al. (1995)). The version used operationally by Storm Weather Center is version 3.7, in a horizontal resolution of 12 km. Data from this model are available for comparison. The model is run with a one-way nesting with initial boundary conditions from the ECMWF model. The models vertical coordinate is terrain following, meaning that the lower grid levels follow the terrain, while the upper surface is flat. Intermediate levels progressively flatten as the pressure decreases toward the chosen top pressure, and the resolution in the boundary layer is much finer than above. In the MM5 model, different schemes are available for parameterization of physical processes. For Cumulus parameterizations, the Kain-Fritsch 2 scheme is utilized (Kain (2004)). MRF is the scheme for the planetary boundary layer and diffusion (Hong and Pan (1996)). The moisture scheme utilized is the The Mixed-Phase (Reisner 1)-scheme (J. Reisner (1998)). The RRTM longwave scheme is used as radiation scheme. See Dudhia et al. (2005) for more details concerning the model. A horizontal interpolation is performed for precipitation forecast at each measurement site. The interpolation method is bilinear interpolation, where a distance weighted average of the four surrounding grid points is used to determine the interpolated value. Ergo, a single point forecast is available for every HOBO rain gauge location. The model runs twice a day, 00 UTC and 12 UTC. Accumulated precipitation from the model is available at hourly basis, and data from forecast hour 06-18 are utilized. For the locations R1-R15 data are available from 21st of June to 28th of October, for the remaining places from 29th of August to 28th of October. The

elevation of the single point forecast in the models topography is not consistent with the observation altitude. The forecast has therefore been adjusted to observation elevation for each particular rain gauge by using a vertical gradient of 5 % / 100 meter. This gradient is identical to the one used for ECMWF.

HIRLAM4: The HIRLAM model - HIgh Resolution Limited Area Model is a regional numerical atmospheric model. Hirlam4 (version 7.1.4) is a fine scale model operational by DNMI, which enables a horizontal resolution 4×4 km^2 and a number of 60 vertical layers. For clouds and condensation parametrizations, the Kain-Fritsch scheme is utilized. Initial and boundary conditions are taken from a larger scale HIRLAM model. See HIRLAM (2009) for more details concerning the model. Only grid data from the nearest grid point to the observation site are available. The data from the HIRLAM4-model are not interpolated to the observation sites, and the grid point closest to the observation site will be used. The model runs at 00 and 12 UTC. Also here, the elevation above sea level is not consistent between the observation altitude and the model altitude, and an average vertical precipitation gradient of 5.0 % / 100 meters (similar to the gradient used in the ECMWF model) is utilized to adjust to the elevation of the nearest rain gauge location.
When refer to the HIRLAM4 data, the following notation is used:
HIRLAM4-fch00 means data from forecast hour 00 in each model run (regardless of run time 00 or 12 UTC) and the following eleven hours, accordingly the twelve first hours in each model run.
HIRLAM4-fch12 means data from forecast hour 12 in each model run (regardless of run time 00 or 12 UTC) and the following eleven hours, accordingly the next twelve forecast hours in the model run.

10.2 Model comparison: At Stordal

The rain gauge observation at R3 Stordal river will in this section be compared with the MM5 model, the HIRLAM4 model and the ECMWF model for the period from 21st of June to 28th of October. The grid point forecast employed from the HIRLAM4 model is about 330 meters northwest of R3, named H3 in Figure 70. Only 24 h values are used in this comparison. Hours when the temperature at AWS-1 Stordal is below 2 °C are removed from the 24 h series.

The histogram for different precipitation intervals is shown in Figure 63. More dry events than forecasted are observed for all the models, which is the same tendency as seen in section 7.3 for the ECMWF model. For the intervals 0.1-1.0 and 1.0-5.0 mm/24h, all the models show more events than the observation. This tendency of too many small amounts when no precipitation is observed, is also clearly for HIRLAM4 in Bremnes and Homleid (2008). In the category $\geq$ 30mm/24 h, the MM5 model has many fewer events than observations. However, both ECMWF and HIRLAM4 agree well with the number of observed events above 30 mm/24h. For the rest of the intervals, varying tendencies are seen.

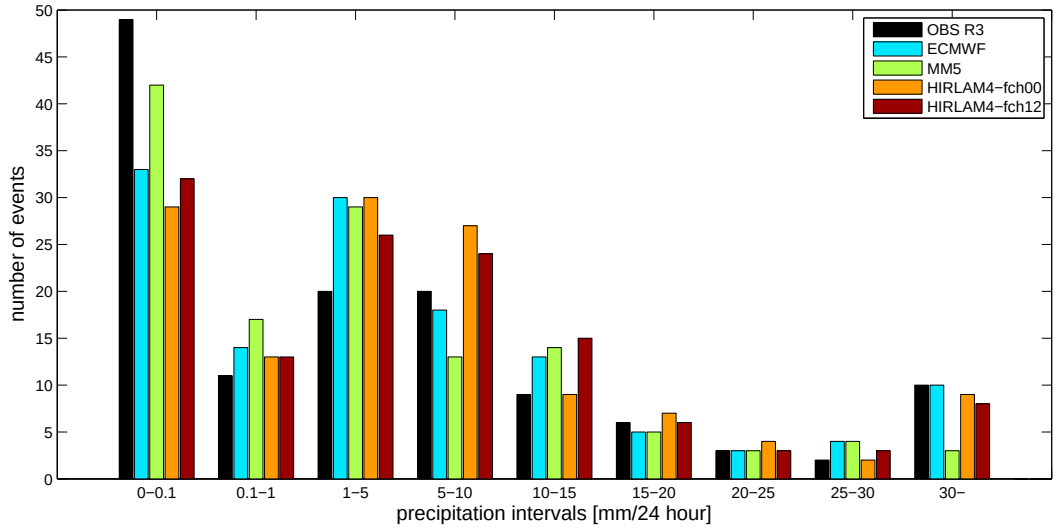

Figure 63: *Number of events for R3 observation and the models ECMWF, MM5, HIRLAM4-fch00 and HIRLAM4-fch12 for different precipitation intervals for mm/24 h. The amount in an interval is higher or equal to the lower boundary and lower than the upper boundary.*

Figure 64 and 65 show the root mean square error, RMSE and mean error, ME (also named bias error) for different precipitation intervals. When studying the RMSE, ECMWF and MM5 seem to have the smallest errors for intervals below 20 mm/24h. The RMSE for both ECMWF and MM5 increases throughout the rest of the intervals, while both HIRLAM4-fch00 and HIRLAM4-fch12 show a tendency for decreasing error for 40-60 mm/24h and for events higher than 60 mm/24h. However, the ECMWF model has overall the smallest RMSE. Figure 65 shows that MM5 has achieved a low ME for small precipitation amounts, while for amounts above 15 mm/24h, the model shows a clear tendency for underestimation. The ECMWF model also shows a small ME for small precipitation amounts. For amounts above 30 mm/24 h, the ECMWF model shows a slight tendency to underestimate. Both HIRLAM4-fch00 and HIRLAM4-fch12 show a small tendency to overestimate amounts below 10.0 mm/24h. Fluctuating values are seen in the remaining intervals. However, both HIRLAM4-fch00 and HIRLAM4-fch12 shows the lowest ME for events above 60 mm/24h. When interpreting the high amount intervals, it has to be taken into consideration that only few events are present within these intervals.

Time series of daily precipitation amounts $[mm/24h]$ for the months July - October 2008 are presented in Figures 66 - 69. The corresponding statistical analysis is given in Tables 15 - 18. In addition to RMSE and ME, mean absolute error, MAE and the correlation coefficient r are given in the tables. Daily minimum and maximum amounts during the month, mean value and standard devitation are also presented in the tables.

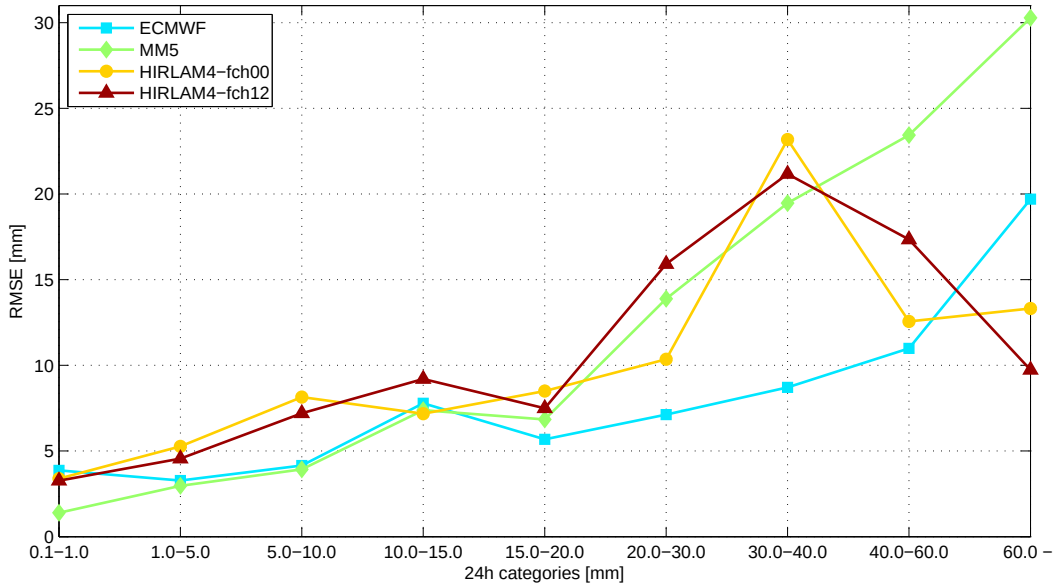

Figure 64: *Root mean square error, RMSE, for the different models compared with the observation R3 Stordal river.*

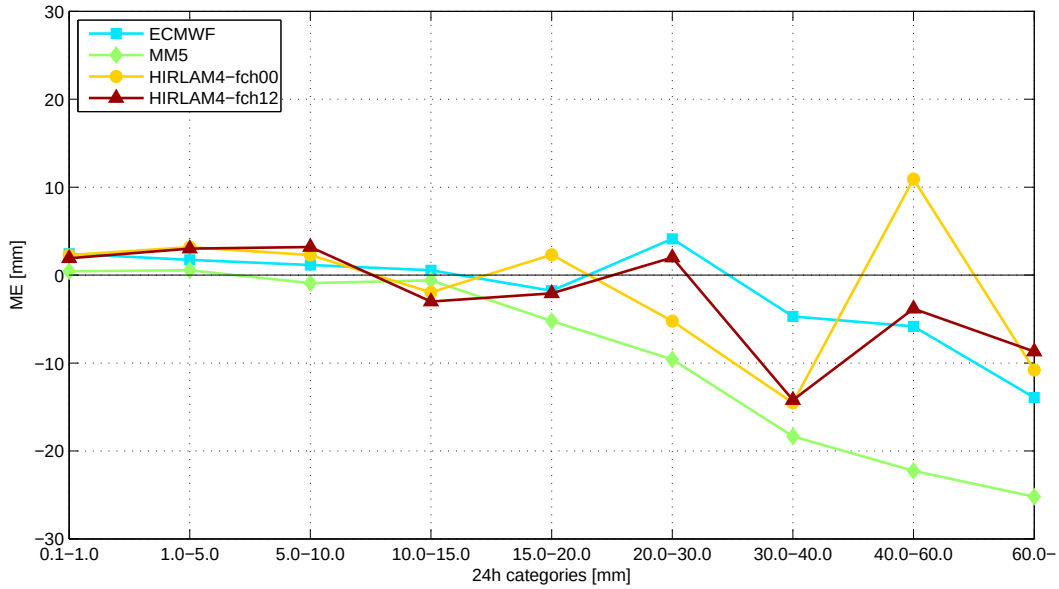

Figure 65: *Mean error, ME, for the different models compared with the observation R3 Stordal river.*

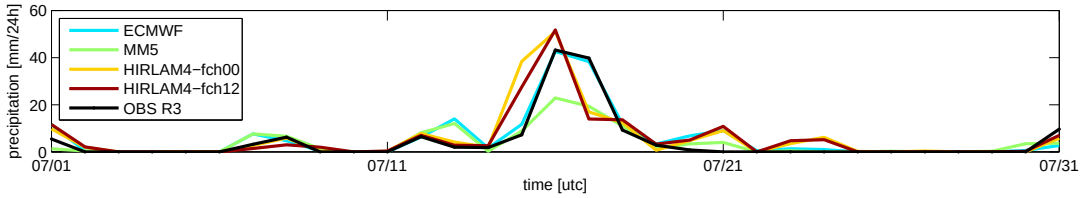

Figure 66: *July 2008. Daily precipitation [mm/24h].*

	Min	Mean	Max	SD
Observation R3	0	4.4	43.2	10.2
ECMWF	0	5.7	42.6	10.1
MM5	0	3.8	22.9	5.8
HIRLAM4-fch00	0	5.9	51.0	11.1
HIRLAM4-fch12	0	5.7	51.8	10.3

	ME	MAE	RMSE	r
ECMWF - Observation R3	1.2	1.9	3.6	0.94
MM5 - Observation R3	-0.7	2.8	5.8	0.88
HIRLAM4-fch00 - Observation R3	1.5	3.4	7.5	0.76
HIRLAM4-fch12 - Observation R3	1.2	3.4	6.7	0.79

Table 15: *Statistics for July [mm/24h].*

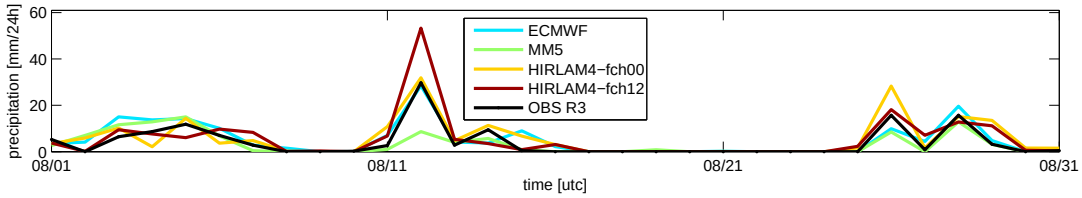

Figure 67: *August 2008. Daily precipitation [mm/24h].*

	Min	Mean	Max	SD
Observation R3	0	4.0	29.7	6.6
ECMWF	0	5.1	28.4	6.8
MM5	0	3.3	15.0	4.6
HIRLAM4-fch00	0	5.7	31.9	7.9
Hirlam4-fch12	0	5.5	53.3	9.9

	ME	MAE	RMSE	r
ECMWF - Observation R3	1.1	2.1	3.3	0.89
MM5 - Observation R3	-0.7	2.1	4.5	0.73
HIRLAM4-fch00 - Observation R3	1.7	2.5	4.1	0.89
HIRLAM4-fch12 - Observation R3	1.5	2.7	5.2	0.90

Table 16: *Statistics for August [mm/24h].*

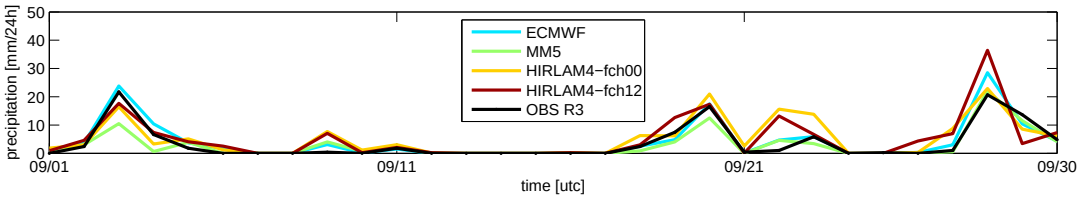

Figure 68: *September 2008. Daily precipitation [mm/24h].*

	Min	Mean	Max	SD
Observation R3	0	3.6	21.7	6.2
ECMWF	0	4.4	28.5	7.0
MM5	0	3.0	22.1	4.9
HIRLAM4-fch00	0	5.2	22.9	6.5
HIRLAM4-fch12	0	5.3	36.4	7.7

	ME	MAE	RMSE	r
ECMWF - Observation R3	0.7	1.2	2.1	0.96
MM5 - Observation R3	-0.6	1.5	2.8	0.90
HIRLAM4-fch00 - Observation R3	1.5	2.6	4.2	0.81
HIRLAM4-fch12 - Observation R3	1.7	2.6	4.7	0.82

Table 17: *Statistics for September [mm/24h].*

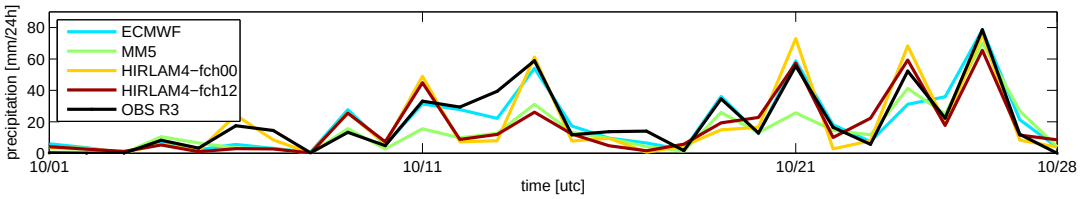

Figure 69: *October 2008. Daily precipitation [mm/24h].*

	Min	Mean	Max	SD
Observation R3	0	19.8	78.6	20.4
ECMWF	0.1	19.1	78.6	19.4
MM5	0	14.3	70.2	15.0
HIRLAM4-fch00	0	18.5	75.6	23.2
HIRLAM4-fch12	0.1	16.5	65.5	18.3

	ME	MAE	RMSE	r
ECMWF - Observation R3	-0.7	5.4	7.8	0.92
MM5 - Observation R3	-5.5	8.3	12.1	0.86
HIRLAM4-fch00 - Observation R3	-1.3	7.9	11.1	0.88
HIRLAM4-fch12 - Observation R3	-3.3	9.2	12.2	0.82

Table 18: *Statistics for October [mm/24h].*

The ECMWF model has the lowest RMSE in all of the months considered. The MAE is lowest for ECMWF in July, September and October and equal to MM5 for August, also here lower than HIRLAM4-fch00 and HIRLAM4-fch12. The ECMWF is consequently the model with the lowest average forecast error. The mean error, ME, shows that ECMWF gives a slight overestimation for the months July, August and September. In October, the month with the highest precipitation amount, the model shows a small underestimation. This corresponds to Figure 65, where the ECMWF model shows a tendency to underestimate high precipitation amounts. The ME for MM5 shows a very small underestimation for the three first months. In October however, MM5 is the model with the evident highest underestimation. According to ME, HIRLAM4-fch00 shows a larger overestimation than ECMWF for the three first months considered. In July, HIRLAM4-fch12 has the same ME as ECMWF, for August and September a larger overestimation is present. In October, both HIRLAM4-fch00 and HIRLAM4-fch12 show an underestimation. The correlation coefficient, r, is highest for ECMWF in all of the months, except August, where HIRLAM4-fch12 has the highest correlation.

Table 19 gives the overall statistics for the months July-October. The column named 'sum', is the accumulated precipitation for the mentioned period. ECMWF shows the smallest RMSE and MAE. Both ECMWF, HIRLAM4-fch00 and HIRLAM4-fch12 show a slightly overestimation, and HIRLAM4-fch12 shows the smallest. The MM5 model shows overall an underestimation. The correlation coefficient, r, is highest for ECMWF, while HIRLAM4-fch12 gives the lowest during the compared period. Based on the models compared in this section for the available period, a single point forecast from the ECMWF model shows the best correspondence to the HOBO rain gauge observation at R3 Stordal river.

	Sum	Mean	SD	
Observation R3	923.6	7.7	13.7	
ECMWF	1000.6	8.3	13.2	
MM5	707.2	5.9	9.7	
HIRLAM4-fch00	1032.8	8.6	14.6	
HIRLAM4-fch12	967.5	8.1	12.9	
	ME	MAE	RMSE	r
ECMWF - Observation R3	0.6	2.6	4.6	0.94
MM5 - Observation R3	-1.8	3.6	7.1	0.88
HIRLAM4-fch00 - Observation R3	0.9	4.0	7.2	0.87
HIRLAM4-fch12 - Observation R3	0.4	4.4	7.7	0.84

Table 19: *Overall statistics for the months July-October 2008 [mm/24h].*

10.3 Model comparison: In the MHS

This section contains a comparison between the accumulated precipitation amounts of the HOBO rain gauge observations and the available forecast for the whole MHS and the ability for MM5 and HIRLAM4 to indicate the gradient found in section 8.4. Precipitation amounts from 30th of June 00 UTC to 28th of October 00 UTC are considered. As in chapter 8, hours when the temperature at AWS-2 Blåfjell are below 2 °C are omitted.

As already mentioned, from HIRLAM4, only grid point data are available. The grid

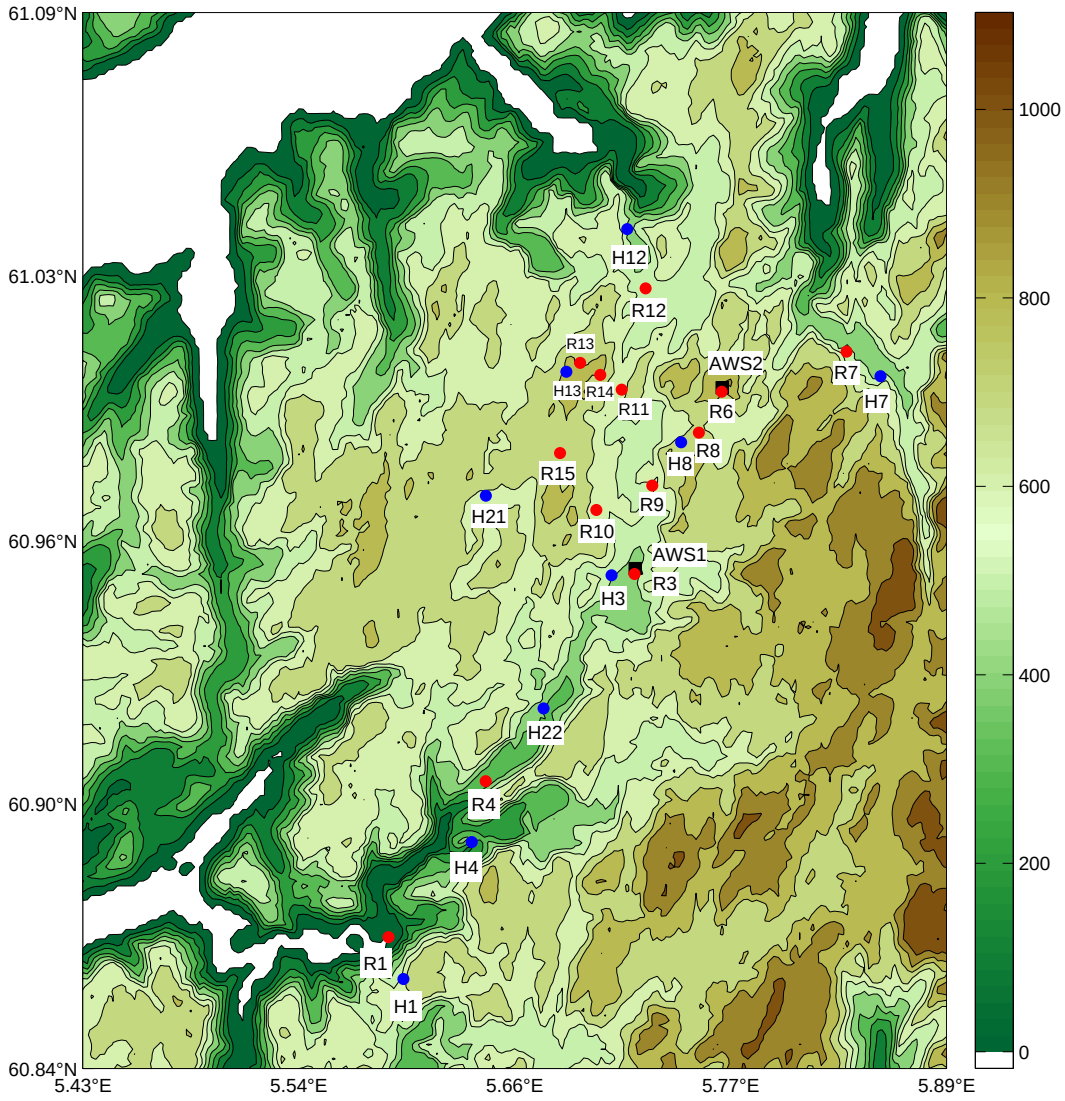

Figure 70: *Blue dots: HIRLAM4 grid point location. Red dots: HOBO rain gauge observations. The MM5 forecast is at the same location as the gauge observations. The colorbar denotes the elevation above sea level [m].*

points of the HIRLAM4-model are marked as the blue dots in Figure 70, the red dots denote the rain gauge locations. The locations R16 Oppedal, R17 Gamle Stølsleitet west, R18 Hareheia, R19 Årnesstøl and R20 Hornsetvatn are omitted from the comparison due to short period of MM5-data, and because of rather few nearby points in the HIRLAM4 model. Points from HIRLAM4 are denoted Hx in the figure and in Table 20, where x stands for the number of the nearest rain gauge locations. Not every HOBO rain gauge observation has a grid point close by, and is therefore denoted with a line in the table. Two grid points from HIRLAM4 are not near any of the gauge observations. These are denoted H21 and H22 in Figure 70, and included for the purpose of the gradient investigation. For the MM5 model, the points match the location of the rain gauges. The data from the MM5 model are denoted Mx in Table 20, where x corresponds to the number of the rain gauge location.

Table 20 shows the accumulated observed and forecasted precipitation for the considered period. The data presented in Table 20 are visualized in a scatter plot in Figure 71. The MM5 model clearly underestimates the observed precipitation amounts for all observation sites, as also seen in section 10.2 for the Stordal location. However, the correlation between the observation and the forecast of MM5 is high (r=0.82). For HIRLAM4, only grid point locations (Hx) that correspond to a rain gauge location (Rx) (see Figure 71) are included in Table 20. Both HIRLAM4-fch00 and HIRLAM4-fch12 show a clear tendency for overestimation. HIRLAM4-fch12 shows the smallest overestimation for all the locations, and is therefore better than HIRLAM4-fch00 when considering the amount. HIRLAM4-fch12 also showed smaller ME than HIRLAM4-fch00 when considering the overall period from July-October 2008 for Stordal location, however, varying tendencies were seen when considering the month-to-month variation. The rather low correlation coefficient of both HIRLAM4-fch00 and HIRLAM4-fch12 is indicating poor correspondence between forecast and observation. The fact that fewer points are considered for HIRLAM4 must be taken into consideration.

For a horizontal gradient investigation, the predicted values in Table 20 have been normalized to the level of R3 Stordal river (480 m a.s.l) with a vertical gradient of 5.0 % / 100 meter. The same method as in section 8.4 is used. The percentage amount of the Stordal-values for the amounts normalized to Stordal-level (R3/M3/H3) for models and observations are given in Table 21. The second last column gives the approximate value for each observation and MM5 location based on the gradient lines in Figure 53. Because the grid points do not coincide with the rain gauge locations, the last column gives the approximate value for each HIRLAM4 location based on the gradient lines in Figure 53. Figure 72 visualizes the table. The observation-column versus the models (column 3-5) is given in Figure 72(a), while the two last columns are utilized in Figure 72(b). The normalized values of MM5 in Table 21 show a relatively high degree of accordance with the observations (Figure 72(a)). The highest percentage is found in the southern part of the area, and the lowest in the northeastern part, which is consistent with the normalized observations. However, the agreement with the observations in the northwestern part of the measurement area, e.g. R13 and R14, is rather poor. The cor-

Location	Observation [mm]	MM5 [mm]	HIRLAM4-fch00[mm]	HIRLAM4-fch12[mm]
R1/M1/H1	632	471	873	837
R3/M3/H3	691	497	862	816
R4/M4/H4	774	539	811	732
R6/M6/-	766	540	-	-
R7/M7/H7	580	394	877	841
R8/M8/H8	684	508	1029	1005
R9/M9/-	687	493	-	-
R10/M10/-	828	528	-	-
R11/M11/-	664	484	-	-
R12/M12/H12	618	441	749	715
R13/M13/H13	798	519	1117	1076
R14/M14/-	920	535	-	-
R15/M15/H15	760	554	-	-

Table 20: *Accumulated precipitation [mm] from 30th of June 00 UTC to 28th of October 00 UTC. Only hours when the temperature at AWS-2 is above 2 °C are included.*

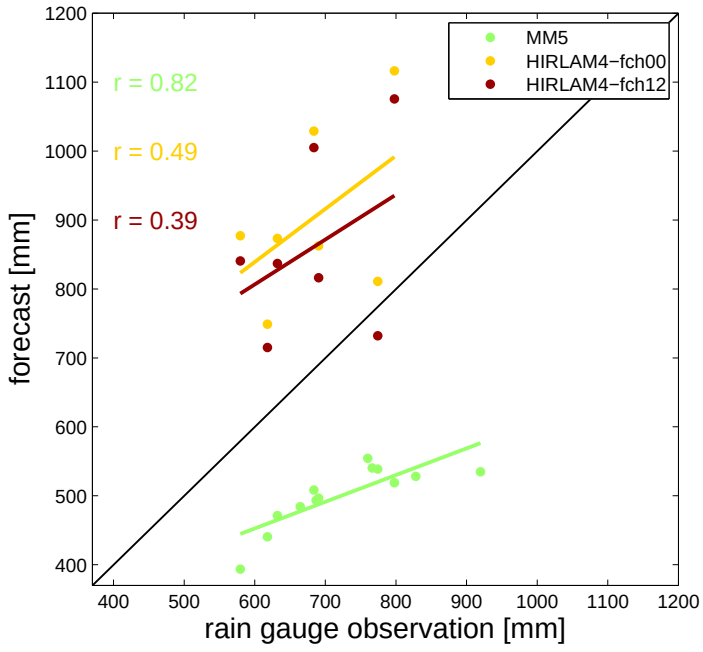

Figure 71: *Observation versus model forecast. Accumulated values [mm].*

relation coefficient is 0.80, and indicates that MM5 has the ability to sense the observed horizontal gradient. Both HIRLAM4-fch00 and HIRLAM4-fch12 show high values for the Matre-location, but H4 is too low compared to the observation. The model does not manage to reproduce the low percentage amount in the northeastern part of the area (H7, H8), but the northermost location (H12) is in well agreement with the percentage of the normalized observations. The correlation coefficient for both HiIRLAM4-fch00 and fch12 is low, indicating that the model does not manage to forecast the observed horizontal gradient in the area.

When comparing MM5 with the values for each location determined by the gradient lines of Figure 53, the correlation is even higher (Figure 72(b)). It is important to point out that the gradient lines are roughly estimated. When comparing with the values of the gradient lines for HIRLAM4, two additional grid points are utilized, H21 and H22. H21 shows some degree of accordance with the gradient lines, H22 does not. The correlation coefficient for both HIRLAM4-fch00 and HIRLAM4-fch12 is somewhat lower when considering gradient lines instead of observations. Omitting locations H21 and H22, which do not have observations to verify against, the correlation coefficients become 0.58 and 0.46 for HIRLAM4-fch00 and fch12, respectively. However, the ability to forecast the horizontal gradient is still poor.

Based on this comparison it is seen that neither the MM5 nor the HIRLAM4 for the different forecast hours are able to forecast the correct amount of observed precipitation. HIRLAM4 overestimates for all the considered observation, while MM5 shows a clear tendency for underestimation. It must be taken into account that HIRLAM4 is not interpolated to the observation sites, and due to the high resolution of the model, strong gradients might be present in a small horizontal scale. It should also be emphasized that not equal number of forecast locations is considered for the two models. For a gradient investigation, the amounts were normalized to the level of Stordal, and the percentage amount of the Stordal-values was considered. MM5 shows a high correlation when comparing with the gradient lines, and therefore a capability to predict the horizontal gradient. HIRLAM4, however, did not show this tendency as clearly, and is, based on this comparison, not suited to forecast the horizontal gradient in the MHS.

	Observation	MM5	HIRLAM4-fch00	HIRLAM4-fch12	gr. lines	gr. lines HIRLAM4
R1/M1/H1	115 %	119 %	127 %	128 %	115 %	115 %
R3/M3/H3	100 %	100 %	100 %	100 %	100 %	100 %
R4/M4/H4	116 %	112 %	97 %	92 %	115 %	115 %
R6/M6/-	90 %	89 %	-	-	88 %	-
R7/M7/H7	84 %	79 %	102 %	103 %	84 %	84 %
R8/M8/H8	88 %	92 %	107 %	110 %	90 %	93 %
R9/M9/-	93 %	93 %	-	-	95 %	-
R10/M10/-	110 %	98 %	-	-	104 %	-
R11/M11/-	90 %	91 %	-	-	97 %	-
R12/M12/H12	85 %	85 %	83 %	84 %	87 %	85 %
R13/M13/H13	100 %	91 %	113 %	115 %	102 %	104%
R14/M14/-	113 %	91 %	-	-	101 %	-
R15/M15/H15	94 %	96 %	-%	- %	106 %	-
H21	-	-	114 %	114 %	-	108 %
H22	-	-	91 %	82 %	-	111 %

Table 21: *Percentage of Stordal location (R3, M3, H3) for the values normalized to Stordal location. The two last columns give the approximate value based on the gradient lines (gr.lines) in Figure 53.*

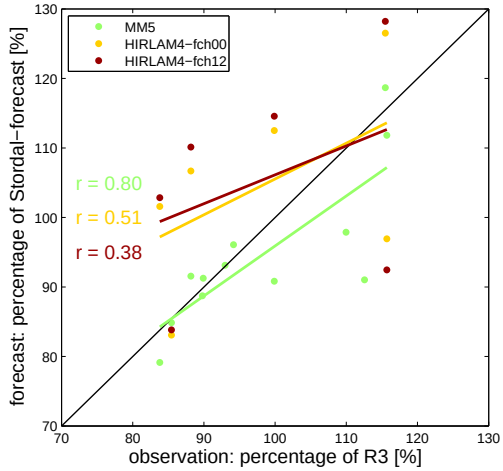

(a) Percentage of normalize Stordal forecast versus percentage of normalize Stordal value for the observations.

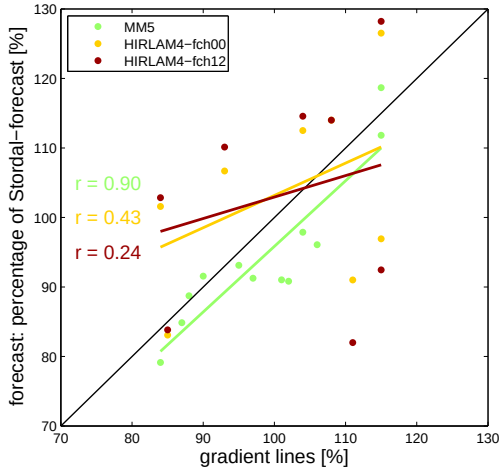

(b) Percentage of normalize Stordal forecast versus the value for the gradient lines from Figure 53 for each location.

Figure 72: *Visualization of Table 21.*

11 Normal versus campaign conditions

The wind conditions during precipitation experienced in the MHS during the field campaign are desirable to compare to normal conditions and conditions observed at nearby official weather stations for clarifying the correspondance to a normal situation. For comparison, wind and precipitation conditions at Fedje, which is located in a coastal area, and therefore less influenced by local topography, would be desirable to use. Unfortunately, Fedje is no longer registrating precipitation, and due to this, official observation at Flesland, Florida (Bergen) and Takle will be used even though these are not well exposed for all wind directions.

The normal annual wind conditions for percentage amount of precipitation at Flesland are presented in Figure 73(a). At Flesland, Bergen Airport, the topography is only believed to have a minor influence on the measurements. In Figure 73(b), the percentage amount of precipitation at Flesland for different wind directions at Flesland in the period from 5th of June to 29th of October (equal period as the weather stations were mounted in the MHS) is given. Precipitation registrations are done 06 and 18 UTC, and the corresponding wind directions when precipitation is registered are utilized. To clarify, the registrated rainfall may have occured until twelve hours before direction registration, or just before registration. This constitute uncertainty, but in the lack of other available data, this will be used. The precipitation observed at Flesland during the measurement period has a broader distribution than normal, with a large amount of the precipitation in a southwesterly direction, while a southeasterly direction is expected more common during a normal year. Approximately the same amount is present for a northerly wind direction, but somewhat more westerly than normal. At both Florida and Takle, the measurement period shows well agreement with the normal conditions, but the ditribution is more narrow than normal. However, Florida and Takle are assumed well influenced by the local topography, and these wind directions are expected common. The percentage amount of precipitation for AWS-2 Blåfjell was presented in Figure 25(b), section 6.3. Here the main amount of precipitation is observed from S to SSW direction, and the distribution is much narrower than observed at Flesland. Like seen for both Takle and Florida, this might be the common distribution at Blåfjell. A comparison of the ratio between convective and frontal precipitation in the project period and normal period is not done. It is expected that the project period has a higher ratio of convective precipitation than an annual normal period, due to convective summer events. The measurement period is rather short, and is therefore difficult to compare to a normal period, because a single event may contribute to a high amount of the total precipitation in a particular wind direction interval. Based on this and the fact that the wind distribution at Flesland during the campaign differs from a normal period, it is hard to consider the precipitation in the project period to be normal, without additional data material.

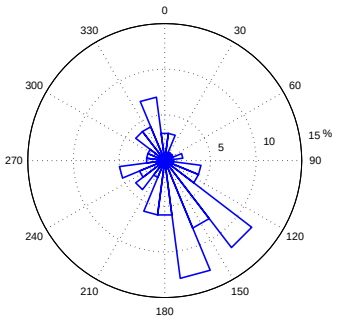

(a) Normal annual percentage amount of precipitation at Flesland.

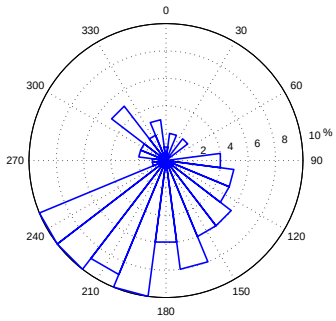

(b) Percentage amount of precipitation from June to October 2008 at Flesland.

Figure 73: *Normal annual conditions and campaign conditions at Flesland.*

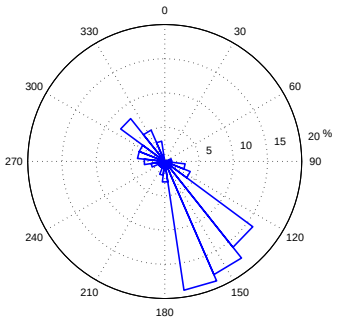

(a) Normal annual percentage amount of precipitation at Florida, Bergen.

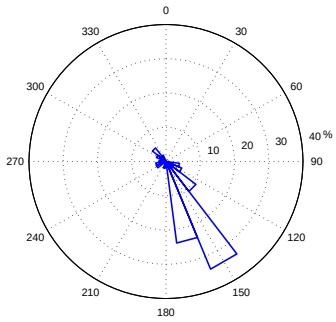

(b) Percentage amount of precipitation from June to October 2008 at Florida, Bergen.

Figure 74: *Normal annual conditions and campaign conditions at Florida.*

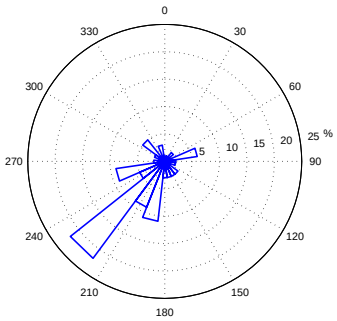

(a) Normal annual percentage amount of precipitation at Takle.

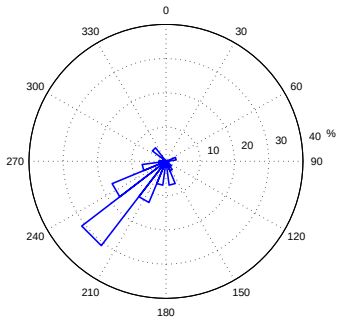

(b) Percentage amount of precipitation from June to October 2008 at Takle.

Figure 75: *Normal annual conditions and campaign conditions at Takle.*

12 Summary and conclusions

The presented thesis can be divided into two main parts. The first part is dedicated to a thorough characterization of the used HOBO rain gauges by laboratory tests and field comparisons. The second part describes the results achieved during the performed field measurement campaign in the MHS.

Laboratory experiments and calibrations of the HOBO rain gauges have been performed at the Geophysical Institute, Bergen. In a laboratory experiment concerning HOBO rain gauges out of level, a tendency of undersampling with increasing tilt angle was discovered. The maximum underestimation is around 10 % for a tilt angle of 6.6° when the tipping bucket in the gauge was parallel to the tilt of the board. A parallel field operation of 12 HOBO rain gauges showed that the total precipitation amounts of the instruments coincide within ±1.8 %. In addition a comparison campaign was performed against the official measurements of DNMI at the station Bergen-Florida. An excellent agreement was found. After removal of events when solid or mixed precipitation occurred, the HOBO rain gauges underestimated precipitation by only 0.9 %. Calibrations of the HOBO rain gauges indicated that the HOBO rain gauges tend to gradually underestimating true precipitation, and the performance of calibration of the HOBO rain gauges has turned out to be very important for accurate precipitation measurements.

The main purpose of this project was to explore the precipitation variability in the MHS and in particular the investigation of the representativeness of single point measurements for larger areas of complex terrain. Therefore a field campaign has been performed in cooperation between the Geophysical Institute, University of Bergen and the power company BKK in the period April to October 2008. During this time 20 rain gauges and two automatic weather stations have been deployed in the MHS. It turned out that a field campaign in the mountains is challenging. First of all by practical reasons, e.g. due to shortage of available tracks and roads in combination with heavy equipment in steep terrain. In addition precipitation can fall as snow during large parts of the year, which limits the accessibility to the higher elevated areas, but also effects the measurements itself, as solid precipitation is one of the major reasons for rain gauge undercatch. In this context a method has been developed and applied to compile an adjusted precipitation data set minimizing uncertainties due to solid precipitation.

As BKK is using a single point measurement for the description of the precipitation in the MHS, a thorough comparison has been performed for the rain gauge at Stordal. The rain gauge maintained by BKK showed unstable values, and a test of this rain gauge is recommended. An investigation of a potential influence caused by the cliff close to the measurement site indicated an undercatch due to wind for the rain gauge situated by Stordal power station compared to the station situated at the location Stordal river. The investigation did not show any clear relationship when comparing for wind direction, and the location of the rain gauge maintained by BKK is therefore

assumed representative for the Stordal area.

In the precipitation distribution for the Matre Hydro System when considering the temperature adjusted time series the highest amounts are present in the northwestern area around Skorvane and Gamle Stølsleitet. The least amounts are found at Matre and Årsdalsvatn. An overall vertical precipitation gradient of 5.2 % / 100 meter is found, and based on this, the precipitation amounts were normalized to the level of Stordal. From this normalized data a horizontal gradient was found present in the area, with approximately 115 % of the Stordal value in Matre (southwest) and gradually decreasing towards northeast with approximately 85 % at Årsdalsvatn and Stølsvatn. The local variability is particularly large in the area around Gamle Stølsleitet and Skorvane, and the gradient lines are therefore more uncertain here. About 80 % of the precipitation measured in the campaign arrived from directions between S and SSW, and the gradient is expected to be common for these directions. However, variations are also seen within this narrow direction. The measurement period is rather short, and longer time series would have been necessary to better describe gradients based on narrow wind direction intervals, because a single event may contribute to a high amount of the total precipitation in a particular wind direction interval. Based on the generalized horizontal gradient lines from the Matre campaign, BKK might be operating with too low normal run-off values for the reservoirs Stølsvatn, Kvanngrøvatn and Holmevatn. However, to make this conclusion more robust, a better comparison between the precipitation in the project period and a normal period should be done. In addition the ratio between convective and frontal precipitation for near normal wind direction conditions should be taken into consideration.

Two case studies for different synoptic situations have been presented. For the frontal passage case the correlation between the case study and the over all precipitation amounts was very high, which indicates that the distribution found in the MHS is mainly obtained from frontal systems. Convective situations like the one examined in case study 2 have a more random precipitation distribution, and are therefore contributing to blur the main gradient. The small scale variation in precipitation in the MHS is shown large, and a denser network of rain gauges, particularly in the area between Matre and Stordal, maybe in the order of a few hundreds of meters, would be desirable for a potential future measurement campaign.

Another purpose of the project was also to study the representativeness of a used single point ECMWF forecast for the reference station at Stordal. The single point forecast from the ECMWF model is typically smoother than the observations. The model neither reaches the intensity tops nor short stops in the observed rainfall time series. Consequently a disagreement is seen when comparing the number of hourly events to the observations for different precipitation intervals. A better accordance is found for daily precipitation amounts, and the agreement is quite well for weekly events. During the measurement period from April to October 2008, the model forecasted in total only about 5 % less then the observed amount, which indicated that the overall vol-

ume forecasted by the model is good when comparing to the observation at Stordal. Good agreement between forecast and observation is also found for the wind direction intervals where most of the precipitation is observed. The model showed also extremely well correspondence to the observation for Stordal in the frontal case study, which is important due to most of the precipitation arriving in frontal passages. The representativeness of the forecast for the Stordal location is therefore considered good. However, for shower activities like the convective case studied, the model showed a poor performance comparing to single point measurements.

The operationally used ECMWF forecast for Stordal comes from a model with rather coarse resolutions of about 25 km. One of the main problems of precipitation modelling for complex terrain is the insufficient resolution of the topography. Therefore the potential for improvement of precipitation prediction by use of operational model runs with higher horizontal resolution has also been addressed. For this purpose, the models MM5, with a horizontal resolution of 12 km, and HIRLAM4, with a horizontal resolution of 4 km, were used. The single point forecast from ECMWF has been compared with the MM5 and HIRLAM4 model for Stordal on the basis of daily precipitation sums for the months July - October 2008. For this period, ECMWF shows the best correspondence with the observations, and it is therefore no need for changing the available forecast to another model if one single point forecast will continue to be utilized in the future.

When comparing MM5 and HIRLAM to the measurements in the whole MHS, it is clear that none of the models are able to predict the correct amount of precipitation. MM5 shows an underestimation, but is highly correlated with the measurements. HIRLAM4 is in general overestimating, but is only weakly correlated to the measurements. The MM5 model describes the gradient in the MHS, and enables a correlation of 0.9 when comparing with the estimated gradient lines for the hydro system. HIRLAM4, however, does not indicate this capability.

Overall the Matre campaign provided a highly valuable data set for an improved understanding of orographic precipitation. These data are important for the estimation and modelling of the hydrology of the MHS. In the future the compiled data set with unique spatial and temporal resolution can be used for detailed model validation purposes of fine scale numerical simulations. On the long term this can lead to the development of improved precipitation parameterization schemes for numerical weather prediction models.

Appendix A

In Table 22 below, the amounts in Table 11 have been normalized to the level of R3 with the aid of equation 8.

AWS-2	R1	R3	R4	R6	R7	R8	R9	R10	R11	R12	R13	R14	R15	R16	R17	R18	R20	
345 < wd ≤ 15	6	15	14	22	29	21	14	9	7	8	4	5	5	5	4	4	4	4
15 < wd ≤ 45	7	4	11	3	2	3	4	4	4	3	4	3	4	2	3	4	3	4
45 < wd ≤ 75	1	0	0	0	1	0	0	0	0	0	0	0	0	3	0	0	0	1
75 < wd ≤ 105	2	1	1	0	0	1	1	0	1	0	0	0	1	1	0	1	0	0
105 < wd ≤ 135	30	18	22	11	14	15	16	17	15	15	17	13	17	25	21	25	29	21
135 < wd ≤ 165	65	31	43	19	24	24	24	31	25	23	29	28	21	39	35	32	29	30
165 < wd ≤ 195	349	316	353	320	251	276	289	357	306	288	348	408	278	332	405	357	151	365
195 < wd ≤ 225	284	255	277	191	207	213	237	277	193	177	214	237	252	180	223	207	93	198
225 < wd ≤ 255	35	27	42	21	23	20	22	25	22	29	24	27	30	25	29	31	15	25
255 < wd ≤ 285	16	12	22	16	19	15	12	18	17	19	20	21	14	23	21	19	11	24
285 < wd ≤ 315	1	4	9	9	7	9	11	8	12	8	13	12	10	11	11	11	6	13
315 < wd ≤ 345	2	7	5	5	2	8	11	11	18	17	16	18	17	3	23	17	18	19

Table 22: *The table gives the normalized amount [mm] for each rain gauge location divided into different wind direction intervals. The values are calculated using equation 8 in section 8.4.*

Table 23 shows the percentage of the value of R3 Stordal river for normalized precipitation for different wind directions at AWS-2 Blåfjell.

AWS-2	R1	R3	R4	R6	R7	R8	R9	R10	R11	R12	R13	R14	R15	R16	R17	R18	R20
345 < wd ≤ 15	-	100	95	152	198	141	94	64	-	-	-	-	-	-	-	-	-
15 < wd ≤ 45	-	-	-	-	-	-	-	-	-	-	-	-	-	-	-	-	-
45 < wd ≤ 75	-	-	-	-	-	-	-	-	-	-	-	-	-	-	-	-	-
75 < wd ≤ 105	-	-	-	-	-	-	-	-	-	-	-	-	-	-	-	-	-
105 < wd ≤ 135	165	100	122	63	78	83	88	96	84	86	94	75	92	138	120	141	119
135 < wd ≤ 165	211	100	140	60	78	79	79	102	81	75	93	90	69	128	114	103	98
165 < wd ≤ 195	111	100	112	101	80	88	91	113	97	91	110	129	88	105	128	113	116
195 < wd ≤ 225	111	100	108	75	81	83	93	109	75	69	84	93	99	71	87	81	78
225 < wd ≤ 255	127	100	153	75	83	73	81	93	82	105	89	98	110	93	108	115	91
255 < wd ≤ 285	137	100	192	134	159	132	103	150	148	166	170	176	124	192	181	164	204
285 < wd ≤ 315	-	-	-	-	-	-	-	-	-	-	-	-	-	-	-	-	-
315 < wd ≤ 345	-	-	-	-	-	-	-	-	-	-	-	-	-	-	-	-	-

Table 23: *Percentage of the value of R3 Stordal river for normalized precipitation for different wind directions. This table should be seen in relation to Table 11, which gives the precipitation amounts in mm (not normalized) for each interval. Values where the precipitation amount in Table 11 have been below 10 mm are omitted. For R3 below 10 mm, all percentage values for that specific wind direction are omitted.*

Table 24 shows a detailed look into the intervals from 170°-225° from Table 23. Table 24 is visualized in Figure 76 and 77.

AWS-2	R1	R3	R4	R6	R7	R8	R9	R10	R11	R12	R13	R14	R15	R16	R17	R18	R20
170 < wd ≤ 175	154	100	147	87	79	65	78	106	90	93	119	122	64	137	143	132	145
175 < wd ≤ 180	127	100	129	99	81	78	90	116	95	99	122	144	78	111	150	137	140
180 < wd ≤ 185	97	100	99	121	81	95	94	115	102	94	118	150	101	100	138	120	122
185 < wd ≤ 190	70	100	85	81	83	90	90	99	78	58	71	80	78	106	80	63	59
190 < wd ≤ 195	108	100	101	106	78	113	109	130	121	110	109	122	123	87	112	92	94
195 < wd ≤ 200	103	100	96	72	88	89	97	106	77	104	82	95	92	79	85	79	74
200 < wd ≤ 205	110	100	111	87	87	94	97	120	84	83	102	107	115	85	105	92	95
205 < wd ≤ 210	109	100	107	79	83	82	98	116	61	58	74	82	89	58	79	72	64
210 < wd ≤ 215	140	100	126	97	99	99	114	135	106	79	100	117	115	77	106	103	95
215 < wd ≤ 220	118	100	79	42	48	46	60	58	47	53	53	59	60	46	59	59	61
220 < wd ≤ 225	111	100	155	61	58	68	74	105	72	69	73	80	117	48	78	80	67

Table 24: *A detailed look into the intervals from 170°-225° in Table 23. The interval 165°-170° is omitted here due to low precipitation amount. It must be taken into consideration that the western intervals contains more precipitation than the easternones.*

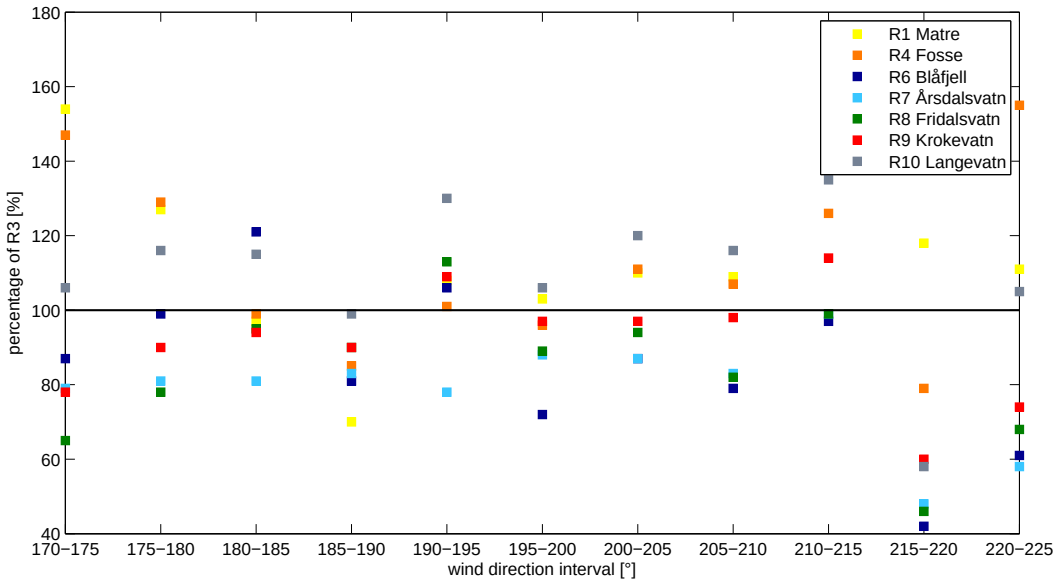

Figure 76: *Percentage of the value of R3 Stordal river for the normalized amounts versus wind direction intervals (170°-225°) for the rain gauge locations R1, R4, R6, R7, R8, R9 and R10. Visualization of Table 24.*

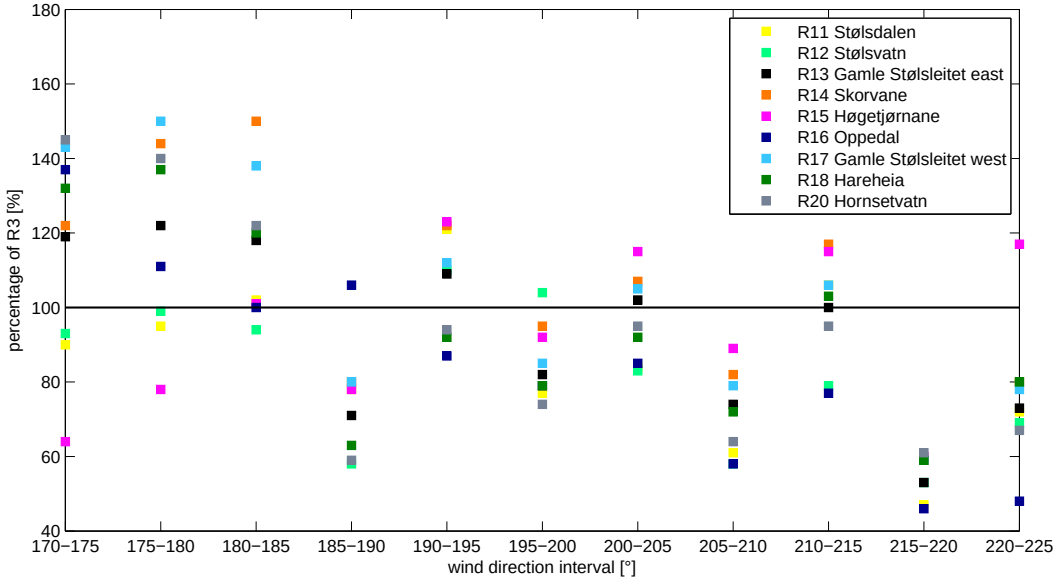

Figure 77: *Percentage of the value of R3 Stordal river for the normalized amounts versus wind direction intervals (170°-225°) for the rain gauge locations R11, R12, R13, R14, R15, R16, R17, R18 and R20. Visualization of Table 24.*

Appendix B

A short description of different statistical parameters used in the master thesis is given here.

Mean error: The mean error, also called the bias error, measures the inclination of a model to overforecast or underforecast a value. The mean error, ME, for a given variable is defined as

$$ME = \frac{1}{N}\sum_{i=0}^{N}(f_i - o_i), \tag{9}$$

where f_1,...,f_N denote the forecast and o_1,...,o_N the corresponding observations. If a model has a positive mean error, on average the model overforecasts or exceeds the observed value. However, it does not measure the correspondence between forecasts and observations, i.e., it is possible to get a perfect score for a bad forecast if there are compensating errors. The range of the mean error is -∞ to ∞, and the optimal score is 0.

Root mean square error: Root mean square error, RMSE, measures the typical size of model forecast errors, and is defined as

$$RMSE = \left[\frac{1}{N}\sum_{i=0}^{N}(f_i - o_i)^2\right]^{1/2}, \tag{10}$$

where f_1,...,f_N denote the forecast and o_1,...,o_N the corresponding observations. The RMSE does not indicate the direction of the deviations, and it tends to give more weight to large errors. The range of the mean error is 0 to ∞, and the optimal score is 0.

Mean absolute error: The mean absolute error, MAE, measures the average magnitude of the forecast errors, and is defined as

$$MAE = \frac{1}{N}\sum_{i=0}^{N}|f_i - o_i|, \tag{11}$$

where f_1,...,f_N denote the forecast and o_1,...,o_N the corresponding observations. The MAE does not indicate the direction of the deviations. The range is from 0 to ∞, and the optimal score is 0.

Correlation coefficient: The correlation coefficient, r, indicates how well the forecast values correspond to the observed values. The correlation coefficient is defined as

$$r = \frac{\frac{1}{N}\sum_{i=0}^{N}(f_i - \bar{f})(o_i - \bar{o})}{SD(f)SD(o)} \tag{12}$$

In the formula for the correlation coefficient r, the following definitions are used for the means and the standard deviations of the forecasts and observations:

$$\bar{f} = \frac{1}{N}\sum_{i=0}^{N} f_i, \qquad \bar{o} = \frac{1}{N}\sum_{i=0}^{N} o_i$$

$$SD(f) = \left[\frac{1}{N}\sum_{i=0}^{N}(f_i - \bar{f})^2\right]^{1/2}, \qquad SD(o) = \left[\frac{1}{N}\sum_{i=0}^{N}(o_i - \bar{o})^2\right]^{1/2}$$

The range of the correlation coefficient is -1 to 1, with 1 as the perfect score.

References

Aaltonen, A., E. Elomaa, A. Tuominen, and P. Valkovuori (1993). Measurement of precipitation. Proc. Symp. on Precipitation and Evaporation. *Slovak Hydrometeorlogical Institute and Swiss Federal Institute of Technology 1*, 42–46.

Andersen, P. (1973). The distribution of monthly precipitation in Southern Norway in relation to prevailing H. Johansen weather types. *Årbok for Universitetet i Bergen. Matematisk-Naturvitenskapelig serie, 1972, Nr. 1*, 20.

Bergeron, T. (1965). On the Low-Level Redistribution of Atmospheric Water Caused by Orography. *Project Pluvius, Reports, 5*.

BKK (2009). *Available from http://bkk.no/servlet/se.ementor.econgero.servlet.presentation.Main?data.node.id=70&data.language.id=2.*

Bolton, D. (1980). The computation of equivalent potential temperature. *Monthly Weather Review 108*, 1046–1053.

Bremnes, J. B. and M. Homleid (2008). Verification of Operational Numerical Weather Prediction Models September to November 2008. *met.no note no. 17.*

Dinku, T., E. Anagnostou, and M. Borga (2002). Improving Radar-Based Estimation of Rainfall over Complex Terrain. *Journal of Applied Meteorology 41*, 1163–1178.

DNMI (2008). *Været i Norge. Klimatologisk månedsoversikt.* met.no-info, no. 5-10. Available at //met.no/observasjoner/maned. The Norwegian Meteorological Institute.

Dudhia, J., K. Manning, W. Wang, and C. Bruyere (2005). PSU/NCAR Mesoscale Modeling System Tutorial Class Notes and Users' Guide (MM5 Modeling System Version 3).

Førland, E. J. (1979). Nedbørens høydeavhengighet. *Klima, Det norske meteorologiske institutt* (2), 3–24.

Førland, E. J. (1981). Sammenligning av nedbørsmålere. *Klima, Det norske meteorologiske institutt* (4), 26–35.

Førland, E. J. (1984). Lokalklima på Vestlandskysten. *Klima, Det norske meteorologiske institutt* (6), 24–36.

Førland, E. J. (1993). Nedbørnormaler: normalperiode 1961-1990. *Klima. Det norske meteorologiske institutt* (39).

Førland, E. J., P. Allerup, B. Dahlström, E. Elomaa, J. Jonsson, H. Madsen, J. Perälä, P. Rissanen, H. Vedin, and F. Vejen (1996). Manual for operational correction of nordic precipitation data. *Klima. Det norske meteorologiske institutt* (24).

Førland, E. J. and G. Bjørbæk (1979). Fordamping fra norske nedbørsmålere. *Klima. Det norske meteorologiske institutt* (2), 37–40.

Grell, G. A., J. Dudhia, and D. R. Staufer (1995). A description of the Fifth-Generation Penn State/NCAR mesoscale model (MM5). *NCAR Techincal Note, NCAR/TN-398+STR*, 122 pp.

HIRLAM (2009). The HIRLAM Consortium. http://www.hirlam.org/.

Hong, S. and H. Pan (1996). Nonlocal Boundary Layer Vertical Diffusion in a Medium-Range Forecast Model. *Mon. Wea. Rev. 124*, 2322–2339.

J. Reisner, R. M. Rasmussen, R. T. B. (1998). Explicit forecasting of supercooled liquid water in winter storms using the MM5 mesoscale model. *The Quarterly Journal of the Royal Meteorological Society 124*, 1071 – 1107.

Jiang, Q. F. and R. B. Smith (2003). Cloud Timescales and Orographic Precipitation. *Journal of the Atmospheric Sciences 60*, 1543–1559.

Kain, J. (2004). The Kain Fritsch Convective Parameterization: An Update. *J. Appl. Meteor. 43*, 170–181.

Karlsen, G. V. (2007). Sammenheng mellom nedbør og utløsende og dynamiske faktorer til jordskred. En studie av Jordal i Fjærland, vest i Norge. Master's thesis, Universitetet i Oslo.

Larson, L. and E. Peck (1974). Accuracy of precipitation measurements for hydrologic modeling. *Water Resour. Res 10*(4), 857–863.

Mass, C. (1981). Topographically-forced convergence in western Washington State. *Monthly Weather Review 109*, 1335–1347.

Nordø, J. and K. Hjortnæs (1966). Statistical studies of precipitation on local, national, and continental scales. *Geophysica Norvegica 26*(12), 1–46.

Onset (2001). *Data logging rain gauge manual*. Onset Computer Corporation.

Persson, A. and F. Grazzini (2007). User guide to ECMWF forecast products. *Meteorological Bulletin M3.2. Available at http://www.ecmwf.int/products/forecasts/guide/user_guide.pdf*.

Reuder, J., G. O. Fagerlid, I. Barstad, and A. Sandvik (2007). Stord Orographic Precipitation Experiment (STOPEX): an overview of phase I. *Advances in Geosciences 10*, 17–23.

Rinehart, R. E. (1983). Out-of-Level Instruments: Errors in Hydrometeor Spectra and Precipitation Measurements. *Journal of climate and applied meteorology 22*, 1404–1410.

Rogers, R. R. Yau, M. K. (1989). *A short course in cloud physics* (3 ed.). Butterworth-Heinemann.

Sælthun, N. R. (1972). Sommernedbørens arealfordeling i et høyfjellsfelt. Master's thesis, Universitetet i Oslo.

Sevruk, B. (1982). Methods of correction for systematic error in point precipitation measurement for operational use. *Operational Hydrology Report. World Meteorological Organization, Geneva 21.*

SIAP (2001). *UM7525 Precipitation Sensor manual.* Available at http://www.siap.com /eng/PDF/UM7525_en.pdf.

Sinclair, M., D. Wratt, R. Henderson, and W. Gray (1997). Factors Affecting the Distribution and Spillover of Precipitation in the Southern Alps of New Zealanl - A Case Study. *Journal of Applied Meteorology 36*, 428–442.

Skaar, E. (1976). Local climates and growth climates of the Sognefjord region: Part III: The Precipitation. *Meteorologiske annaler 7*(2), 19–67.

Skartveit, A. (1976). *Energy exchange at the earth's surface with emphasis on an alpine tundra ecosystem.* University of Bergen.

Smith, R. B. (1979). The influence of mountains on the atmosphere. *Advances in Geophysics 21*, 87–230.

Smith, R. B. (1982). A differential advection model of orographic precipitation. *Monthly Weather Review 110*, 306–309.

Smith, R. B. (1989). Mechanisms of orographic precipitation. *Meteorological Magazine 118*, 85–88.

Smith, R. B. and I. Barstad (2004). A Linear Theory of Orographic Precipitation. *Journal of the Atmospheric Sciences 61*, 1377–1391.

Smith, R. B. and S. Grønås (1993). Stagnation points and bifurcation in 3-d mountain airflow. *Tellus 45A*, 28–43.

Spinnangr, F. (1943a). Synoptic studies on precipitation in Southern Norway. I. Instability showers. *Meteorologiske annaler 1*(12), 324–356.

Spinnangr, F. (1943b). Synoptic studies on precipitation in Southern Norway. II. Front precipitation. *Meteorologiske annaler 1*(17), 434–468.

Spinnangr, F. and H. Johansen (1954). On the distribution of precipitation in maritime tropical air over Norway. *Meteorologiske annaler 3*(14), 352–424.

Spinnangr, F. and H. Johansen (1955). On the influence of the orography in Southern Norway on instability showers from the sea. *Meteorologiske annaler 4*(3), 18–35.

Villanger, F. (2009). Personal communication.

Wallace, J. and P. Hobbs (2006). *Atmospheric science : An introductory survey* (2 ed.). International Geophysics Series. Elsevier.

Yang, D., B. Goodison, J. Metcalfe, V. Golubev, R. Bates, T. Pangburn, and C. Hanson (1998). Accuracy of NWS 80 Standard Nonrecording Precipitation Gauge: Results and Application of WMO Intercomparison. *Journal of atmospheric and oceanic technology 15*, 54–68.